Zonally symmetric monsoon dynamics in a general circulation model

by

Nikki C. Privé

B.S., University of Maryland, College Park (1999)

Submitted to the Department of Earth, Atmospheric, and Planetary Science
in partial fulfillment of the requirements for the degree of

Master of Science in Atmospheric Science

at the

MASSACHUSETTS INSTITUTE OF TECHNOLOGY

May 2002

Author ....
Department of Earth, Atmospheric, and Planetary Science
May 10, 2002

Certified by ....
R. Alan Plumb
Professor
Thesis Supervisor

Accepted by ....
Ronald G. Prinn
Professor, Head of Department

Zonally symmetric monsoon dynamics in a general circulation model

by

Nikki C. Privé

Submitted to the Department of Earth, Atmospheric, and Planetary Science
on May 10, 2002, in partial fulfillment of the
requirements for the degree of
Master of Science in Atmospheric Science

Abstract

The MIT general circulation model is used with simplified setup to study steady zonally averaged monsoon circulations. Two dimensional model runs are made with a zonally symmetric continent north of 15N and a slab ocean of uniform sea surface temperature to study the applicability of axisymmetric theory. Forcing to drive the monsoon is applied by heating the subtropical land surface. The dynamical constraints of axisymmetry prevent low-level cross-equatorial flow and inhibit the northward transport of moisture onto the continent when there is no temperature gradient across the equator. The ocean cannot supply adequate moisture to feed the monsoon, and the ground hydrology strictly controls the behavior of the monsoon. A second set of two dimensional runs with similar continent, but with an SST gradient across the equator, result in a viable steady monsoon with low-level cross-equatorial flow providing moisture to the monsoon. The surface forcing required to induce a monsoon is reasonable given the constraints of the axisymmetric model setup. A series of three dimensional model runs with a zonally symmetric continent are made to study the role of zonally asymmetric flow on the zonal mean monsoon. It is found that greater land surface forcing is required to induce a zonally averaged monsoon circulation in the three dimensional runs than in similar axisymmetric runs. The behavior of the monsoon disturbances in the three dimensional runs is similar to the observed Asian monsoon in that there is low-level cross-equatorial flow which is southwesterly along the coastline, and in that a large-scale angular momentum conserving meridional circulation develops with ascent over the continent and subsidence in the opposite hemisphere. Moisture transport is found to play a very strong role in the monsoon dynamics in all of the model runs.

Thesis Supervisor: R. Alan Plumb
Title: Professor

Acknowledgments

I am indebted to many people, but in the interest of keeping an already overlong document contained, I shall endeavor to be brief. I am deeply grateful to the following people: for direction, discussions, and helpful advice, my advisor, Alan Plumb; for assistance above and beyond the call of duty, Olivier Pauluis; for help with the MITGCM, Chris Hill; for all sorts of aid at all times of the day and all days of the week, the denizens of the 17th floor computer lab, Kirill Semeniuk, Jessica Neu, Alan Kuo, and Will Heres; for inspiration, Tieh-Yong Koh; for tolerating a lot of mess, my officemates, Fabio Dalan and Irene Lee; for being relentlessly cheerful and inordinately helpful, Mary Elliff; for patience with repeated mistakes, the bridge-players (your identities are safe!); for putting up with extended absence, my housemates Wendy, Josh, Geoff, and George; for gourmet care packages, my parents; for always being on time, the late night drivers of the #80 bus; for advice and entertaining chats, Tony; and for the gentle darkness of the lab at night, Richard Shindell's *Courier,* Steve Earle's *Train a Comin',* and the self-titled album by *Cry Cry Cry.*

This material is based upon work supported under a National Science Foundation Graduate Research Fellowship. Any opinions, findings, conclusions or recommendations expressed in this publication are those of the author and do not necessarily reflect the views of the National Science Foundation.

Contents

List of Figures

Chapter 1

Introduction

1.1 Background

Current theory of steady axisymmetric meridional circulations in the tropics is based on Hide's theorem. Hide (1969) was the first to specifically note that for viscous, axisymmetric, steady flow, there can be no extrema of angular momentum away from the surface by conservation of angular momentum (AMC). Therefore, thermal equilibrium states which result in a westerly jet aloft at the equator cannot attain, in which case a meridional circulation is present instead. Held and Hou (1980) and Lindzen and Hou (1988), building on the work of Hide (1969), Schneider and Lindzen (1977), and Schneider (1977), examined the conservation of angular momentum in axisymmetric tropical regions in order to explain the existence and behavior of Hadley cells.

Plumb and Hou (1992) examined the threshold behavior of meridional circulations when the regularity condition for the thermal equilibrium solution is violated in the subtropics. This threshold is the vanishing of absolute vorticity at upper levels. Since the absolute vorticity of a fluid at rest in the subtropics is small but nonzero, there is a minimum forcing below which the thermal equilibrium solution does not violate Hide's theorem. When the thermal equilibrium solution attains, the cross-equatorial circulation is weak and driven by viscous effects. For supercritical forcing, an AMC cross-equatorial circulation attains, and the flow strengthens rapidly with increased forcing.

The critical transition to a thermally direct axisymmetric circulation was expanded to moist atmospheres by Emanuel (1995). Zheng (1998) performed numerical calculations in a moist, axisymmetric model to test the theory of Emanuel (1995). Using a model with an explicit hydrological cycle and saturated lower boundary, with forcing due to a specified surface temperature profile, Zheng found that threshold behavior of the meridional circulation was still present, and qualitatively followed the theory of Emanuel (1995).

Studies of monsoons with general circulation models (GCMs) often employ highly detailed setups, including realistic configurations of continents and complex surface parameterizations. In contrast to the usual approach, Xie and Saiki (1999) used a GCM with minimal land surface parameterizations and a simplified continent roughly similar in form to the Eurasian/African landmass to investigate the onset and seasonal evolution of the monsoon. They found that the development of instability in the easterly jet which occurs offshore of the heated continent during early summer played a role in sudden onset of the monsoon by generating baroclinic disturbances which initiate deep convection over the continent. A series of perpetual summer runs showed that the bucket-type ground hydrology encouraged the inland spread of the monsoon by providing moisture to supply deep convection in the interior of the continent.

1.2 Motivation

Previous studies of axisymmetric subtropical circulations have been based on highly simplified dynamics, usually with specified, non-interactive forcing and idealized background states. The introduction of more realistic dynamics, with the complicated feedbacks that are thus implied, may significantly alter the dynamical behavior of the axisymmetric circulations.

We wish to turn the investigation of axisymmetric circulations to the study of monsoon-type dynamics by introducing an axisymmetric 'continent' to the picture, and by using a GCM which includes moist convective processes. The intention is to determine how the axisymmetric theory of Plumb and Hou (1992), Emanuel (1995), and Zheng (1998) might pertain to actual monsoon dynamics, and also how well an axisymmetric setup can hope to represent the monsoon. The land surface is treated in a highly simplified manner, but in such a way that the fundamental nature of convective and surface flux feedbacks is captured. By applying a meridionally localized surface temperature anomaly to the land surface, representing the heating of the land surface in the subtropics during the early summer, it is hoped to simulate the most basic nature of monsoonal flows. Although this type of simplified, axisymmetric model is clearly not able to reproduce a realistic monsoon, the idealized setup may help to clarify the nature of the dynamical interactions and feedbacks involved in the monsoon.

A series of different model setups are used to highlight various aspects of steady, zonal mean monsoon dynamics. First, an axisymmetric setup similar to that of Zheng (1998) is used to examine the existence of threshold behavior with land and a uniform background equilibrium surface temperature profile. A realistic background temperature profile is then assumed for the second set of axisymmetric experiments. A series of three-dimensional runs are investigated with zonally symmetric surface conditions, in order to examine the role of eddies in monsoon dynamics and to explore the dynamical limitations of axisymmetry in representing the monsoon.

Unlike previous investigations, wherein specified forcing (be it applied vertical heating or surface temperature perturbation) was not affected by the resulting circulation, the setup used in the current experiments allows for many and various types of feedbacks between the forcing and the dynamics. The importance of such feedbacks to monsoon circulations has been illustrated by the work of Xie and Saiki (1999). The progression and extent of the monsoon region was limited in their model by the ground hydrology, as the land surface was gradually moistened with the advance of the monsoon rains. A simple bucket hydrology as used by Xie and Saiki can lead to self-sustaining feedback: a moist surface can provide local moisture for convection and thus encourage precipitation, while a dry surface may have a local θ_e minimum, and precipitation will favor other regions. We expect that a variety of such feedbacks will be present in our model runs.

The zonally symmetric setup used is not representative of the real monsoon, which has important longitudinal variations. The simplified land parameterizations are also not realistic, although it is hoped that the parameterizations capture the basic nature of the land processes. We are clearly not attempting to recreate a realistic monsoon in the model. Likewise, the three-dimensional model runs are not intended to recreate any actual monsoon as observed in the real world. Instead, the three-dimensional runs are designed to look at the differences in the dynamics between axisymmetric and zonal mean 3D circulations so that the role of eddies can be evaluated. To what extent can an axisymmetric model hope to represent a monsoon? What aspects of the monsoon are only captured in three dimensions? Is longitudinal variation of landmass needed to create a viable monsoon? These are the main questions that we wish to address through the three-dimensional model runs.

An additional goal of this work is to test the behavior of the MITGCM in an atmospheric framework. The model is relatively untested in atmospheric mode, although the oceanic platform is somewhat more studied. The MITGCM has previously been used only in aqua-planet situations, and does not yet have a fully developed set of land parameterizations. As our setup is highly simplified, we cannot quantitatively check our model results against observations, but we can make qualitative assessments of the large-scale model behavior.

1.3 Defining the Monsoon

As there is no agreed-upon definition for the monsoon, it behooves us to specify exactly what we will consider a 'monsoon circulation' for the purposes of this work. Although the monsoon is generally associated with seasonal changes in wind direction and precipitation fields, a seasonal definition is not useful for steady runs such as are used here. The large monsoons, such as the Asian and Australian monsoons, are associated with intense precipitation over land surfaces and with low-level poleward meridional flow across the land-sea boundary. For our purposes, we shall define a monsoon circulation to be one in which

1. the zonally averaged meridional circulation features ascent over the land surface, with subsidence in the opposite hemisphere and northward low-level flow across the equator
2. significant zonal mean precipitation occurs over the land surface in the region of ascending circulation

Thus, circulations with ascent over the ocean near the land-sea boundary, so that only a small amount of precipitation occurs over the land, are not considered to be monsoonal. Whether this definition excludes circulations similar to those associated with real monsoons is uncertain, as there are no existing continents which are zonally symmetric as in the model runs. As we are interested in the behavior of the zonal mean circulation, this requires that the majority of the circulation in the three-dimensional runs revert to a monsoon regime, so that small longitudinally-isolated disturbances are not considered monsoonal.

Chapter 2

Model

All model runs were done using the MIT atmospheric general circulation model. The model was run in an channel between 60N and 60S, with varied meridional resolution, and 40 vertical levels at 25 mb intervals between 1000 mb and 25 mb. The channel had free-slip sides, and flow was not allowed through the sides. Runs were made with a timestep of 5 minutes for both dynamics and physics calculations. Topology is not yet available for the atmospheric mode of the MITGCM, so all runs were made with no orography. The land surface was taken to be on the 1000 mb pressure surface.

The dynamical kernel of the MITGCM is described in Marshall et al. (1997b) and Marshall et al. (1997a). In atmospheric mode, the dynamics were coupled to a single-column physics package, important aspects of which are described here.

2.1 Radiation

Instead of using the built-in radiation package from the MITGCM, the atmosphere underwent Newtonian cooling to a specified vertical temperature profile. This was done to exclude any possible radiative feedbacks and to save considerably on computational time. The radiative timescale was set to be 60 days. The vertical temperature profile was varied between runs, and is described in later sections.

2.2 Convection

The convection scheme used in the atmospheric physics package was developed by Emanuel (1991) and later refined by Emanuel and Živković Rothman (1999). The convection scheme has been tuned to data from the Intensive Flux Array of the Tropical Ocean Global Atmosphere Coupled Ocean-Atmosphere Response Experiment, but has not yet been extensively tested in general circulation models.

2.3 Boundary Layer

The height of the momentum boundary layer was set to be constant for all locations, with a depth of either 100 mb or 200 mb. The rationale for choosing this boundary layer thickness will be discussed in detail in the next chapter. The vertically averaged momentum was calculated over the depth of the boundary layer in each column, and the momentum at each level within the boundary layer was relaxed to this average value to emulate mixing. At the lowest model level, there was also a momentum tendency term due to turbulent surface fluxes, of the form

$$\vec{F}_s = \frac{-g\rho_s c_D \vec{u}_s v_s^* L}{dp_s} \tag{2.1}$$

where $\vec{F}_s$ is the momentum tendency, rho_s is the density of the surface air, c_D is the surface drag coefficient, $\vec{u}_s$ is the surface velocity, L is a vertical wind profile coefficient, and dp_s is the pressure difference between the surface and the first model layer. v_s^* is a modified surface velocity, defined as

$$v_s^* = \sqrt{w_D^2 + w_{s0}^2 + v_s^2 + u_s^2} \tag{2.2}$$

where w_{s0} is a minimum surface wind speed, w_D is a convective downdraft velocity scale, and v_s and u_s are the surface meridional and zonal velocities. There was no similar boundary layer mixing for temperature or moisture.

2.4 Surface Physics

The surface physics of the MITGCM has not yet been fully developed. In order to investigate monsoonal dynamics, surface parameterizations for the land were added, and are explained in the following subsections. The physics package includes surface ocean parameterizations with a slab ocean, here taken to have a specified, constant sea surface temperature (SST) profile. The surface fluxes from the land surface are applied to the lowest model layer.

2.4.1 Land Surface Hydrology

The large-scale circulation of the tropical atmosphere is significantly affected by the choice of ground hydrology. The latent heat flux at the surface is strongly dependent on the choice of ground hydrology, and feedbacks between precipitation, evaporation, and the hydrology can strongly affect surface heating of the atmosphere.

A ground hydrology for the modeled land surface was developed with the aim of capturing the aspects of hydrology needed to create a reasonably realistic monsoon circulation over the land with the simplest possible parameterizations. A simple bucket hydrology following that of Manabe (1969) was used over the land surface. With the bucket hydrology, surface evaporation was modified by a factor $\mathcal{B}$

$$\mathcal{B} = \begin{cases} 1 & B \geq 0.75B_0 \\ \frac{B}{0.75B_0} & B < 0.75B_0 \end{cases} \tag{2.3}$$

$$\frac{\partial B}{\partial t} = P - E$$

where B_0 is an assigned bucket depth indicating the amount of moisture that can be stored per unit surface area, B is the current moisture in the bucket per unit area, E is the evaporation rate, and P is the precipitation rate. Any excess moisture gained by precipitation was considered to be runoff, so that the maximum value for B was B_0, and likewise the bucket moisture content was constrained to a minimum value of 0 cm. For all runs, the land was assigned a uniform bucket depth of 20 cm. This type of bucket hydrology has been used extensively in a variety of GCMs and simpler models (ex. Cook and Gnanadesikan (1991), Webster (1983)).

2.4.2 Land Surface Temperature

Although the ocean SST was prescribed in the GCM, the land surface temperature could not be similarly assigned, as high land temperatures coupled with the bucket hydrology can lead to unrealistically high surface evaporation and extreme convection. Instead, the land surface temperature, T_s, was determined interactively with the sensible and latent heat fluxes at the surface. The land surface temperature in GCMs is often determined by a balance of incoming and outgoing radiative fluxes, as well as latent and sensible heat fluxes. However, as our intention was to use a very simple model of the land processes, we chose not to use radiation in order to isolate other feedbacks without complications due to radiative effects. The surface temperature was instead relaxed back to a specified temperature profile, and was only modified by the sensible and latent heat fluxes at the surface. To maintain simplicity, the land was assumed to have zero heat capacity. The balance equation for the land surface temperature was given by

$$T_s = T_r - \frac{1}{A}(SHF + LHF) \tag{2.4}$$

where T_r is the specified relaxation temperature field, SHF and LHF are the sensible and latent heat fluxes from the surface to the atmosphere, and A is a parameter representing the ratio of the soil heat capacity to the relaxation timescale, set to a value of 10 for all runs. A was chosen by performing several different GCM runs to determine a value which resulted in realistic changes to both the land surface temperature and the latent heat flux after onset of precipitation over the land.

The evaporation over the continent, and thus the latent heat flux at the surface, were dependent on the local moisture content of the buckets. Over the ocean, all buckets were assumed to be completely full. The latent heat flux was given by

$$\begin{aligned} LHF &= 100 L_v \rho_s C_d \mathcal{B} e (v_s^* (q_s - q) - v_s^{'} q') \\ v_s^{'} &= \sqrt{w_D^2 + v_s^2 + u_s^2} \end{aligned} \tag{2.5}$$

where C_d is the surface drag, e is an efficiency factor, $v_s^{'}$ is the perturbation surface wind speed, ρ_s is the air density at the surface, L_v is the latent heat of vaporization at the surface, q_s is the saturated specific humidity at the surface, q is the specific humidity of the air just above the surface, e_s is the saturation vapor pressure, and $q^{'}$ is the turbulent specific humidity perturbation scale.

The sensible heat flux was affected by the surface temperature, but not directly by the hydrology:

$$SHF = 100 \rho_s C_d c_{pp} (v_s^* (T_S - T_{Sa}) - v_s^{'} T^{'}) \tag{2.6}$$

where T_S is the surface temperature, c_{pp} is the heat capacity of moist air at constant pressure, T_{Sa} is the temperature of air at the surface and $T^{'}$ is the turbulent temperature perturbation scale. For all model runs, the land surface drag coefficient was set to be $3.6E-3$ and the ocean surface drag coefficient was set to be $1.2E-3$.

Since the surface temperature and latent and sensible heat fluxes were dependent upon each other, the physics package iteratively determined the three values for each timestep with a Newton-Raphson type calculation. At very hot land surface relaxation temperatures, the intensity of heat fluxes at the surface may become considerably larger than those observed in the real atmosphere.

The interactive land surface temperature was expected to result in various feedbacks of a complicated nature. For instance, high latent heat flux of evaporation of moist buckets will result in a lower surface temperatures, thus discouraging convection. However, the reduced surface temperature also reduces the surface evaporation, which both decreases the amount of moisture available for precipitation and prevents the rapid depletion of bucket moisture content. The interwoven feedbacks of the land surface temperature and hydrology can result in complicated effects on the strength and location of the deep convection, and thus on the large-scale circulation.

The land surface processes tend to self-organize the convection and dynamics, especially at middle and high latitudes. An axisymmetric run was conducted with latitude ranging from 90S to 90N, with 1° meridional resolution, and land conditions with uniform temperature relaxation profile at all surface points. The run was spun up from a resting state

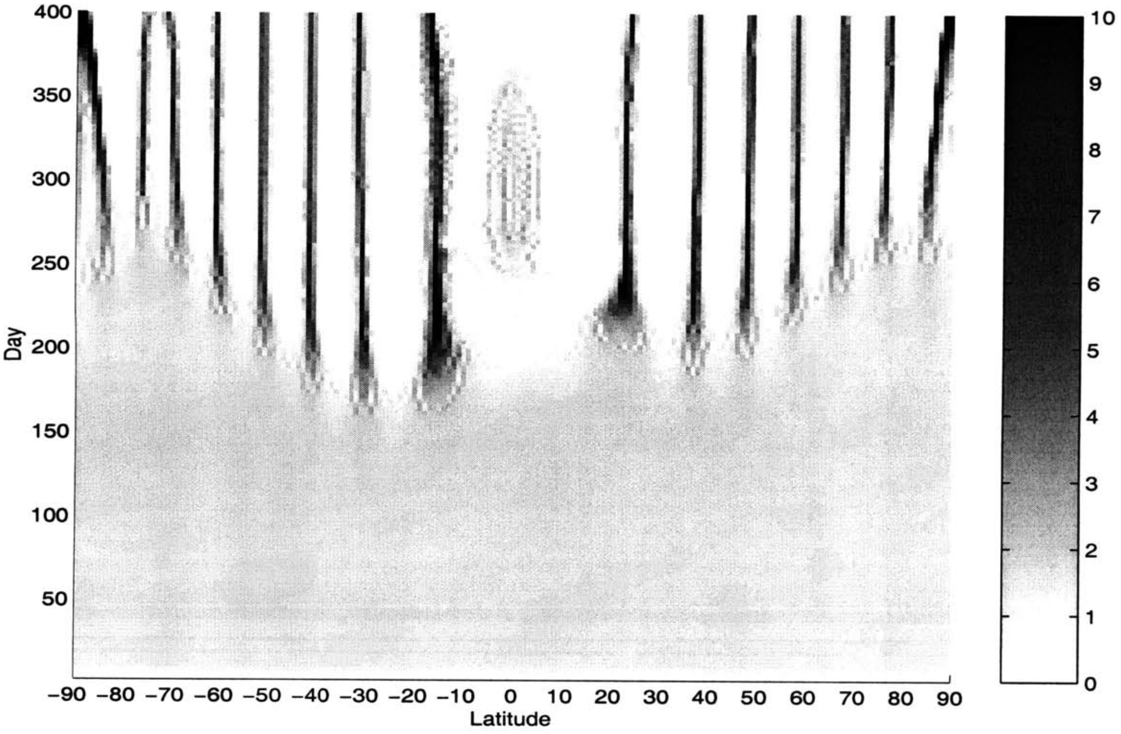

Figure 2-1: Evolution of precipitation field with global continent of uniform surface temperature. Precipitation in mm/day.

with completely dry land. After approximately 100 days, small local variations in the rate of rainfall and evaporation began to organize into alternating regions of excess rainfall and excess evaporation, as seen in Figure 2-1. Under the regions of excess rainfall, the land buckets began to fill, while the buckets under regions of excess evaporation began to empty. The moisture was supplied from the initial moisture of the atmosphere specified at the start of the model run. The convection anomalies were spaced approximately 10 degrees apart, with horizontal width of 1.5°-2°, and were nearly stationary once established. No strong anomalies occurred within 15 degrees of the equator. It seems that this organization was due to feedbacks between the bucket hydrology and the dynamics. The effects of this were seen in many of the model runs, where strong stationary convective anomalies formed over the land in the midlatitudes. However, this type of behavior did not seem to play a significant role the tropical and subtropical regions of the later model runs.

Chapter 3

Axisymmetric Circulations in the MITGCM

3.1 MITGCM Setup

The form of the land surface temperature perturbation is

$$T_s = \begin{cases} T_{sb}(\phi) + T_{es}(\phi) & |\phi - \phi_0| \leq \Delta\phi \\ T_{sb}(\phi) & |\phi - \phi_0| > \Delta\phi \end{cases} \tag{3.1}$$

where T_s is the relaxation surface temperature, T_{sb} is the background surface temperature, T_{es} is a localized temperature perturbation, ϕ_0 is the location of the maximum temperature perturbation, and $\Delta\phi$ is the meridional scale of the perturbation.

As the model includes viscous effects, a meridional circulation is expected to occur even when the regularity condition for the thermal equilibrium solution is not violated. Since we are interested in monsoon-type circulations in the northern hemisphere of our model, the circulation of greatest interest will be one which crosses the equator, with southward flow at upper levels across the equator.

The model was first run for 100 days with the momentum tendency due to pressure set to zero in order to approximate a radiative-convective equilibrium state. The end of the RCE run was then used to initialize a longer run with the full dynamics turned on. The surface temperature perturbation was introduced at the beginning of the RCE model run, and there was precipitation onset over the land surface during the initial spin-up of the model once the dynamics were turned on. This may predispose the circulation towards a monsoon state by wetting the land surface.

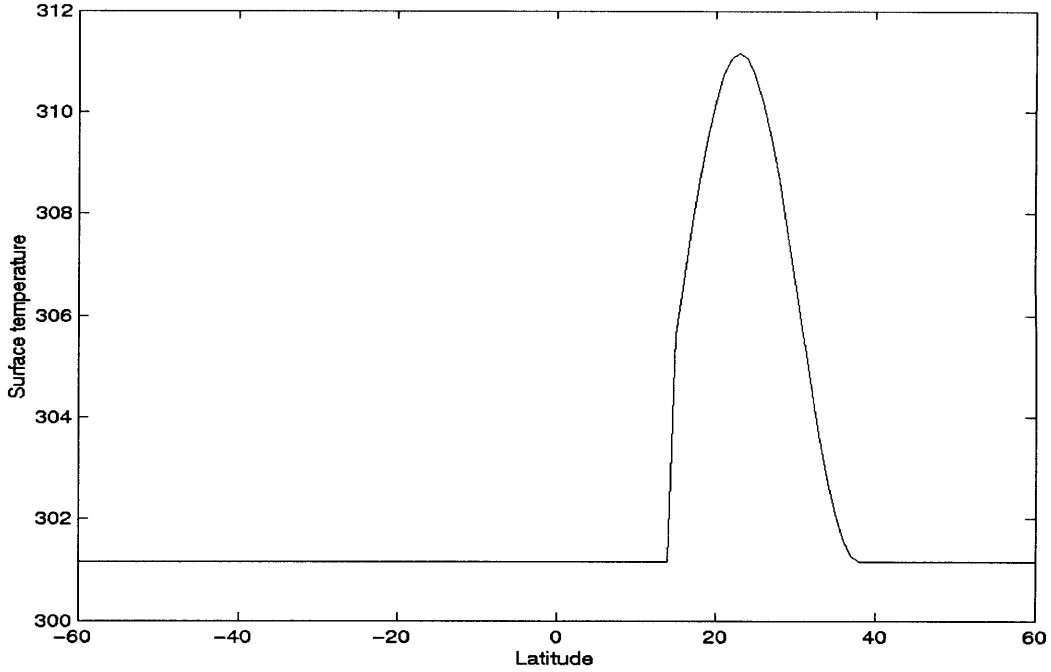

Figure 3-1: Surface temperature relaxation profile for Case 1, example with ΔT of 10K. Land/sea boundary is located at 15N.

3.2 Case 1: Uniform Background Temperature

A reasonable first step in investigating cross-equatorial monsoon circulations is to perform a set of experiments similar to that of Plumb and Hou (1992) and Zheng (1998), with a subtropical heat source against a uniform background temperature field. Thus, the surface background temperature profile in (3.1) for the first set of runs was given by

$$T_{sb}(\phi) = \overline{T_{sb}}$$

The localized land relaxation temperature perturbation was given by

$$T_{es} = \Delta T \, cos^2\left(\frac{\pi}{2}\frac{\phi - \phi_0}{\Delta\phi}\right) \tag{3.2}$$

where ΔT is the maximum strength of the localized surface temperature perturbation. ϕ_0 was chosen to be 23N, and $\Delta\phi$ was taken to be 15° for all Case 1 runs. An example of the meridional surface temperature relaxation profile for the first set of axisymmetric runs is seen in Figure 3-1. The momentum boundary layer was set to a constant depth of 100 mb. The radiative equilibrium temperature profile was set to be 200 K above 500 mb and increased linearly with pressure below 500 mb to 260K at the surface. The minimum surface

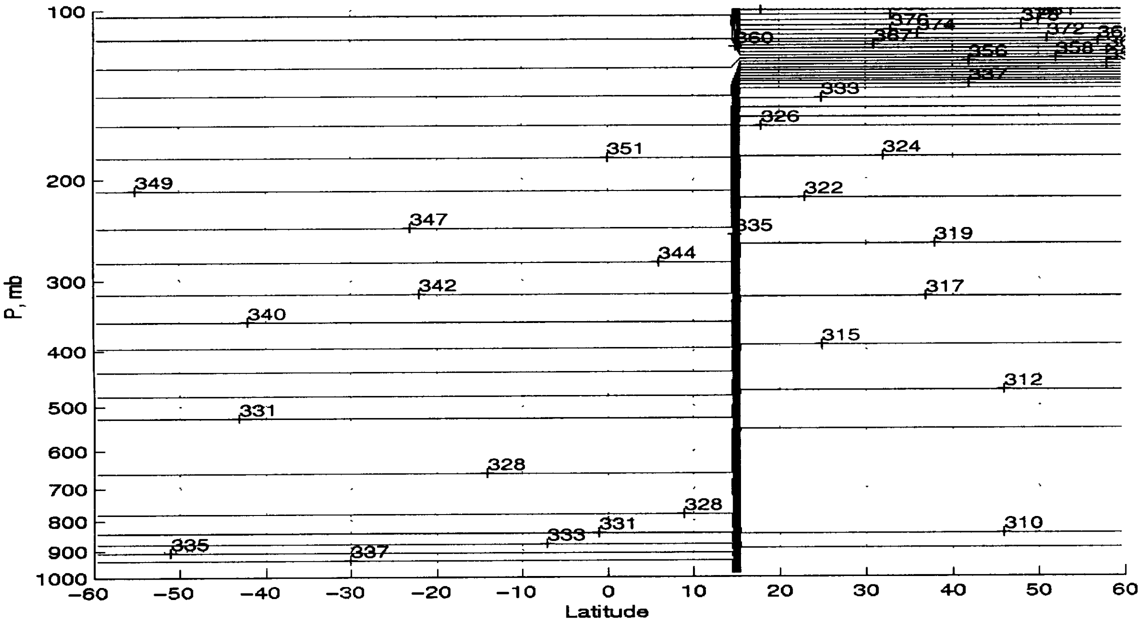

Figure 3-2: Equivalent potential temperature, Θ_e for RCE state with $\Delta T = 0K$

wind speed was set to 2 m/s, and the winds were set to be uniform from lowest model layer to the surface. The model was run with full dynamics for at least 200 days, and a steady state was usually reached within 100 days. All Case 1 runs were made with 1° meridional resolution.

This simple setup excludes complicating effects such as Hadley cells which might compete with the monsoon circulation, and allows us to compare results directly with those of Plumb and Hou (1992) and Zheng (1998). Numerous model runs were run with $\overline{T_{sb}}$ set to 301.15K, and with varying land surface perturbation temperature forcings (i.e., different values of ΔT in (3.2)).

The inclusion of a continent in our model greatly complicates the moist dynamics. The continent is very dry overall, especially in the subtropics, so that the equivalent potential temperature of the radiative convective equilibrium state over the dry land surface is lower than that over the oceans for the same surface temperature, as illustrated in Figure 3-2. The tropopause is clearly lower over the land surface than over the ocean, occurring near 150 mb over the land but above 100 mb elsewhere. The temperature difference is especially large in the upper troposphere, as the air over the dry land surface will tend toward a dry adiabat in RCE, while the air over the ocean will tend toward a moist adiabat. As the land surface temperature is increased, the effects of the surface heating are restrained to the lower levels of the atmosphere while the land remains dry. Thus, even when the land

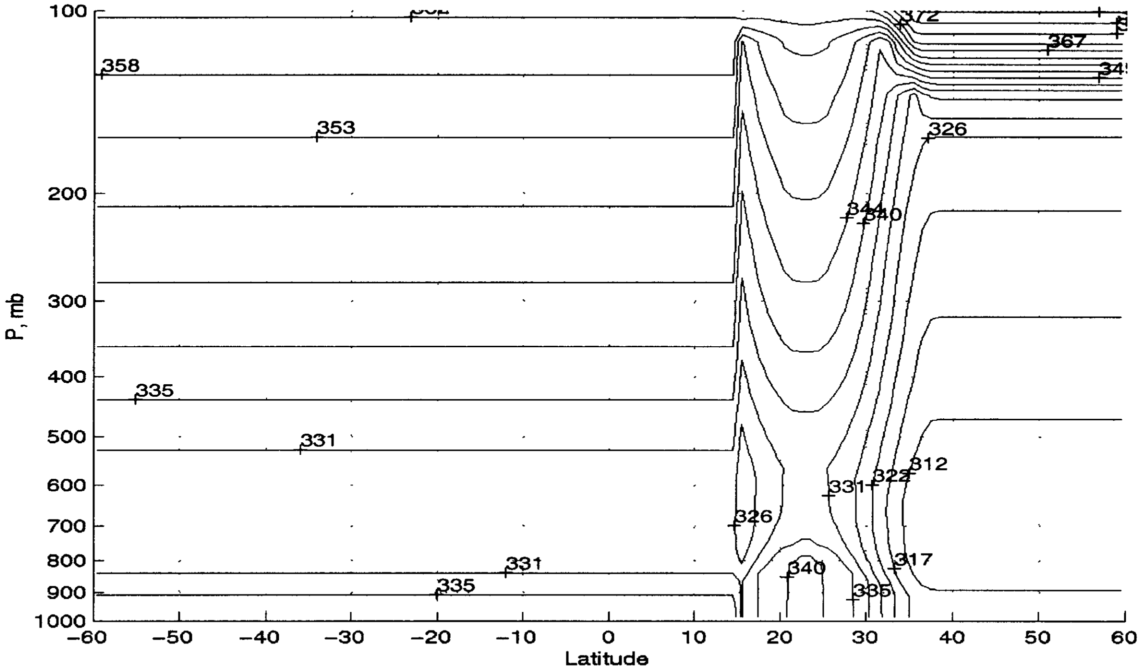

Figure 3-3: Equivalent potential temperature, Θ_e for RCE state with $\Delta T = 23K$

surface temperature is very warm, it is possible for the large-scale meridional gradient of temperature to be positive (increasing northwards) at lower levels, but negative in the upper troposphere, an example of which is shown in Figure 3-3. There is also a sharp discontinuity in temperature at the land-ocean boundary in the RCE state. In order for the temperature maximum to occur over land in the upper troposphere, deep convection must be sustained over the warm, moist land surface. To achieve this, a source of moisture over the land surface is needed; this may be provided by advection of moisture over the land from the ocean and by wetting of the buckets

One of the objectives of this work is to evaluate the applicability of the axisymmetric theory of Plumb and Hou (1992), Emanuel (1995), and Zheng (1998) to more complex flows. Case 1 of the axisymmetric runs is most similar to the model tests in Plumb and Hou (1992) and Zheng (1998), and these offer the clearest comparison. The maximum absolute strength of the upper tropospheric streamfunction for the cross-equatorial monsoon circulation is calculated for the last 50 days of each model run, and plotted against the magnitude of the land surface temperature forcing (ΔT) with triangles in Figure 3-4. There clearly seems to be a threshold in the strength of the circulation at ΔT = 29K, separating two different flow regimes. When the forcing is too weak ($\Delta T < 29K$), there is no steady monsoon circulation, and little or no precipitation over the land surface, as seen in Figure

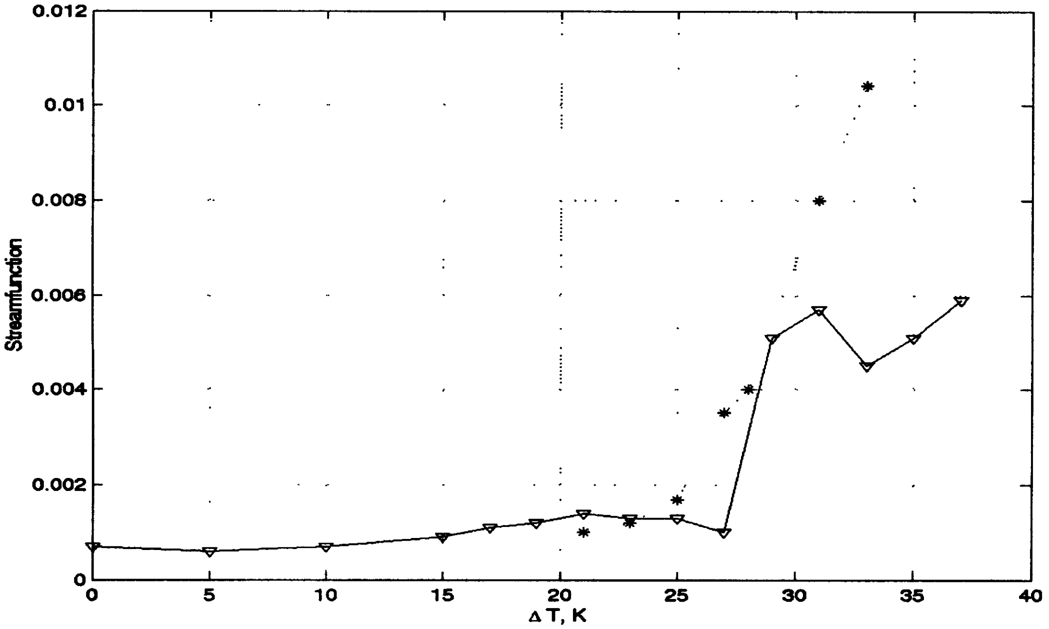

Figure 3-4: Maximum absolute streamfunction for cross-equatorial cell (Pa/s). Solid line with triangles indicates 'free' bucket hydrology, asterisks denote fixed moist bucket results.

3-5f. In these cases, the 'summer' circulation cell over the land is dominant, and the ascent region of the circulation is located over the ocean surface near the coast. Since the SST is set to a uniform temperature, so long as the deep convection and ascent region of the circulation is located over the ocean, we expect there to be little variation in the strength of this circulation. As the land surface temperature forcing is increased, a region of negative streamfunction begins to form in the upper troposphere to the south of the region of deep convection. This upper level circulation seems to be AMC, but is not strong enough to distort the momentum contours significantly, and is thus restricted to a narrow region near the equator, where the gradient of M is small. The M contours are primarily distorted in a small region near the coastline where there is a strong thermally-balanced jet, seen in Figure 3-6c and 3-6e.

In the monsoonal regime, for $\Delta T \geq 29K$, the behavior is quite different, as shown in Figure 3-7. The cross-equatorial circulation cell becomes much stronger, and considerably broader as well. The region of ascent and deep convection occurs over the land surface, with high precipitation rates there. The exact location of the deep convection is dictated by the land surface parameterizations and the location of the wetted buckets. As these circulations tend to 'jump' aloft across the equator when returning northward, very little moisture is advected from the ocean surface onto the land, so that the majority of the moisture for the deep convection over the land surface is supplied by evaporation from the nearby land surface. When the land surface temperature forcing is increased, deep convection and the region of wetted buckets moves northward until balanced evaporation and precipitation rates are established over the continent. The strength of the monsoon circulation cell does not continue to increase with increasing surface temperature forcing, but instead remains roughly constant. As the region of deep convection is pushed further north, the land surface temperature at the location of the monsoon does not increase appreciably with increasing ΔT. Although the circulation cell may become wider as the region of ascent moves further north, the area of subsidence does not increase very much, due to the 'jumping' of the circulation. Thus, the strength of the ascending branch of the circulation cell does not increase with increasing ΔT. The cross-equatorial circulation is nearly AMC, as seen in Figure 3-7. The M-contours are now significantly deformed in both hemispheres.

In order to elucidate the effects of the land surface parameterization on the behavior of the large-scale circulation, we perform several runs at various ΔT, but with the bucket moisture near the coast set to a specified, constant moisture content. At 18N, the buckets were assigned to be full, while the buckets at 17N and 19N were set to have a moisture content of 7.5 cm, and all other land buckets were allowed to change freely as in previous runs. The resulting circulation cells for these 'fixed moist bucket' runs have their region of ascent and deep convection located over the land near the coast, and the deep convection does not move northward with increasing ΔT. The maximum upper-tropospheric streamfunction of the cross-equatorial circulation cells for these fixed moist bucket runs are shown as asterisks in Figure 3-4. The fixed moist bucket runs have a more gradual transition into the monsoonal regime than the 'free' bucket runs, and the monsoon circulation continues to increase in strength with increasing land surface temperature forcing. This behavior is similar to that found by Plumb and Hou (1992) and Zheng (1998), with the threshold occurring around $\Delta T = 26K$.

There appear to be three different regimes of dynamical behavior for Case 1. In the first regime, for $\Delta T \leq 25K$, the land surface temperature forcing is too weak to induce an upper-tropospheric temperature maximum, even when deep convection occurs over the land. Even though the land surface temperature forcing may seem to be very large, the intense evaporation which occurs in the presence of wetted buckets severely reduces the actual surface temperature. A cross-equatorial monsoonal circulation does not occur in this regime. In the second regime, where $27K < \Delta T < 29K$, deep convection over the warmed land surface can result in a cross-equatorial monsoon circulation, but the land surface parameterizations cannot reach an equilibrium state. A steady monsoon will only attain if the buckets are forced to remain moist. In the third regime, for $\Delta T \geq 29K$, the cross-equatorial monsoon circulation is viable for both free and fixed bucket moisture, but the land hydrology selects the location and strength of the circulation. The effect of the land

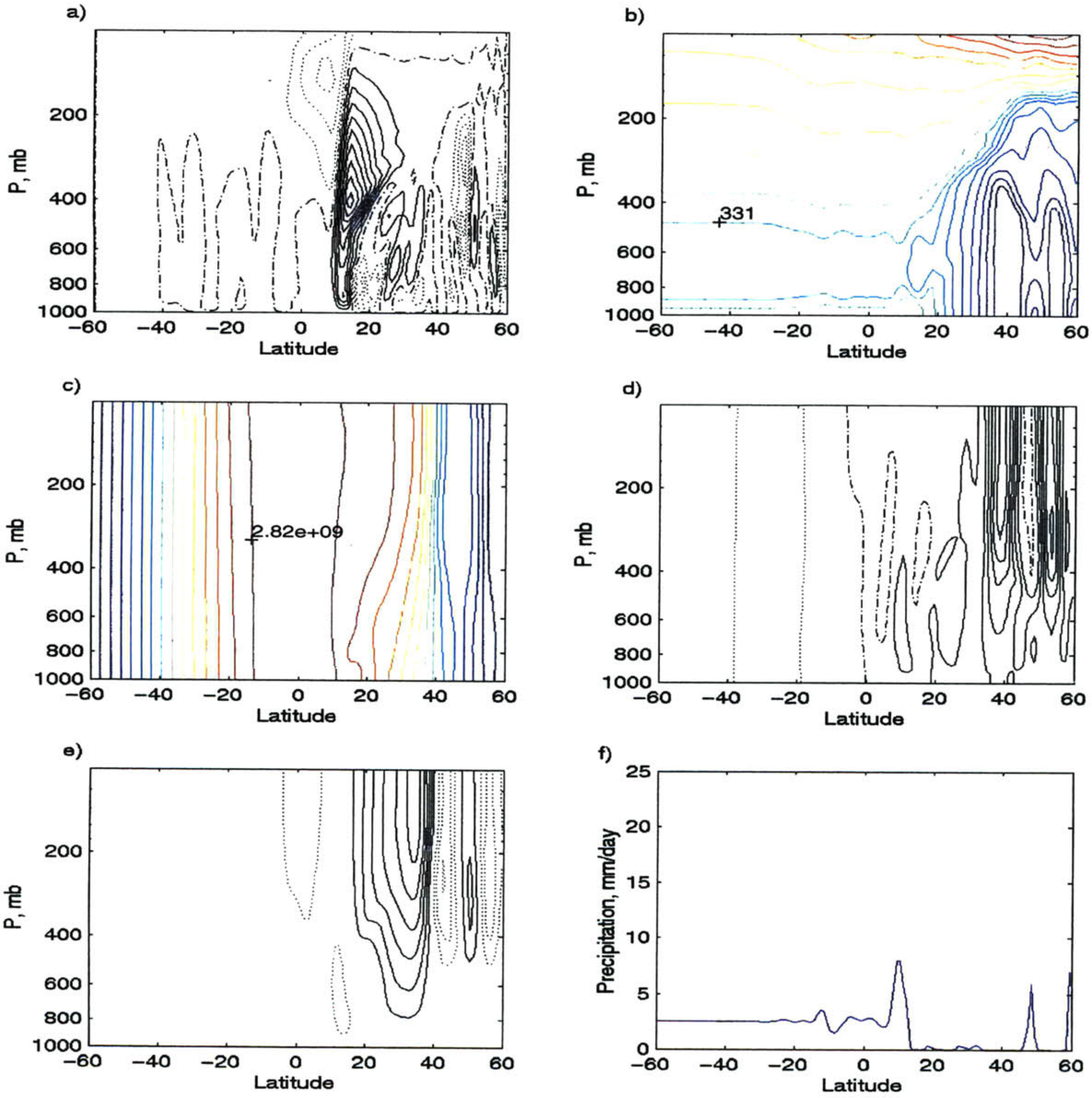

Figure 3-5: Model results for Case 1 with $\Delta T = 23K$, all fields averaged over days 150-200. Solid lines indicate positive contours, dotted lines indicate negative contours, zero contour in dash-dots. a) Streamfunction, contour interval 1.0E10 kg/s; b) Θ_e, contour interval 5 K; c) M, contour interval 1.5E8 m^2/s; d) absolute vorticity, ζ_a, contour interval 4.5E-5 1/s ; e) zonal wind u, contour interval 13 m/s; f) precipitation, mm/day.

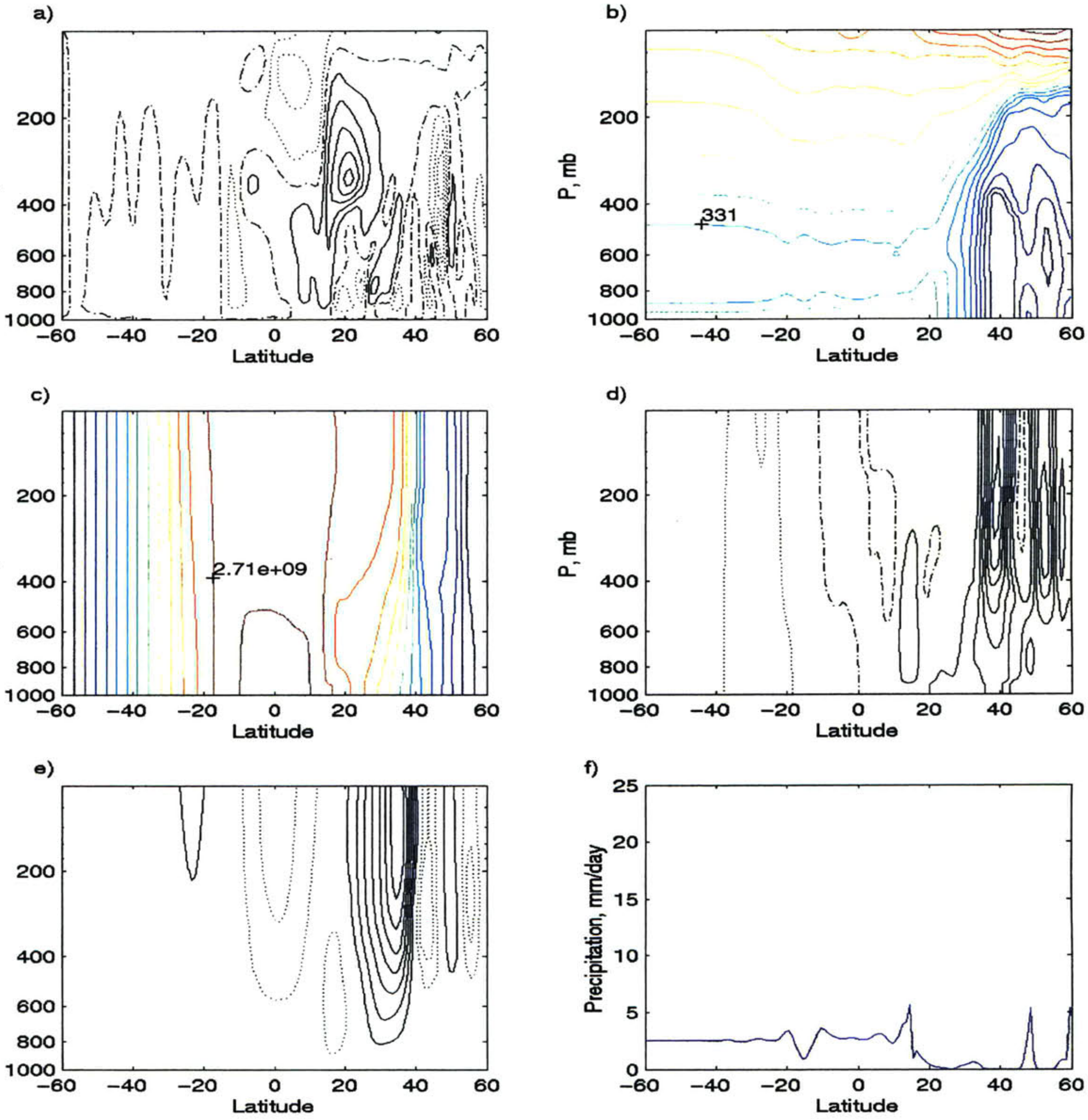

Figure 3-6: Model results for Case 1 with $\Delta T = 27K$, all fields averaged over days 150-200. Solid lines indicate positive contours, dotted lines indicate negative contours, zero contour in dash-dots. a) Streamfunction, contour interval 1.0E10 kg/s; b) Θ_e, contour interval 5 K; c) M, contour interval 1.5E8 m^2/s; d) absolute vorticity, ζ_a, contour interval 4.5E-5 1/s ; e) zonal wind u, contour interval 13 m/s; f) precipitation, mm/day.

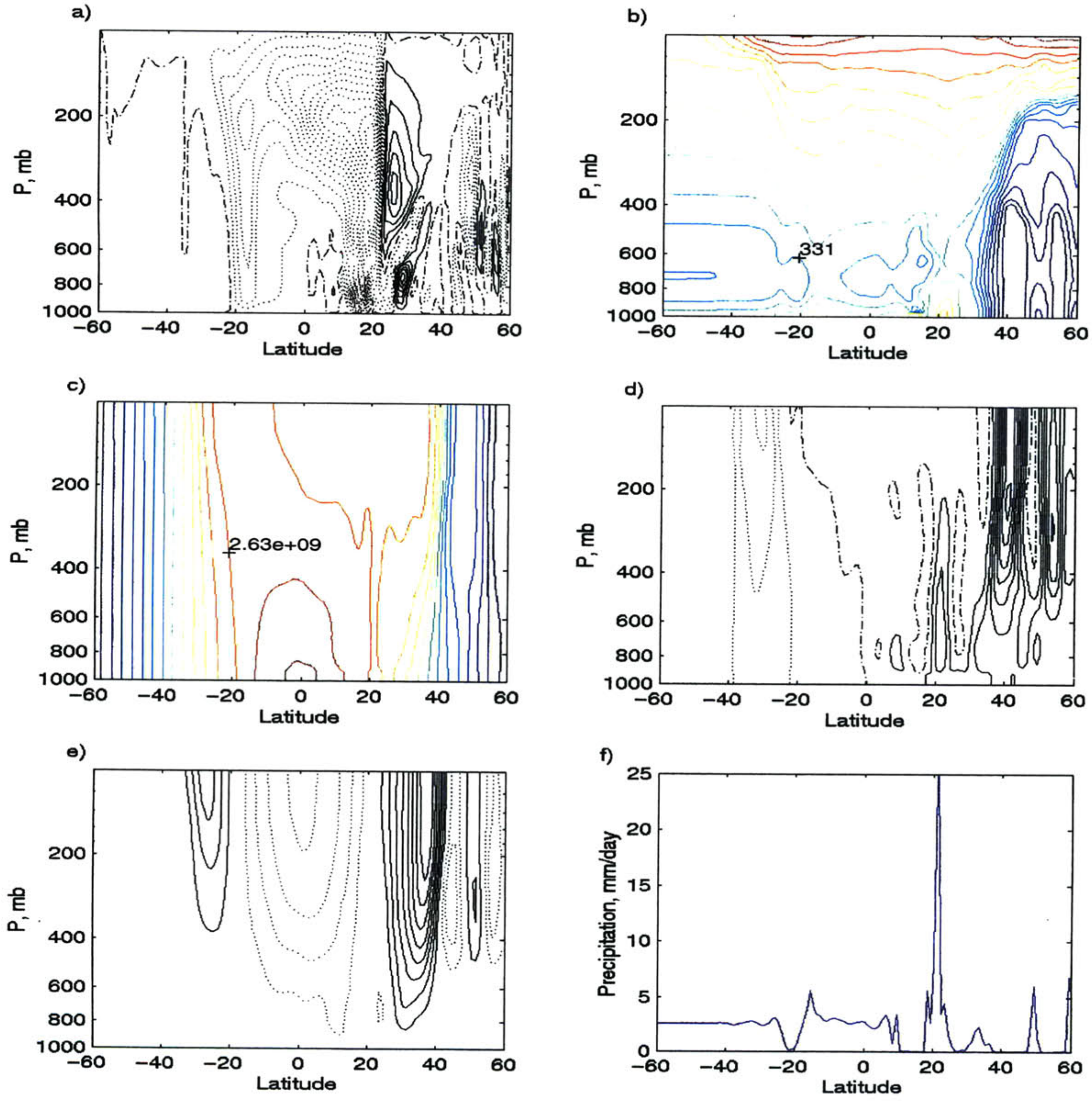

Figure 3-7: Model results for Case 1 with $\Delta T = 31K$, all fields averaged over days 150-200. Solid lines indicate positive contours, dotted lines indicate negative contours, zero contour in dash-dots. a) Streamfunction, contour interval 1.0E10 kg/s; b) Θ_e, contour interval 5 K; c) M, contour interval 1.5E8 m^2/s; d) absolute vorticity, ζ_a, contour interval 4.5E-5 1/s ; e) zonal wind u, contour interval 13 m/s; f) precipitation, mm/day.

surface parameterizations on the monsoon dynamics seems to be to sharpen the nature of the threshold behavior, and to limit the strength of the monsoon circulation to two different plateaus.

With a uniform SST profile, the northward return flow of any cross-equatorial cells has a tendency to conserve angular momentum, following M-contours aloft over the equator before returning to the boundary layer in the northern hemisphere. This type of behavior is also seen in the circulation acquired by Zheng (1998), and to a lesser extent in Plumb and Hou (1992), where the streamfunction appears to 'jump' over the equator. In the MITGCM, the circulation tends to rise very high - to a height of nearly 300 mb - losing much of its moisture in the process. The flow does not approach the boundary layer in the northern hemisphere until it has moved northward over the land surface, and thus there is no moisture supply from the ocean to feed monsoonal convection and precipitation over the continent. The only moisture supply for the monsoon is from the wetted buckets, which gain moisture during spin-up, so that the bucket hydrology strictly controls the monsoon behavior.

Why does the circulation tend to jump over the equator? This question is extensively addressed by Pauluis (2001); a synopsis will be given here. In an axisymmetric model, cross-equatorial flow can occur either as angular momentum conserving flow in the nearly inviscid free troposphere, or as flow through the mixed layer where surface drag and turbulent mixing allows the flow to cross M-contours. In the absence of a meridional temperature gradient in the equatorial region and with easterlies in the free troposphere, a pressure minimum occurs at the equator. The trough is in geostrophic balance with the easterlies, but the pressure minimum is generally weak due to the small Coriolis parameter. As there are easterlies in the free troposphere just above the top of the mixed layer, the Ekman transport within the mixed layer will be equatorward in both hemispheres. Thus, a southerly (equatorward) flow in the southern hemisphere will be unable to cross the equator in the mixed layer, and will instead ascend into the free troposphere near the equator. The flow can then cross the equator along M-contours, and may become westerly as it moves northward in the northern hemisphere. This westerly flow induces a poleward Ekman transport in the mixed layer, and the flow is able to return to the mixed layer as it continues northward. In order for the flow to cross the equator while remaining within the mixed layer, there must be a meridional temperature gradient of a minimum strength, which can depend on boundary layer parameterizations of drag, turbulent mixing, and the depth of the mixed layer. If the mixed layer is not sufficiently deep, a considerable fraction of the low-level circulation may ascend to the free troposphere and 'jump' over the equator even in the presence of a meridional temperature gradient, as illustrated in Figure 1 of Pauluis (2001). This is why a depth of 200 mb has been chosen for the momentum boundary layer in our subsequent axisymmetric model runs.

3.3 Case 2: Meridionally Varying Background Temperature

A second set of axisymmetric runs was done with a more realistic background surface temperature profile. The sea surface temperature over the ocean was given by

$$T_{sb} = 301.15 - 28\,sin^2\left(\frac{\pi}{180}(\phi - \phi_{SST})\right)$$

where the SST maximum was at $\phi_{SST} = 8$N. This was chosen to mimic the actual SST profile during the summer in the northern hemisphere in the vicinity of the Asian monsoon. The background land surface temperature was similarly given by

$$T_{sb} = 301.15 - 28sin^2\left(\frac{\pi}{180}(\phi - \phi_{land})\right)$$

but the location of the land temperature maximum was instead set to be $\phi_{land} = 18$N. The land surface temperature perturbation was given by

$$T_{es} = \begin{cases} \Delta T & \phi < \phi_0 \\ \Delta T\,cos^2\left\{\frac{\pi}{2}\left(\frac{\phi-\phi_0}{\Delta\phi}\right)\right\}; & \phi_0 < \phi < (\phi_0 + \Delta\phi) \\ 0 & otherwise \end{cases}$$

where ϕ_0 was chosen to be 20N, and $\Delta\phi$ was 15°. A schematic of the relaxation surface temperature distribution is shown in Figure 3-8. The momentum boundary layer was set to a uniform depth of 200 mb. The radiative equilibrium temperature profile was set to be 200K at all altitudes in order to give stronger circulations than those achieved in the Case 1 runs. The minimum surface wind speed, w_{s0} in Equation 2.2, was increased to 4 m/s, and the winds in the lowest model layer were assumed to have a logarithmic profile in an effort to strengthen the circulation and thus induce low-level cross-equatorial flow. The full-dynamics runs were made for 300 days from the end of the RCE run.

Unlike Case 1, the cross-equatorial circulations of Case 2 predominantly remain in the mixed layer while traveling northward across the equator, and can thus transport moisture to the continent. Three different runs with ΔT = 25K, 30K, and 35K were performed so that monsoonal and non-monsoonal circulations could be compared. Several different meridional resolutions were used with each choice of ΔT.

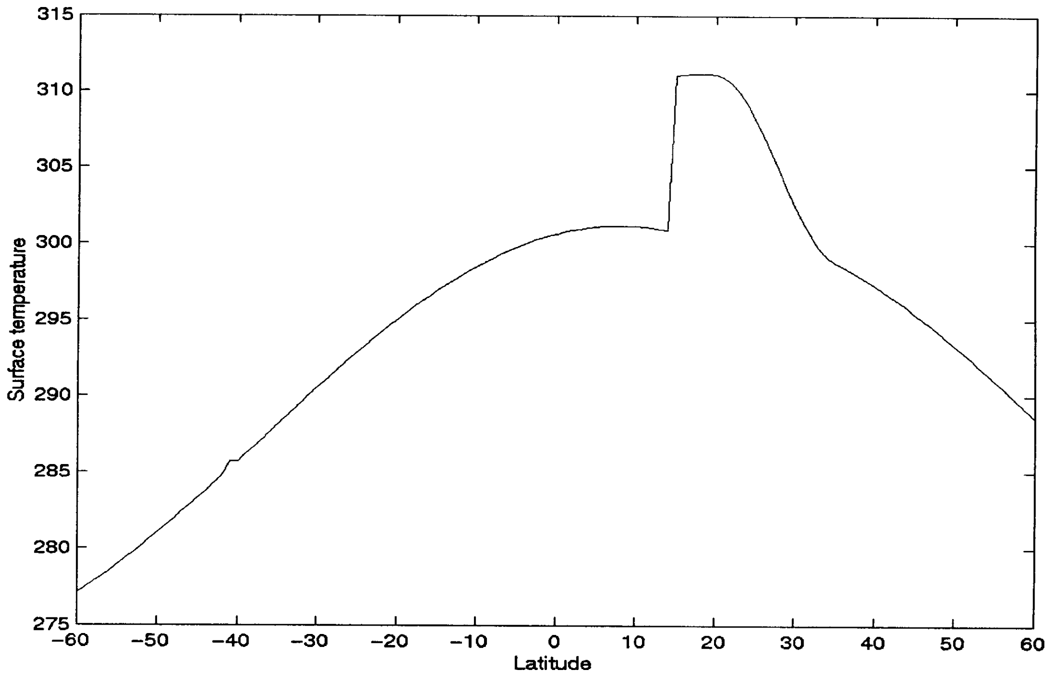

Figure 3-8: Surface temperature relaxation profile for Case 2, example with $\Delta T = 10$K. Land/sea boundary at 15N.

3.3.1 $\Delta T = 25$K

The $\Delta T = 25$K run is non-monsoonal in nature. The 'winter' cross-equatorial Hadley cell has a broad region of ascent and moderate precipitation over the ocean surface, and a weaker 'summer' cell is present to the north.

The 1° resolution run for $\Delta T = 25$K shows fine structure in the circulation and convection, as seen in Figure 3-9. A very intense, narrow region of deep convection associated with the ascent region of the summer cell is located between 10N and 15N. This region is also home to a low-level local intense easterly jet in thermal balance with the lower tropospheric temperature maximum over the continent. These easterlies penetrate to the surface, so that the surface winds reach a local maximum between 10N and 15N, increasing the latent heat flux at the surface considerably, and leading to the intense deep convection. The near-surface θ_e peaks just south of the land-sea boundary, near 13N, and steeply falls off to the north. The land surface temperature near the heated coast is reduced to slightly more than 315K by a sensible heat flux of approximately 100 W/m^2. The surface air temperature has a maximum of 310K near 23N.

The low-level, intense dry circulations which are seen over the land surface between 15N and 40N are highly transient in nature, and are tilted in the vertical along M-contours.

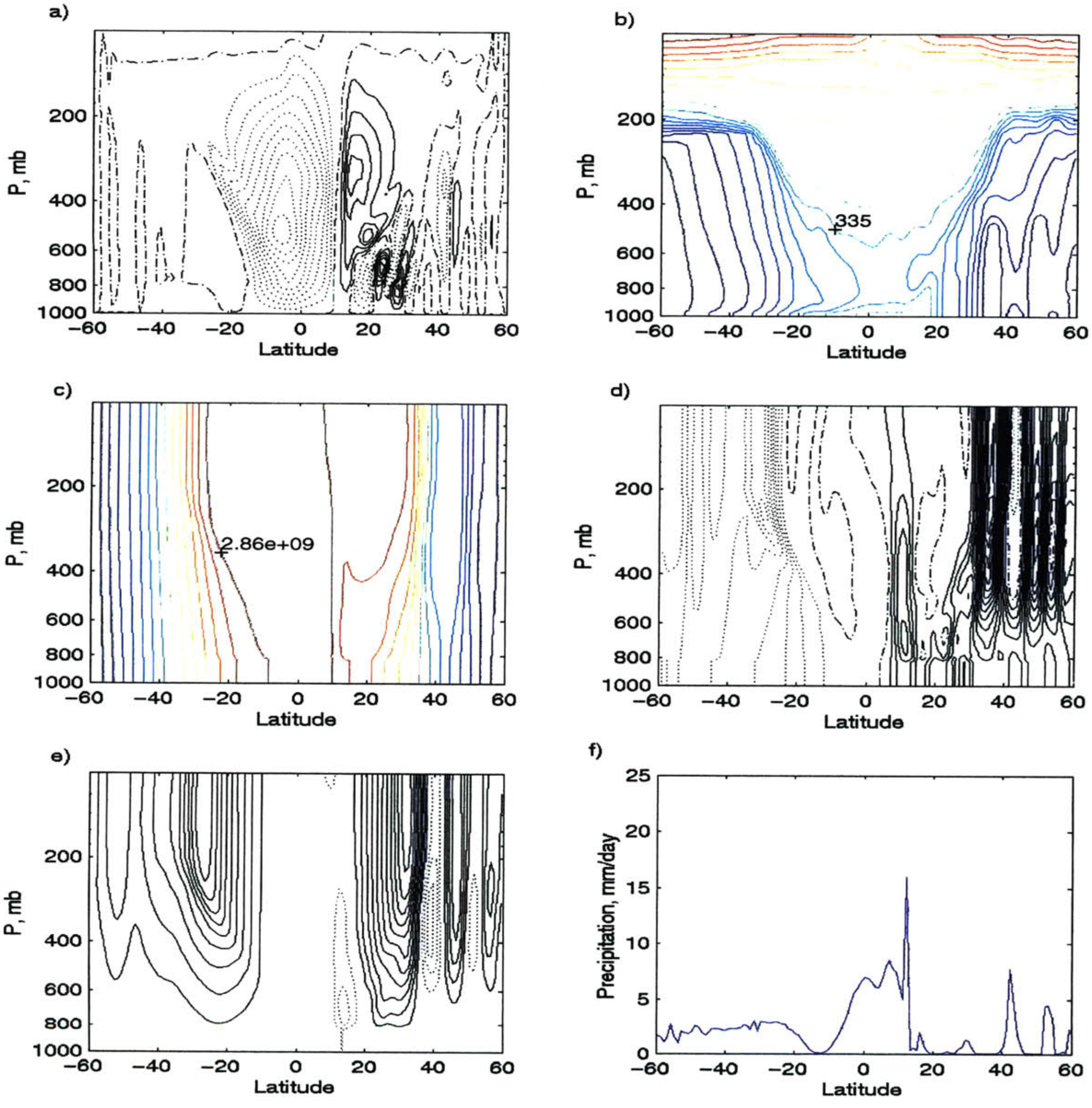

Figure 3-9: Model results for Case 2 with $\Delta T = 25K$ with 1° resolution, all fields averaged over days 200-300. Solid lines indicate positive contours, dotted lines indicate negative contours, zero contour in dash-dots. a) Streamfunction, contour interval 2.0E10 kg/s; b) θ_e, contour interval 6 K; c) M, contour interval 1.5E8 m^2/s; d) absolute vorticity, ζ_a, contour interval 2.0E-5 1/s ; e) zonal wind u, contour interval 9.0 m/s; f) precipitation, mm/day.

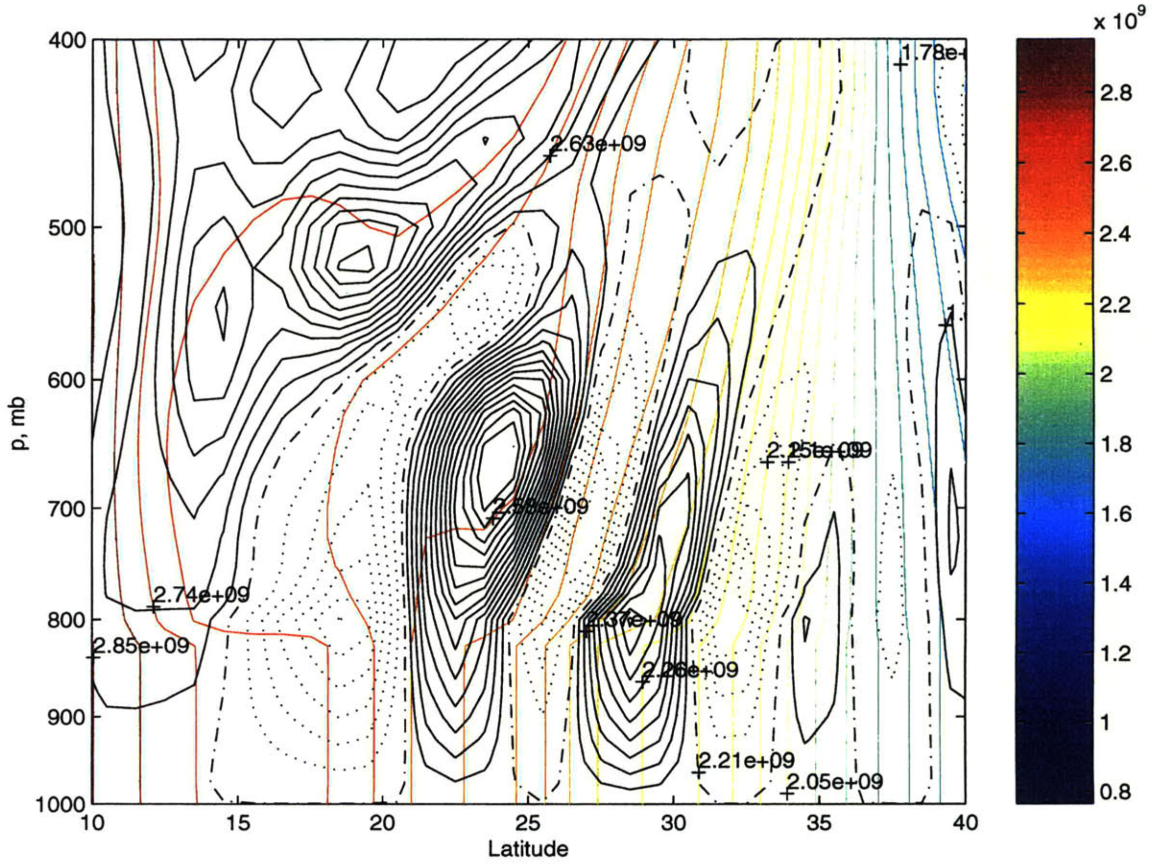

Figure 3-10: Streamfunction (solid and dotted black lines) and M (color lines), average of days 297.5 to 300 of the Case 2 $\Delta T = 25K$ run.

These disturbances are characteristic of symmetric instability, and θ_v is nearly constant with height in this region. These circulations seem to interfere with the lower portion of the 'summer' Hadley cell, which is confined to the middle and upper troposphere over the land surface.

Decreasing the meridional resolution to 2° does not significantly alter the strength or location of the large scale meridional circulations. The convection associated with the ascent of both the 'summer' and 'winter' Hadley cells merges into a strong, deep convective region between 5N and 10N, where the SST peaks. There is a broad local precipitation maximum near the equator associated with ascent in the 'winter' cell. The narrow region of strong low-level easterlies which was present in the 1° run between 10N and 15N is considerably weaker, and the θ_e maximum is weaker but still located around 13N. The low-level, dry circulations over the land surface are less intense and localized than in the 1° case, which can be expected due to the blurring of features with the reduced resolution.

Similarly, running the $\Delta T = 25$K case with 3° resolution tends to broaden the convective regions even more, as seen in Figure 3-11. The 'winter' meridional cell is slightly wider latitudinally than in the higher resolution cases, reaching from 15S to 15N at lower levels, but the strength of the circulation is not significantly different. The low-level disturbances seen over the warm land surface in the higher resolution runs are almost completely absent, and are presumably too meridionally narrow to be captured at this low resolution. The effects of these disturbances on the large-scale circulation can be seen by comparing the summer Hadley cells in the 1° and 3° cases. In the high resolution cases, the summer Hadley cell slants upward and poleward near the surface, as the low-level disturbances seem to eat away at the base of the circulation. In the low resolution case, however, the summer Hadley cell does not have this slant, and reaches low levels more easily.

Another effect of the dry low-level disturbances is to carry warm air above the boundary layer over the land surface near the coastline. Thus, in the high resolution runs, a strong low-level easterly jet forms in thermal wind balance along the coast, with very warm air poleward over the land. In the low resolution runs, the ascent region of the cross-equatorial circulation occurs further to the north than in the high resolution runs, and weak, low-level westerlies form near 10N as equatorial air is carried to the north. There is only weak easterly shear in the low-level free troposphere at 10N, due to very weak positive poleward temperature gradient. As the low-level disturbances are not present in the low-resolution runs, and the Hadley subsidence region reaches down to the boundary layer over the coastline, the temperature maximum caused by the heated land surface does not penetrate much above the top of the boundary layer, and the easterly jet present in the high resolution runs is lost. The near-surface θ_e peak is still near 13N, but the sharp nature of the peak in the higher resolution runs has been smeared out in the 3° run. The broad precipitation maximum, which is centered near 10N, tapers off rapidly over land, with significant rainfall confined to within 5° of the coast.

The lower troposphere near the coastline shows the possibility of baroclinic instability. In the high resolution runs, the northward gradient of Ertel's potential vorticity is negative in the subtropics in the lower troposphere, while the low-level θ gradient is positive with a maximum near 20N. As there is easterly shear in this region for the high resolution runs, baroclinic instability may be possible. This is very similar to the pre-onset conditions found by Xie and Saiki (1999). There are also reversals of PV gradient along θ_v surfaces in the subtropics in both high and low resolution runs. In the midlatitudes, positive northward PV gradients throughout the lower and middle troposphere coupled with westerly shear and negative northward surface θ gradient indicate a second region of potentially unstable flow. The lower resolution cases may be barotropically unstable, as the meridional gradient of absolute vorticity is negative between 10N and 15-20N in the 2° run from 800 mb upward, and from 500 mb upward in the 3° resolution run.

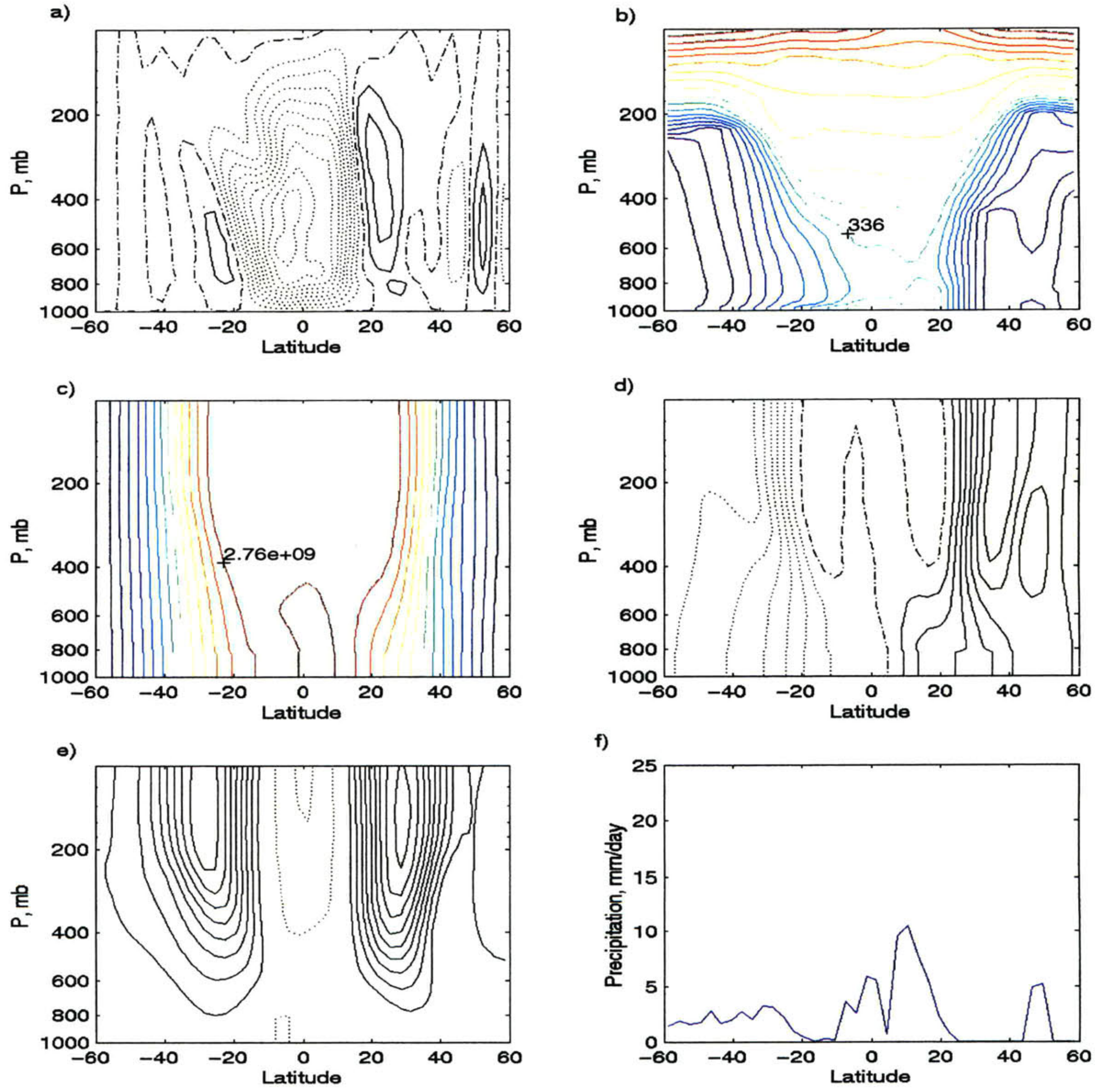

Figure 3-11: Model results for Case 2 with $\Delta T = 25K$ with 3° resolution, all fields averaged over days 200-300. Solid lines indicate positive contours, dotted lines indicate negative contours, zero contour in dash-dots. a) Streamfunction, contour interval 2.0E10 kg/s; b) θ_e, contour interval 6 K; c) M, contour interval 1.5E8 m^2/s; d) absolute vorticity, ζ_a, contour interval 2.0E-5 1/s ; e) zonal wind u, contour interval 9.0 m/s; f) precipitation, mm/day.

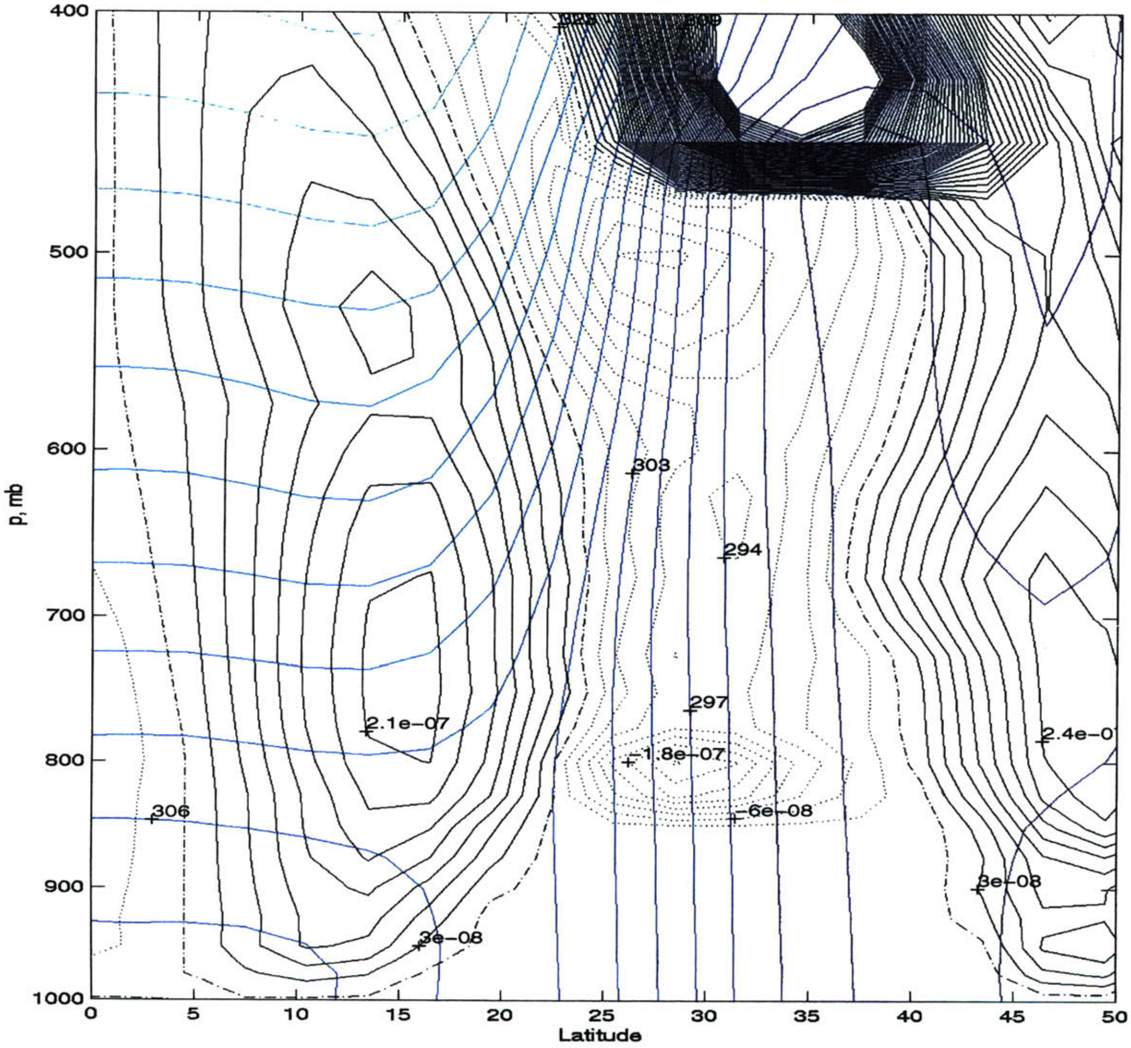

Figure 3-12: Zonal mean Ertel's PV, contour interval 3E-8, solid black lines indicate positive values, dotted indicate negative values. Zonal mean θ_v, contour interval 2K, color lines. ΔT of 25K, 3° resolution.

3.3.2 ΔT = 30K

The 1° meridional resolution case with ΔT = 30K shares several characteristics with the ΔT = 25K at case the same resolution: the width and strength of the 'winter' cell; the presence of low-level disturbances over the warmed land surface; the locations and intensities of deep convection regions at 13N, 5N-10N, and near the equator. The near-surface θ_e peak is located slightly northward of that in the ΔT = 25K case, near 14N-15N. The low-level region of enhanced easterlies between 10N-20N is also present, and again seems to be the cause of strong latent heat fluxes and intense deep convection in this region. The offshore latent heat flux reaches a peak of nearly 140 W/m^2, while the sensible heat flux over the heated land surface reaches a maximum of 120 W/m^2 between 15N and 20N. The land surface temperature peaks at almost 320K, while the surface air temperature only reaches up to 313K. These temperatures are a few degrees higher than that observed over India prior to monsoon onset (Xie and Saiki, 1999).

The 2° resolution case begins to show differences from the higher resolution run. The 'winter' meridional circulation widens and strengthens, spanning a region from 20S to 15N. The deep convection near the coastline has strengthened and broadened, and is centered around 13N. The region of enhanced low-level easterlies between 10N and 20N in the higher resolution case is gone, similar to the lower resolution runs of the ΔT = 25K case. The triple-peaked tropical precipitation of the 1° case has merged into a double peaked profile, with the northern hemisphere precipitation peak greatly strengthened and centered around 12-13N. The near-surface θ_e profile is similar in form to the 1° resolution case, with a strong localized peak around 15N, the small peak at 7N in the higher resolution case is gone, and the values of surface θ_e are higher across the entire equatorial region by about 5K.

In both the 1° and 2° resolution runs, our criteria for a monsoonal circulation are not met, as there is little precipitation over the land surface associated with the winter meridional circulation cell. However, for lower resolution runs (3° and 4°), a monsoon-type circulation does develop. For these cases, the winter circulation cell is quite broad, ranging from 20S to 20N, with strong ascent between 15N and 20N, as seen in Figure 3-15. The overall circulation is considerably stronger than for either of the higher resolution cases. In the low-resolution runs, the near-surface θ_e maximum shifts poleward to around 17N. The precipitation maximum in the northern hemisphere becomes broader with decreasing resolution, and spreads from 10N to 25N in the 3° case and from 10N to 30N in the 4° case, with the peak over the land surface near 17N in both cases. This is in contrast to the very narrow precipitation band in the higher resolution cases, with a width of around 5° latitude. As with the $\Delta T = 25K$ case already discussed, the vigorous dry low-level circulations which are present over the land surface in the high resolution runs are almost completely absent in

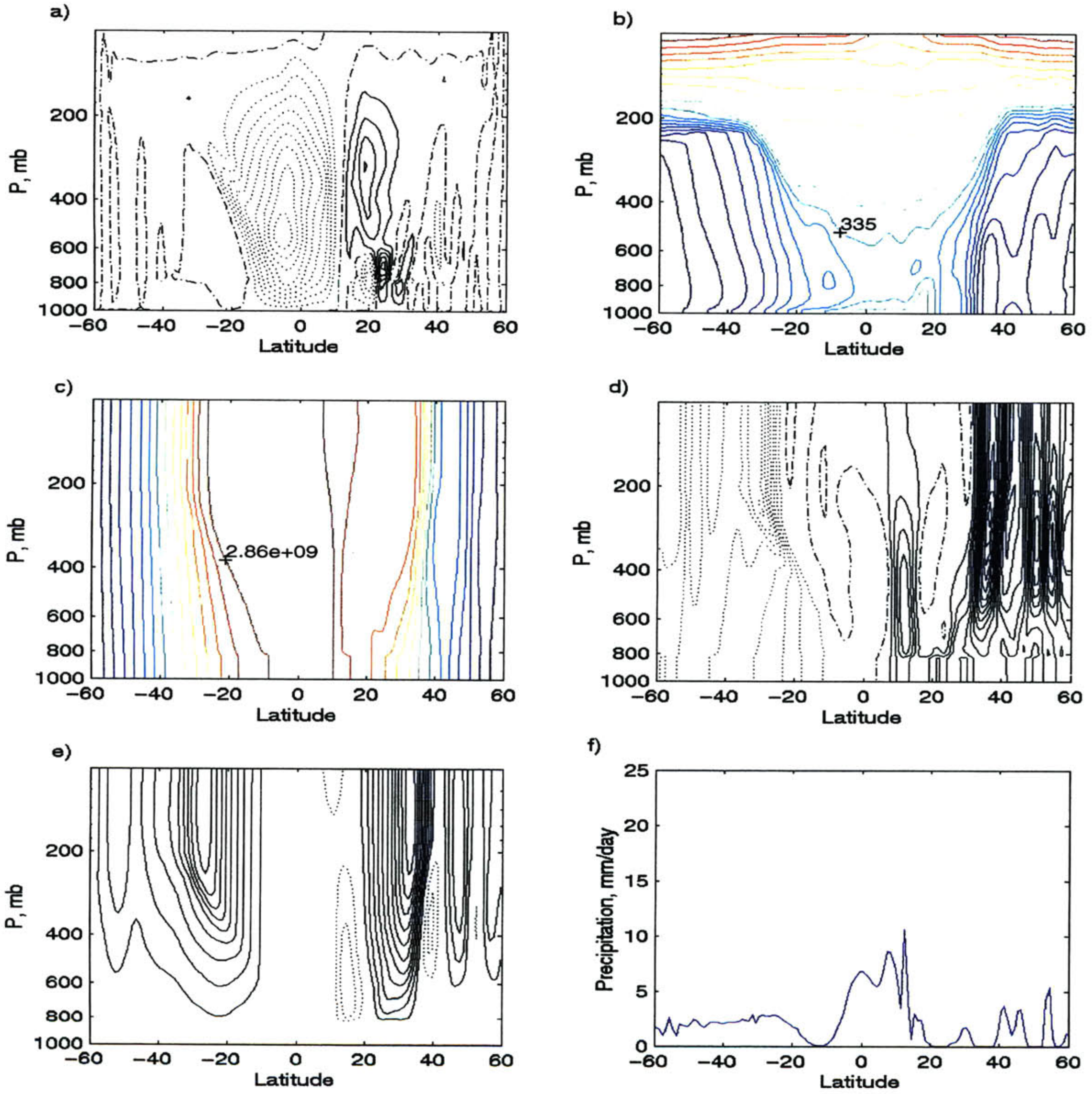

Figure 3-13: Model results for Case 2 with $\Delta T = 30K$ with 1° resolution, all fields averaged over days 200-300. Solid lines indicate positive contours, dotted lines indicate negative contours, zero contour in dash-dots. a) Streamfunction, contour interval 2.0E10 kg/s; b) θ_e, contour interval 6 K; c) M, contour interval 1.5E8 m^2/s; d) absolute vorticity, ζ_a, contour interval 2.0E-5 1/s ; e) zonal wind u, contour interval 9.0 m/s; f) precipitation, mm/day.

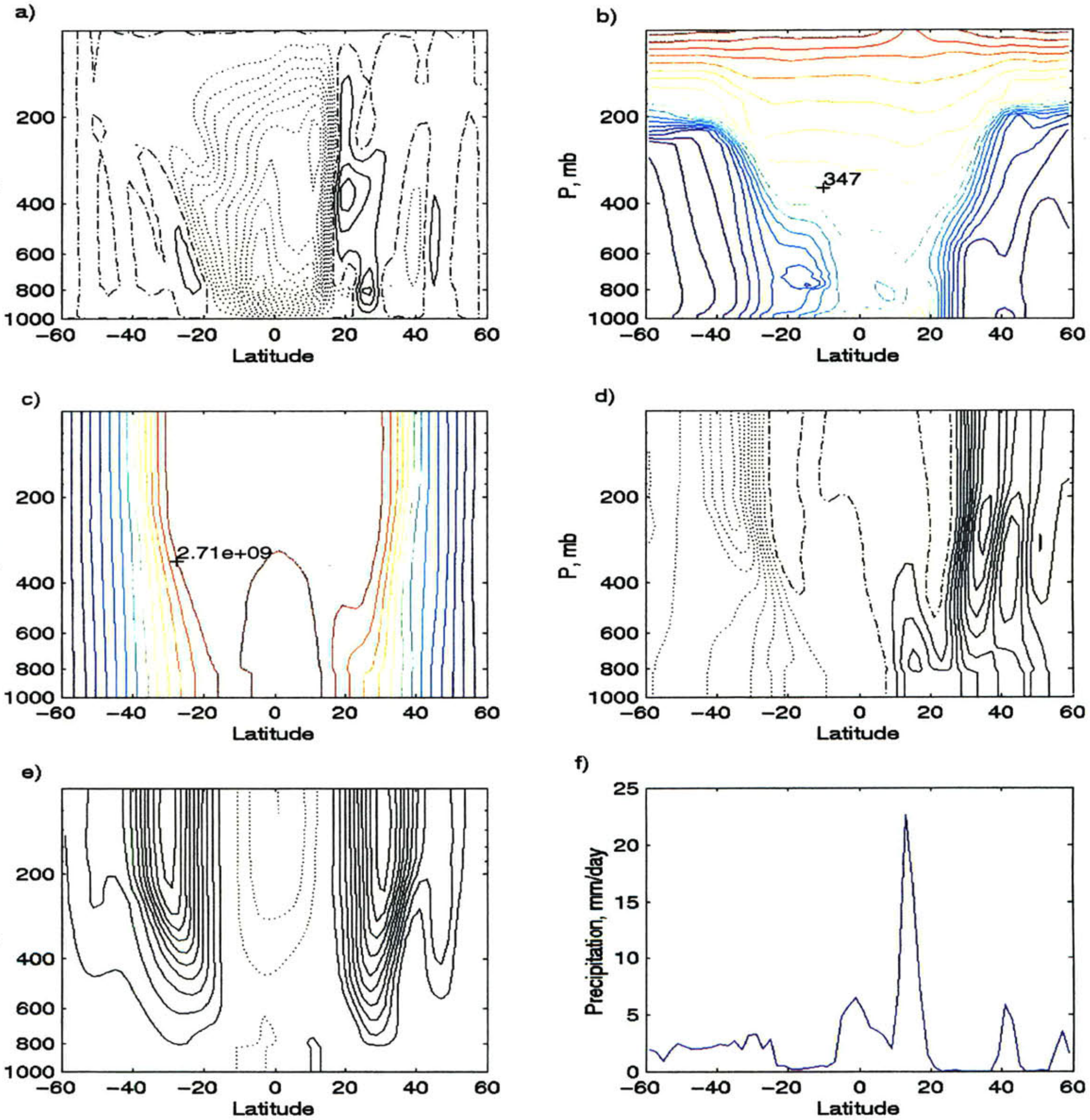

Figure 3-14: Model results for Case 2 with $\Delta T = 30K$ with 2° resolution, all fields averaged over days 184-284. Solid lines indicate positive contours, dotted lines indicate negative contours, zero contour in dash-dots. a) Streamfunction, contour interval 2.0E10 kg/s; b) θ_e, contour interval 6 K; c) M, contour interval 1.5E8 m^2/s; d) absolute vorticity, ζ_a, contour interval 2.0E-5 1/s ; e) zonal wind u, contour interval 9.0 m/s; f) precipitation, mm/day.

the low resolution runs. In all runs except for the 4° resolution run, there is a local pressure minimum very near the equator. In the 4° resolution case, we note that the circulation shows no tendency for convergence at the equator, and the moisture transport in this region is greatly enhanced. As the pressure minimum in the higher resolution runs is extremely weak at the equator, it seems likely that this feature is simply blurred out in the lowest resolution run.

The flow for these runs is potentially baroclinically unstable, as illustrated in Figure 3-16. The meridional gradient of Ertel's potential vorticity changes sign both in the subtropics and in the midlatitudes on θ_v surfaces throughout the lower troposphere. The easterly jet in the subtropics of the high resolution case may also be unstable, as there is a region of negative PV gradient in the lower troposphere between 10N and 15N where the surface θ gradient is positive northward. The midlatitudes are also potentially unstable, as in the ΔT = 25K run. The meridional gradient of absolute vorticity changes sign in the mid troposphere near 15N in all runs except for the 4° resolution case.

The striking differences between the high and low resolution runs in the $\Delta T = 30K$ case may be due to interactions between the land surface processes, moisture transport, and the resolution. In order to test this, we perform two runs, one at low resolution and one at high resolution, with the bucket content on the near-coastal land fixed to specific wetted values. For the fixed moist bucket runs, the buckets were set to be full over the land between 15N and 16.5N, have a water content of 8 cm between 16.5N and 18.5N, and were allowed to change freely over the rest of the land surface. One run was made at 1° resolution, and a second run was made at 3° resolution. The overall size and form of the winter circulation cell was similar for both runs, encompassing the region from 20S to around 20N in both runs, although the circulation of the lower resolution run was once again stronger. The precipitation peak for both runs was located around 16N, with the precipitation region being somewhat broader for the low resolution run.

A careful examination of the fixed moist bucket runs is quite revealing. The meridional moisture advection from the ocean onto the land in the low resolution case is nearly twice as strong at the coastline as in the high resolution case, as demonstrated in Figure 3-17. In the high resolution run, much of the circulation is diverted upwards in the region of deep convection near the equator, and part of the circulation becomes cut off, never crossing the equator. The circulation in the low resolution run shows less of a tendency to avoid the equator, and the deep convection near the equator is weaker. This type of behavior in the high resolution run is due to the same cause as that behind the jumping of the circulation in the Case 1 runs. The easterlies in the low-level equatorial region tend to cause convergence toward the equator, and the flow is thus reluctant to cross the equator at low levels. The low-level pressure gradient near the equator is very similar for the low and high resolution

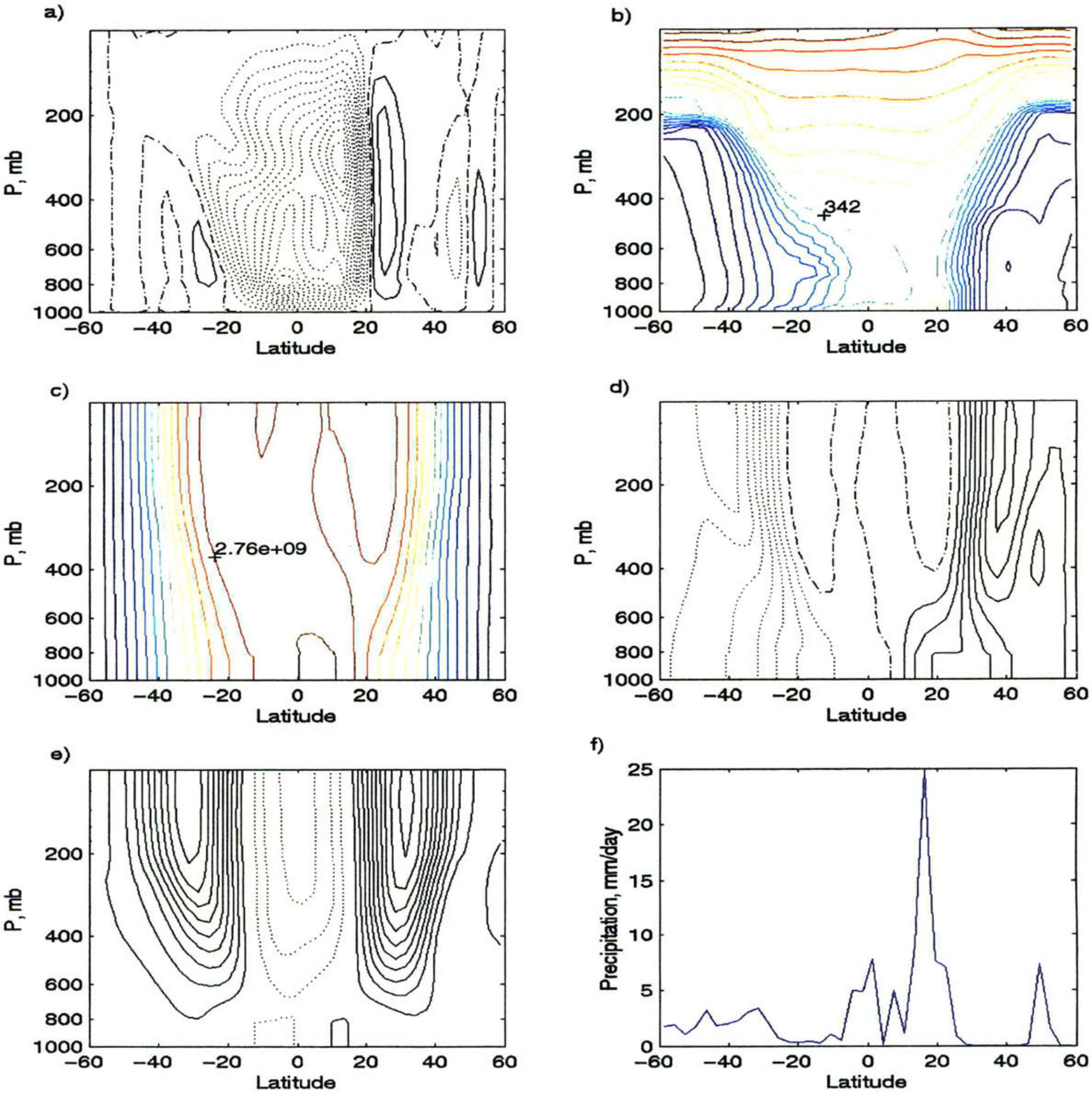

Figure 3-15: Model results for Case 2 with $\Delta T = 30K$ with 3° resolution, all fields averaged over days 200-300. Solid lines indicate positive contours, dotted lines indicate negative contours, zero contour in dash-dots. a) Streamfunction, contour interval 2.0E10 kg/s; b) θ_e, contour interval 6 K; c) M, contour interval 1.5E8 m^2/s; d) absolute vorticity, ζ_a, contour interval 2.0E-5 1/s ; e) zonal wind u, contour interval 9.0 m/s; f) precipitation, mm/day.

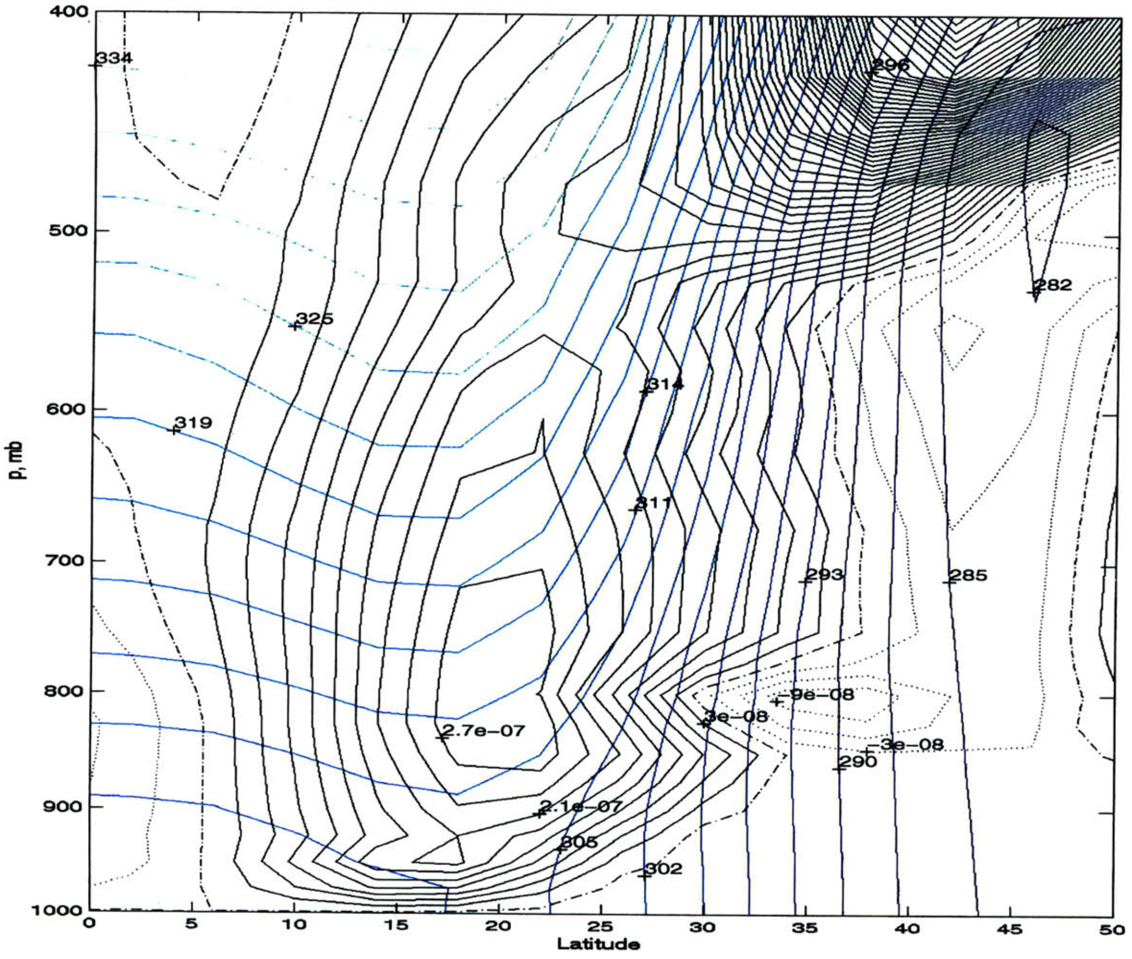

Figure 3-16: Zonal mean Ertel's PV, contour interval 3E-8, solid black lines indicate positive values, dotted indicate negative values. Zonal mean θ_v, contour interval 2K, color lines. ΔT = 30K, 4° resolution.

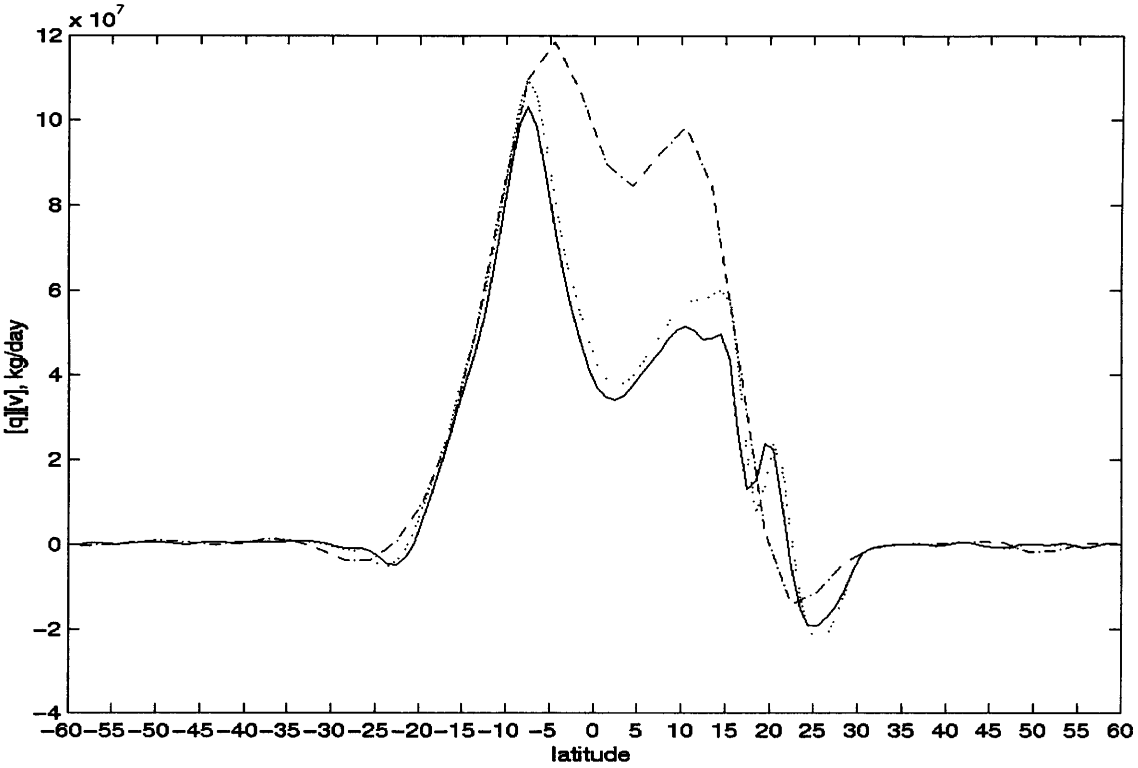

Figure 3-17: Column integrated northward moisture vapor transport, $[q][v]$, kg/day, for Case 2 with $\Delta T = 30K$ with fixed moist buckets, all fields averaged over days 200-300. Solid lines indicate 1° resolution with narrow band of prescribed moist buckets, dashed lines indicate 1° resolution with broad band of prescribed moist buckets, dash-dot lines indicate 3° resolution with narrow band of prescribed moist buckets. All fields vertically integrated over the depth of the atmosphere.

runs, with a small local minimum in geopotential at the equator. In the low resolution run, the actual equator is blurred due to the wide gridpoint spacing so that the equatorial pressure minimum is smeared out, and numerical diffusion allows cross-equatorial flow to occur more easily.

Since the low resolution case results in a larger region of wetted buckets and deep convection than the high resolution case, we perform another run with prescribed bucket moisture at high resolution, with the bucket moisture set to a similar profile to that achieved by the low resolution fixed moist bucket run. We wish to determine whether the strength of the circulation in the high resolution run is weaker than that of the low resolution run due to the greater wetting of the land in the low resolution case, as this could result in stronger heating and thus a stronger large-scale circulation overall. In this run, the circulation was nearly as strong as in the low resolution fixed moist bucket run, but the moisture advection over the land was still considerably smaller than in the low resolution run, as seen in Figure 3-17. As in the previous high resolution fixed moist bucket run, the major difference in the northward moisture advection seems to stem from the tendency of the circulation to enter the free troposphere rather than crossing the equator near the surface.

3.4 $\Delta T = 35$K

The $\Delta T = 35$K runs develop monsoonal-type circulations at all tested resolutions. The near-surface θ_e maximum and precipitation peak are both located over the land surface between 15N and 20N. The size, spread, and strength of the 'winter' meridional circulation cells are very similar for runs at 1°, 2°, 3°, and 4° resolution. Profiles of various quantities are shown in Figure 3-18 for the highest resolution run. The precipitation region is somewhat broader but less intense in the low resolution runs. The latent heat flux over the land in the monsoon region is quite high - nearly 350 W/m^2- although the land surface temperatures in this area are reduced almost to 300K. To the north of the monsoon region, the land surface heats up to almost 320K, with the surface air temperature near 315K, and sensible heat fluxes between 100 and 150 W/m^2. While these sensible heat fluxes are comparable to those observed over the Tibetan Plateau during the summer (Xu and Chan, 2001), the latent heat fluxes are somewhat higher than the observed maximum fluxes, which are on the order of 300 W/m^2 near India.

Again, the moisture transport onto the land from the ocean increases with decreasing resolution, which appears to be related to the behavior of the low-level flow in the near-equatorial region. Except for the 4° resolution run, there is a region of moderate precipitation just south of the equator, where the circulation jumps slightly over the equator, and a great deal of moisture is lost. In the 4° resolution case, this feature does not seem to be resolved. In all runs except for the 4° resolution runs, there is a pressure minimum of similar magnitude at the equator; this feature is lost in the lowest resolution run. As in the $\Delta T = 30$K case, this removes the tendency for convergence in the lowest resolution case, and increases the northward moisture transport.

Although the high resolution cases have less net moisture import onto the land than the low resolution runs, as seen in Figure 3-19, there is sufficient moisture import over the land to sustain the monsoonal circulation. There is again a tendency for deep convection near the equator to divert the circulation aloft, but there is strong boundary layer flow over the ocean surface in the northern hemisphere. Evaporation from the ocean surface is able to replace most of the moisture lost when the flow jumps over the equator. The moisture flux across the coastline for all of the $\Delta T = 35$K runs is greater than the moisture flux for the high resolution fixed moist bucket cases with $\Delta T = 30$K.

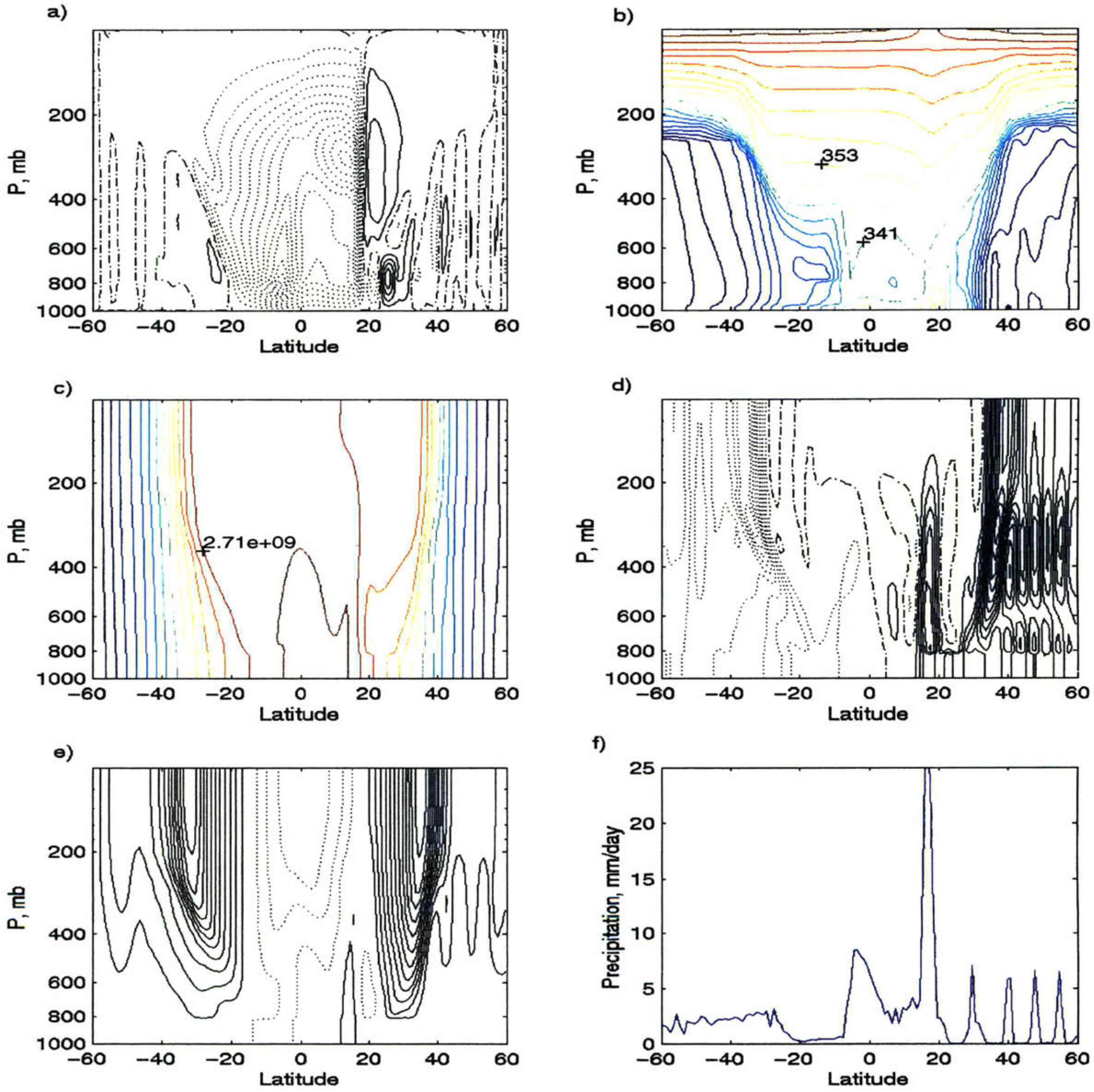

Figure 3-18: Model results for Case 2 with $\Delta T = 35K$ with 1° resolution, all fields averaged over days 200-300. Solid lines indicate positive contours, dotted lines indicate negative contours, zero contour in dash-dots. a) Streamfunction, contour interval 2.0E10 kg/s; b) θ_e, contour interval 6 K; c) M, contour interval 1.5E8 m^2/s; d) absolute vorticity, ζ_a, contour interval 2.0E-5 1/s ; e) zonal wind u, contour interval 9.0 m/s; f) precipitation, mm/day.

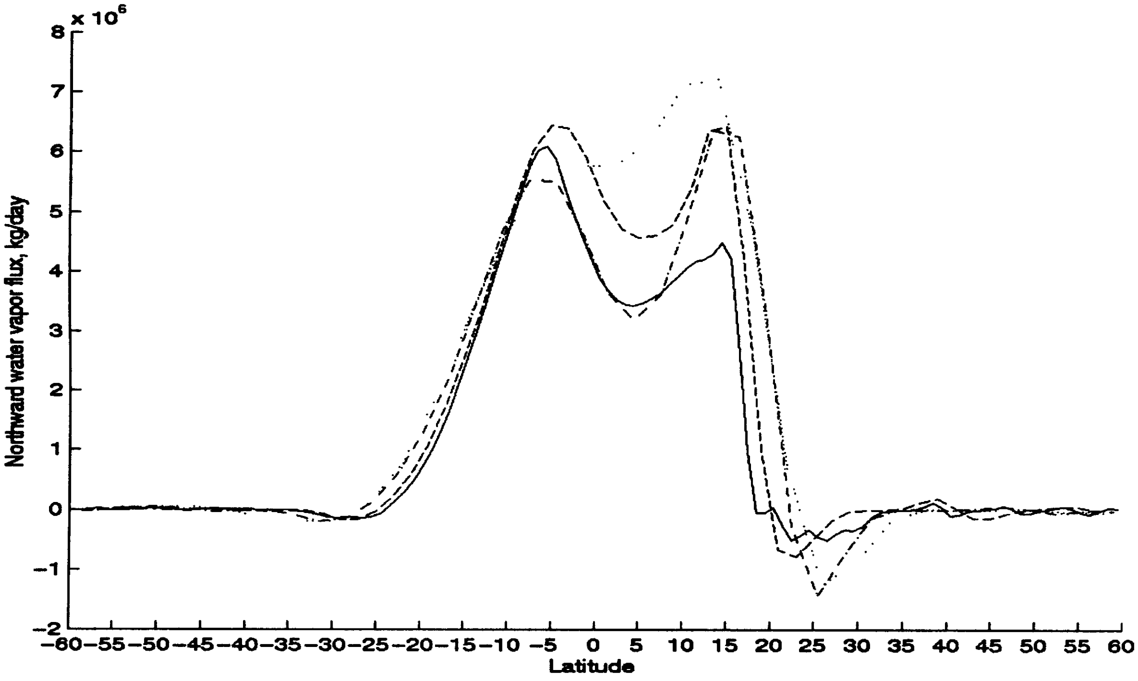

Figure 3-19: Northward water vapor transport, kg/day, model results for Case 2 with $\Delta T = 35K$ with all fields averaged over days 200-300. Solid lines indicate 1° resolution, dashed lines indicate 2° resolution, dash-dot lines indicate 3° resolution, dotted lines indicate 4° resolution. All fields vertically averaged over the entire depth of the atmosphere.

However, if the moisture availability over the land surface is disrupted in the highest resolution (1°) run, the monsoon cannot be sustained. This is demonstrated by a run in which 20% of the precipitation was assumed to automatically run off, reducing the availability of moisture for evaporation over the land surface. In this case, the monsoon circulation cell is not viable over the land surface, and the winter circulation cell recedes so that the ascending branch is colocated with the SST maximum near 8N, as in the ΔT = 25K case. This indicates that the high resolution case has northward moisture transport near to the minimum amount needed to sustain the steady monsoon.

Figure (3-20) shows the zonal mean θ_v and Ertel's potential vorticity for the lowest resolution run. All of the ΔT = 35K runs have a reversal of PV gradient in the lower tropospheric subtropics near 20N. The midlatitudes are also potentially unstable as in runs with smaller ΔT. The meridional gradient of absolute vorticity changes sign in the mid-tropospheric subtropics for the high resolution runs, and in the lower troposphere for the lowest resolution run, indicating that barotropic instability may also be possible there.

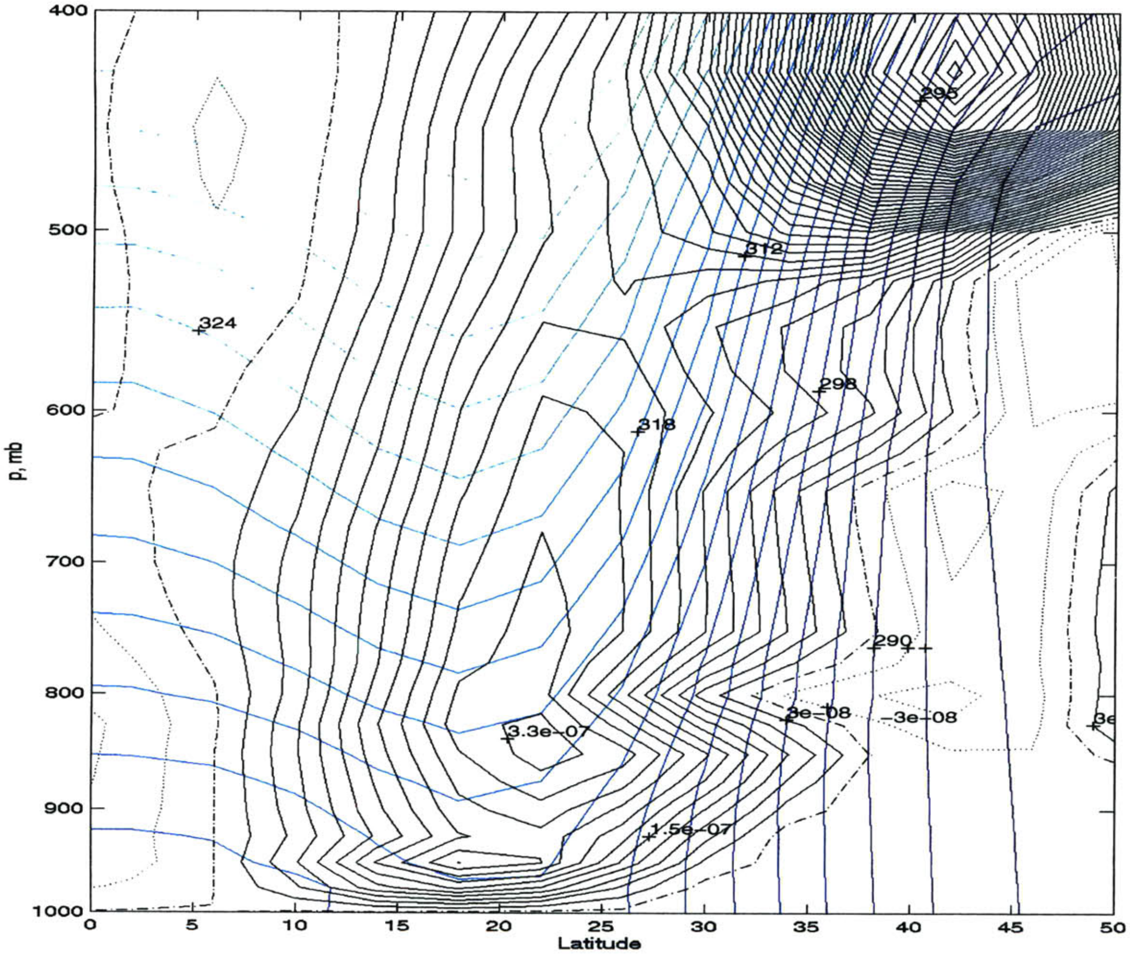

Figure 3-20: Zonal mean Ertel's PV, mean days 200-300, contour interval 3E-8, solid black lines indicate positive values, dotted indicate negative values. Zonal mean θ_v, contour interval 2K, color lines. $\Delta T = 35$K, 4° resolution.

Chapter 4

Three Dimensional Runs

The three-dimensional MITGCM runs were made with a resolution of 6° in longitude and 4° in latitude, with 40 vertical levels of 25 mb spacing in a channel between 60S and 60N. All other parameters were the same as with Case 2 of the axisymmetric runs. Four different runs were made, with land surface forcing of ΔT = 20K, 30K, 35K, and 45K.

The 3D runs had a zonally symmetric land surface, with the coastline at 15N and land continuing north to the poleward edge of the channel at 60N. The land surface relaxation temperature and SST were also zonally symmetric, and had the same form as in Case 2. The GCM was first run for 100 days with the momentum tendency due to pressure gradients set to zero throughout to approximate a RCE state. Then the GCM was run for 300 additional days, starting from the zonal mean of the end state of the RCE run. Small, random, longitudinal perturbations to the near-surface air temperature were added to the initial state of the full-dynamics run to induce the creation of eddies.

4.1 $\Delta T = 20K$

In the ΔT = 20K run, the steady state zonal mean land surface temperature is only a few degrees warmer than the tropical sea surface temperature, and the extreme dryness of the continent results in a sharp drop in low-level θ_e across the subtropics. The inter-tropical convergence zone (ITCZ) is located near 6N, with a broad equatorial peak which sharply drops off at 10N. The 'winter' Hadley cell is predominantly AMC in nature except along the subtropical edge, while the 'summer' Hadley cell is very much not AMC, as seen in Figure 4-1. There are weak easterlies in the low and mid-troposphere, but no easterly jet aloft.

As the continent remains almost completely dry throughout the subtropics, the zonal mean latent heat flux is near zero over the land except for the region of the midlatitude rainband. The sensible heat flux over the heated land surface is on the order of 100 W/m^2. The surface air temperature over the continent peaks at around 308 K. The observed surface potential temperatures over India and south Asia prior to monsoon onset are greater than 310K over a large area, and greater than 315 K in some regions (Luo and Yanai, 1984), so that the temperatures found in the model run are reasonable.

Although the eddy moisture flux tends to transport moisture northward onto the continent, the strong 'summer' Hadley circulation acts in the opposite fashion to remove moisture from the continent (Figure 4-3). The net water vapor flux across the coastline is northward, but much smaller than the transport seen in the monsoonal axisymmetric runs. The subsidence region of the 'summer' Hadley cell is located over the subtropical continent, and can act to suppress deep convection there. Figure 4-2 shows that the eddy disturbances which occur over the subtropical continent have only weak, transient precipitation. As seen in Figure 4-4, the convection associated with these eddies occurs when the eddies pull moist ocean air northward over the coast. These precipitation events seem to be controlled by the large scale eddies, and do not induce significant flow of their own.

The lower tropospheric eddies over the subtropical continent are primarily baroclinic in nature. The meridional gradient of absolute vorticity is positive throughout the northern hemisphere at low levels, so that barotropic instability is unlikely. As seen in Figure 4-5, there is a region in the lower tropospheric northern hemisphere subtropics where the meridional gradient of Ertel's PV along θ_v contours is near zero and may change sign. There is a second region where the PV gradient changes sign in the midlatitudes, in the mid-troposphere. In the midlatitudes, the positive northward PV gradient and negative northward surface θ gradient also indicate the possibility of baroclinic instability in westerly shear flow. The Eliassen-Palm flux, seen in Figure 4-6, shows a broad region with characteristic baroclinic eddy signatures between 15N and 50N.

The zonal wavenumber phase speed covariance spectra of the eddy fluxes of heat and momentum at 750mb are compared between 22N and 42N. We see from Figure 4-7 that the waves most active in the midlatitudes have different wavenumbers and phase speeds from those occurring along the subtropical continent, and are therefore presumed to have different sources. At 22N, both $[v^*T^*]$ and $[u^*v^*]$ are concentrated in three different wavenumbers: wavenumber 7 with eastward phase speed of approximately 3.5 m/s, and wavenumbers 4 and 6 with eastward phase speed of approximately 2 m/s. At 42N, the heat flux spectra is concentrated primarily in wavenumber 5 disturbances with eastward phase speeds of either 4 m/s or 5.5 m/s. The momentum flux spectra at 42N is dominated by westward-moving waves, however, with only some contribution to eastward moving waves at wavenumber 4, phase speed of 1.5 m/s. The wavenumber 7 and wavenumber 4 disturbances are relatively weakly present in the midlatitudes, so that it is uncertain whether these waves originated in the midlatitudes or elsewhere.

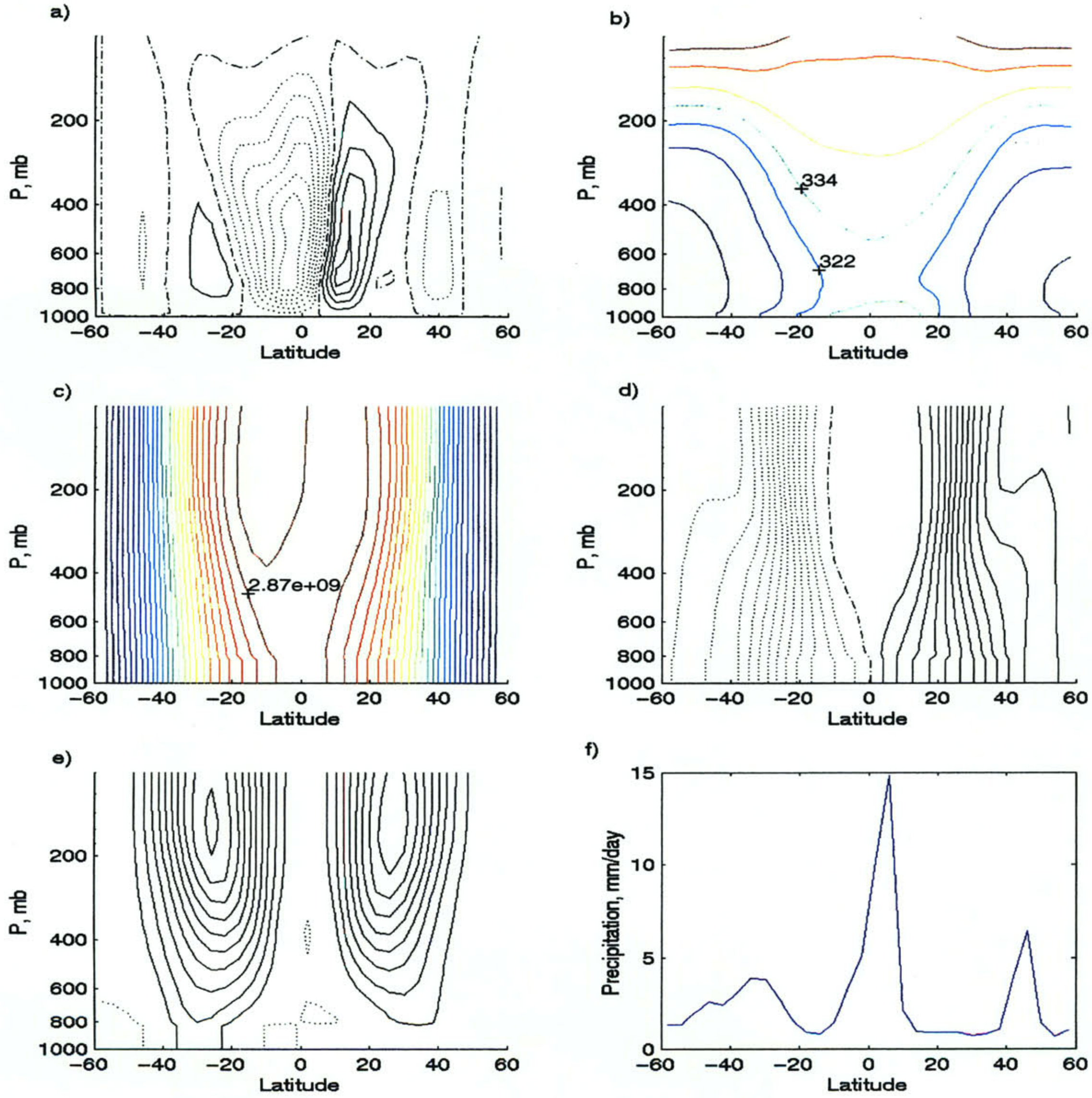

Figure 4-1: Model results for 3D run with $\Delta T = 20K$, all fields averaged over days 200-300. Solid lines indicate positive contours, dotted lines indicate negative contours, zero contour in dash-dots. a) Streamfunction, contour interval 2.5E10 kg/s; b) θ_e, contour interval 12 K; c) M, contour interval 8.6E7 m^2/s; d) absolute vorticity, ζ_a, contour interval 1.0E-5 1/s ; e) zonal wind u, contour interval 6.0 m/s; f) precipitation, mm/day.

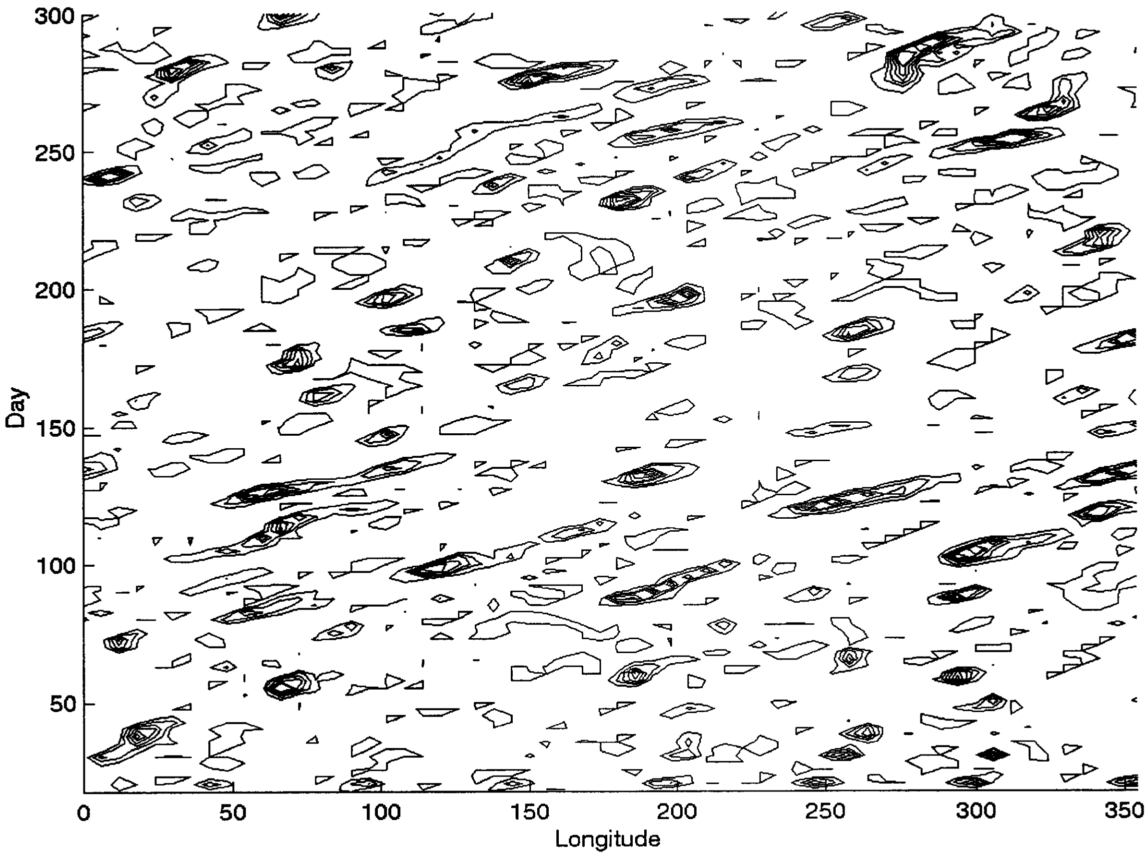

Figure 4-2: Longitude-time diagram of precipitation at 22N for three dimensional run with ΔT = 20K. Precipitation contour interval 3 mm/day.

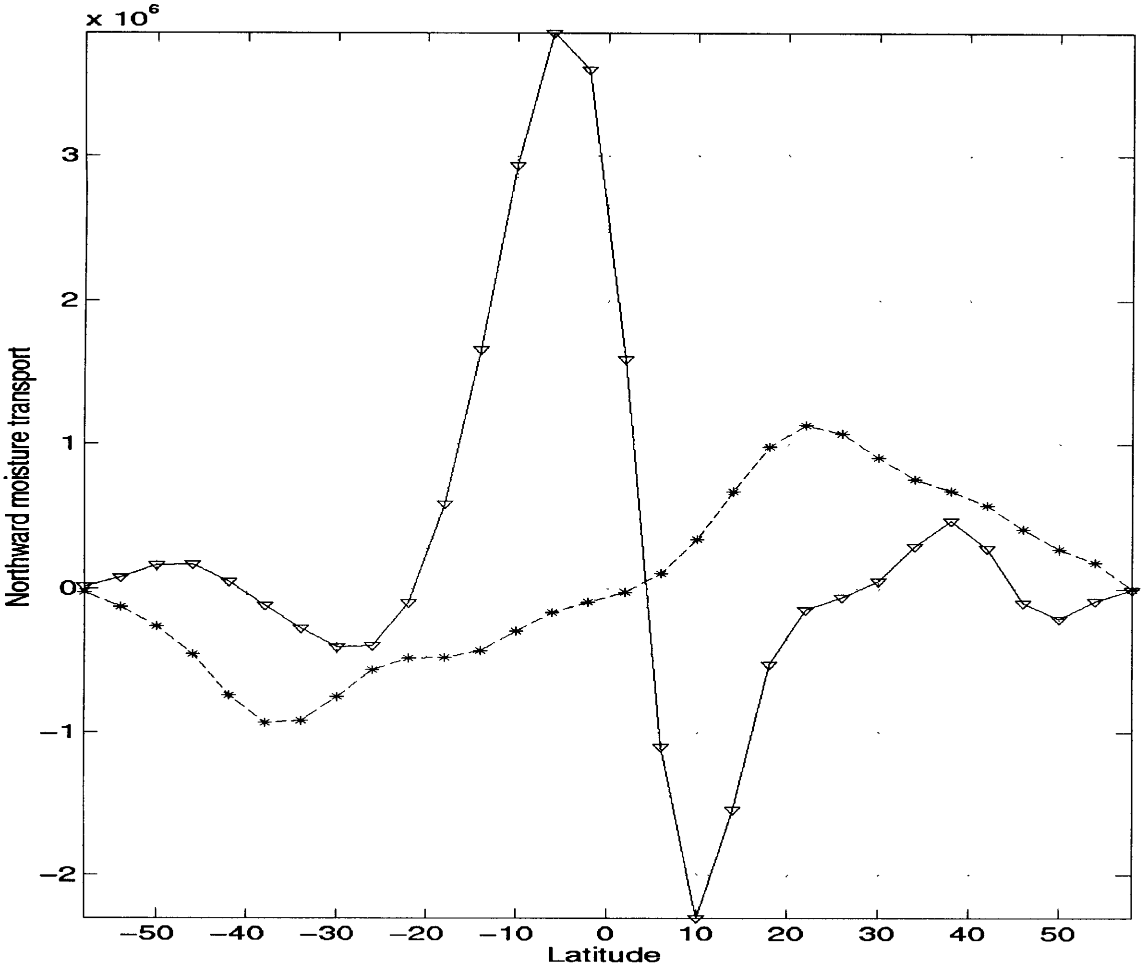

Figure 4-3: Column integrated zonal mean northward water vapor flux, kg/s, mean days 200-300, ΔT = 20K. Solid line with circles indicates [q][v], dashed line with asterisks indicates eddy flux $[q^*v^*]$.

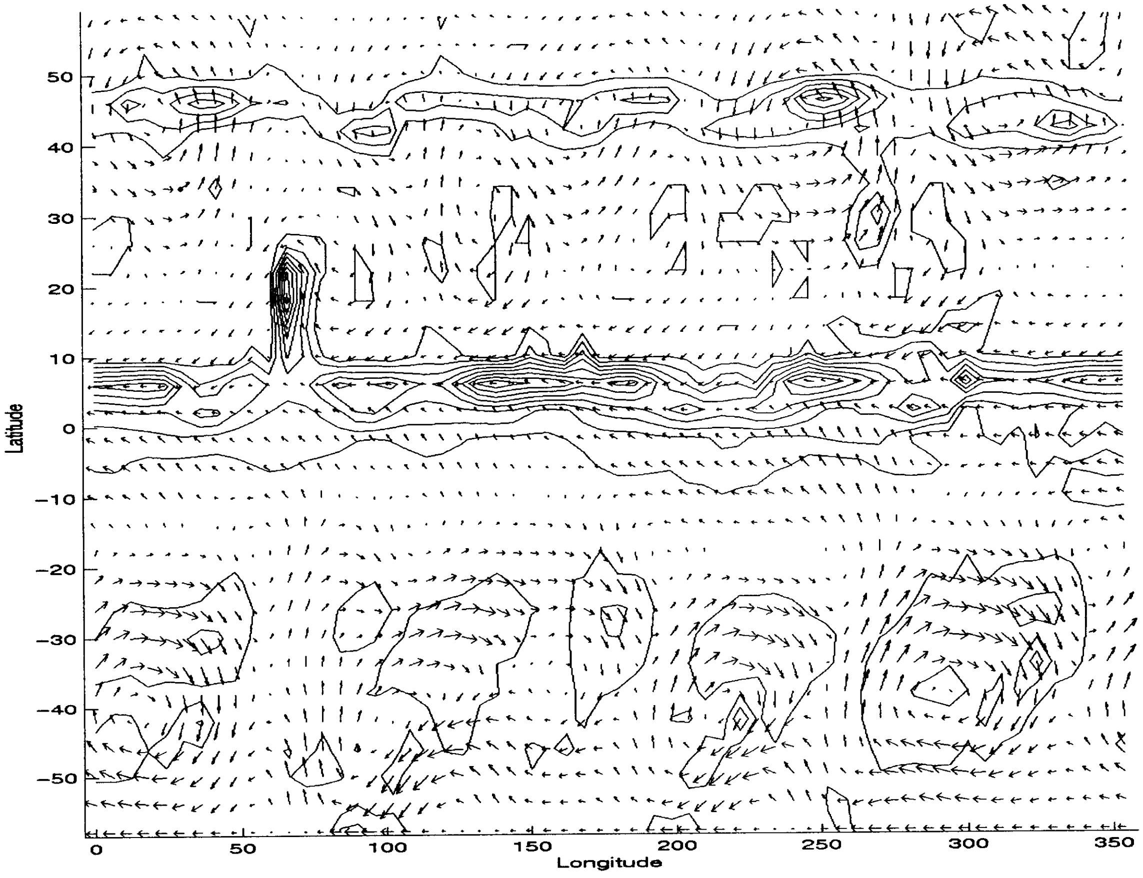

Figure 4-4: Winds at 1000 mb (arrows), mean days 297.5-300, with precipitation contours for the three dimensional run with $\Delta T = 20$K. Precipitation contour interval 3 mm/day, maximum wind speed 16.3 m/s.

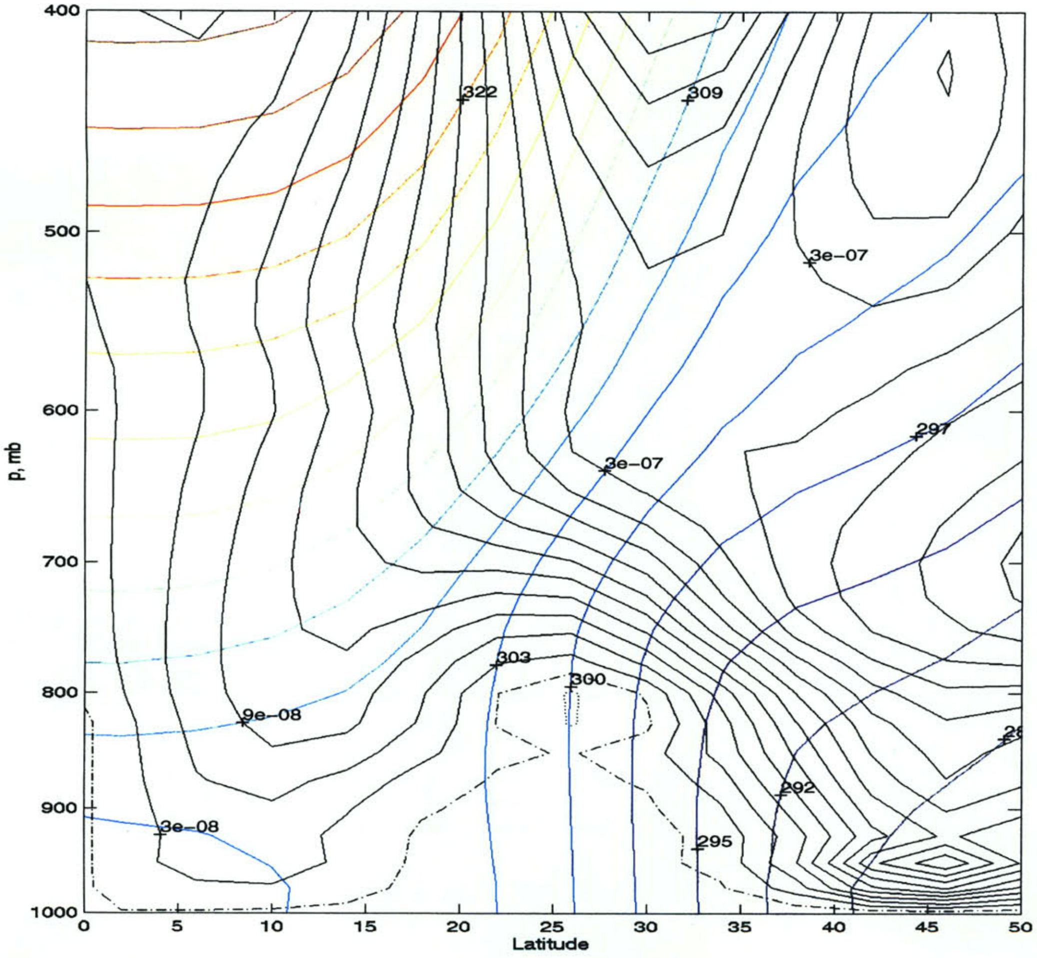

Figure 4-5: Zonal mean Ertel's PV, contour interval 3E-8 $Km^2kg^{-1}s^{-1}$, solid black lines indicate positive values, dotted indicate negative values. Zonal mean θ_v, contour interval 2K, color lines. 3D run with ΔT = 20K.

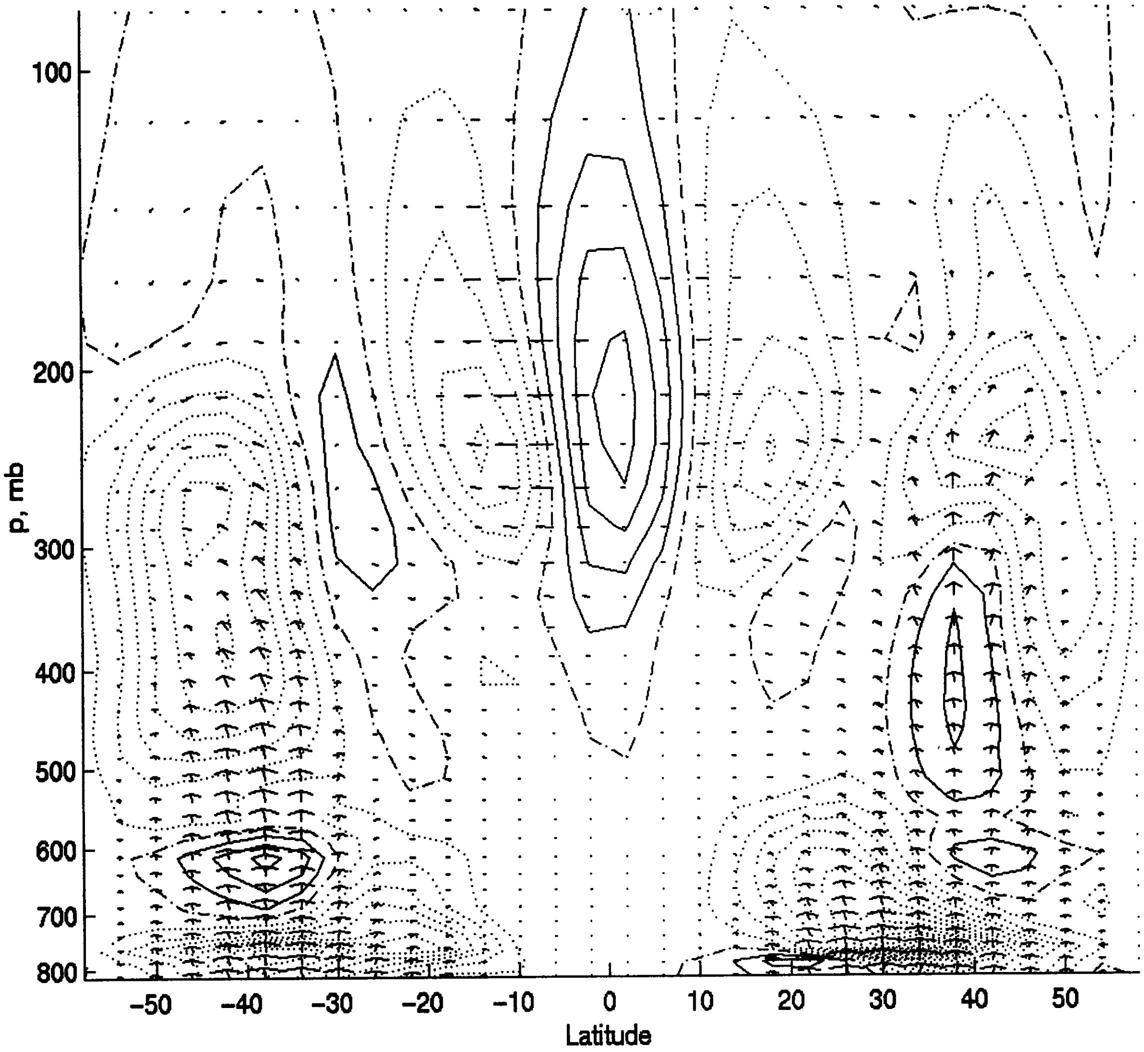

Figure 4-6: Eliassen-Palm flux, arrows, and EP divergence, contours, contour interval 40 m^3, ΔT = 20K. Solid contours indicate divergence, dotted contours indicate convergence.

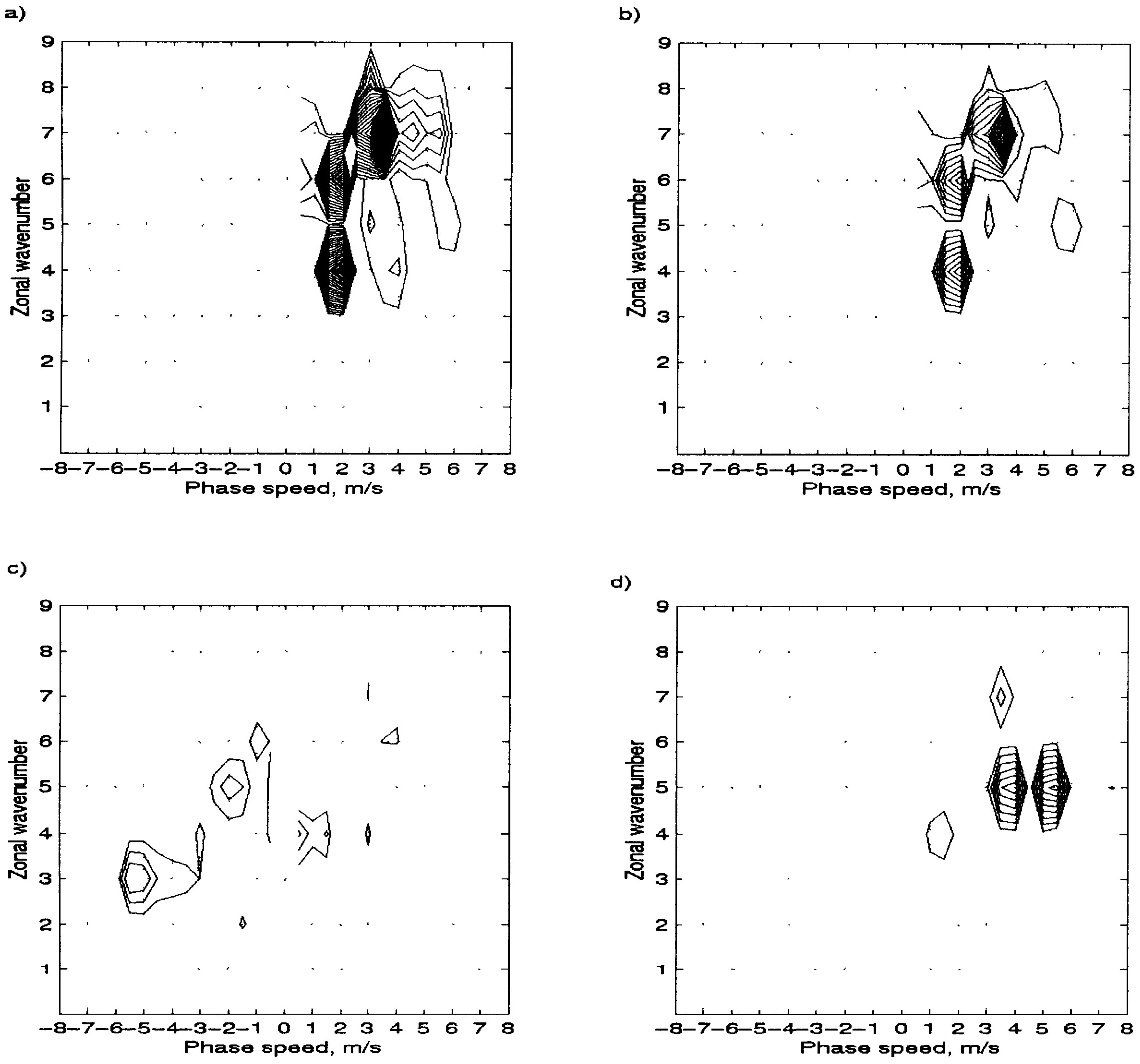

Figure 4-7: Zonal wavenumber phase speed covariance spectra, ΔT = 20K at 750 mb. a) spectra for $[u^*v^*]$ at 21N, contour interval 2.5E-8 m^3s^{-3}; b) $[v^*T^*]$ at 21N, contour interval 1.0E-8 Km^2s^{-2}; c) $[u^*v^*]$ at 42N, contour interval 2.5E-8 ; m^3s^{-3}d) $[v^*T^*]$ at 42N, contour interval 3.5E-8 Km^2s^{-2}

4.2 $\Delta T = 30K$

The zonally averaged circulation of the ΔT = 30K run is not monsoonal in nature. The ITCZ is located near 5N, with only a small amount of zonal mean precipitation over the land surface. The subsidence region of the northern Hadley cell is located in the subtropics, as seen in Figure 4-8. The northern Hadley cell is not AMC, and is strongly driven by eddies, especially along the northern slope of the cell. The larger southern Hadley cell is more nearly AMC, especially in the equatorial region, although the southernmost edge of the cell also shows some eddy effects as the streamlines begin to cross M-contours. The zonal mean circulation over the subtropical land areas seems to be dominated by a low-level circulation with ascent between 20N and 25N, confined to altitudes below 500 mb. This is not terribly dissimilar to the high resolution axisymmetric case for ΔT = 30K, although the ITCZ is located slightly more to the south in the 3D run. The eddy momentum fluxes weaken the subtropical westerly jets in the three dimensional run in comparison to the axisymmetric runs, although these jets are still quite strong.

The land surface temperatures approach 315K over the dry land regions, with a strong sensible heat flux of nearly 150 W/m^2. The surface air temperature is considerably lower than the surface temperature, and only reaches a maximum of 305K, and it is not unreasonable that a monsoon does not occur at this level of surface forcing. The sensible heat fluxes over the land are similar to those observed over the Tibetan Plateau during the summer months (Xu and Chan, 2001).

The limited amount of precipitation which occurs near the land coast takes the form of longitudinally narrow disturbances which slowly travel to the east. A longitude-time diagram of the precipitation a 22N is shown in Figure 4-9. Although some of the disturbances may result in locally heavy precipitation, the eddies tend to be short-lived, so that the zonal average of the precipitation shows only a small maximum between 15N and 25N. As in the ΔT = 20K case, the precipitation events along the coastline seem to be controlled by eddies which carry moist air inland from the ocean. The subtropical precipitating anomalies are transported and fed by the eddies, so that if an eddy ceases to supply adequate moisture to the deep convection, the precipitating anomaly will die off.

The mean flow tends to transport water vapor southward across the coastline, but the moisture transport due to the mean flow is weaker than in the ΔT = 20K case. The eddy water vapor flux is northward, but not significantly greater than in the ΔT = 20K case, so that the net northward water vapor flux across the coastline is positive but small. The eddies act to transport moisture to the midlatitudes, gradually filling the buckets in a band between 40N and 50N and maintaining a region of precipitating eddies there.

The EP flux diagram (Figure 4-12) is similar to that of the ΔT = 20K case. The

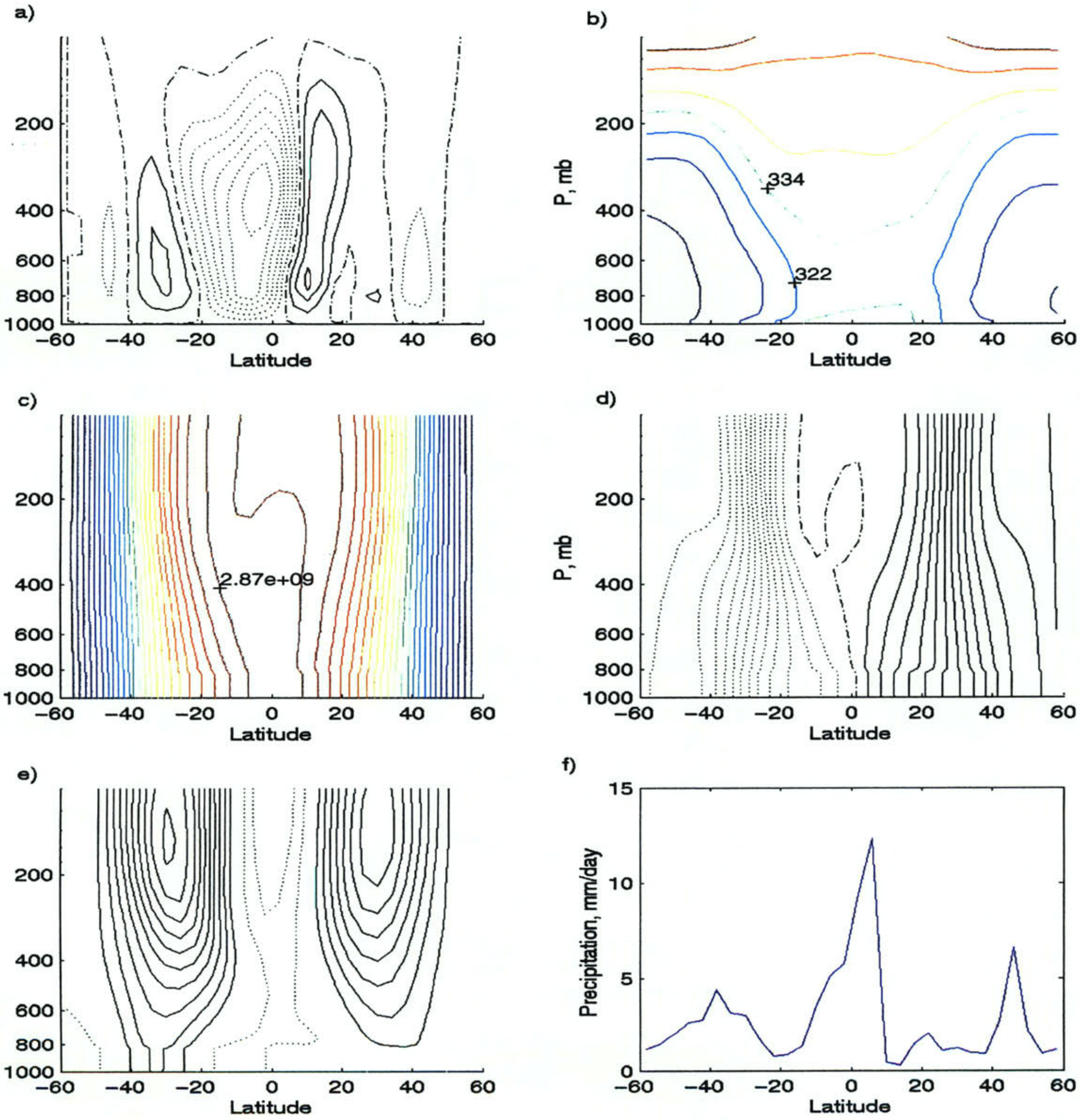

Figure 4-8: Model results for 3D run with $\Delta T = 30K$, all fields averaged over days 200-300. Solid lines indicate positive contours, dotted lines indicate negative contours, zero contour in dash-dots. a) Streamfunction, contour interval 2.5E10 kg/s; b) θ_e, contour interval 12 K; c) M, contour interval 8.6E7 m^2/s; d) absolute vorticity, ζ_a, contour interval 1.0E-5 1/s ; e) zonal wind u, contour interval 6 m/s; f) precipitation, mm/day.

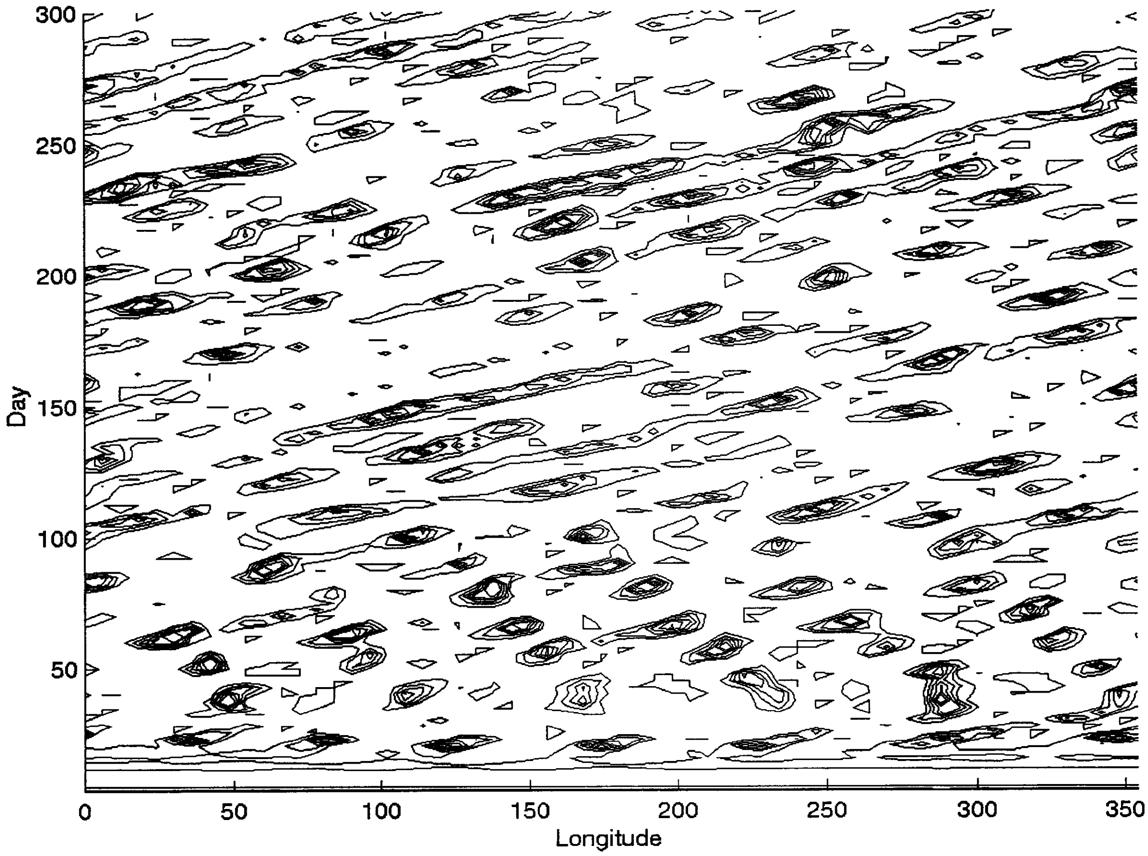

Figure 4-9: Longitude-time diagram of precipitation at 22N for three dimensional run with ΔT = 30K. Precipitation contour interval 3 mm/day.

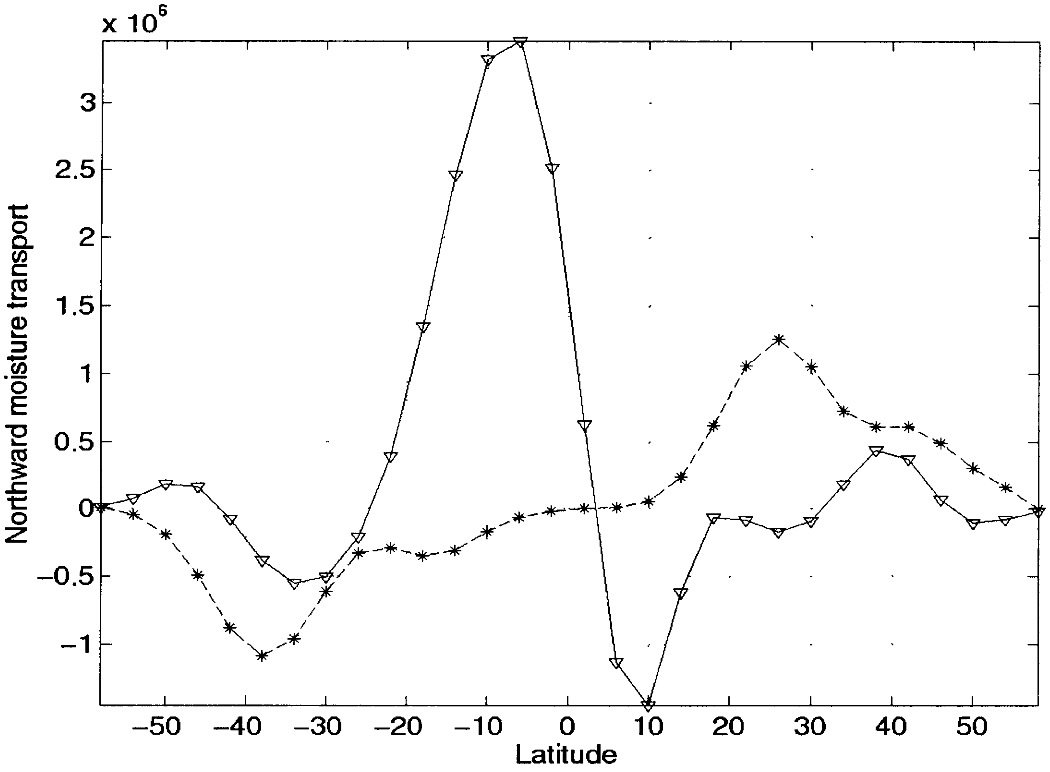

Figure 4-10: Column integrated zonal mean northward water vapor flux, kg/s, mean days 300-400, $\Delta T = 30K$. Solid line with circles indicates [q][v], dashed line with asterisks indicates eddy flux $[q^*v^*]$..

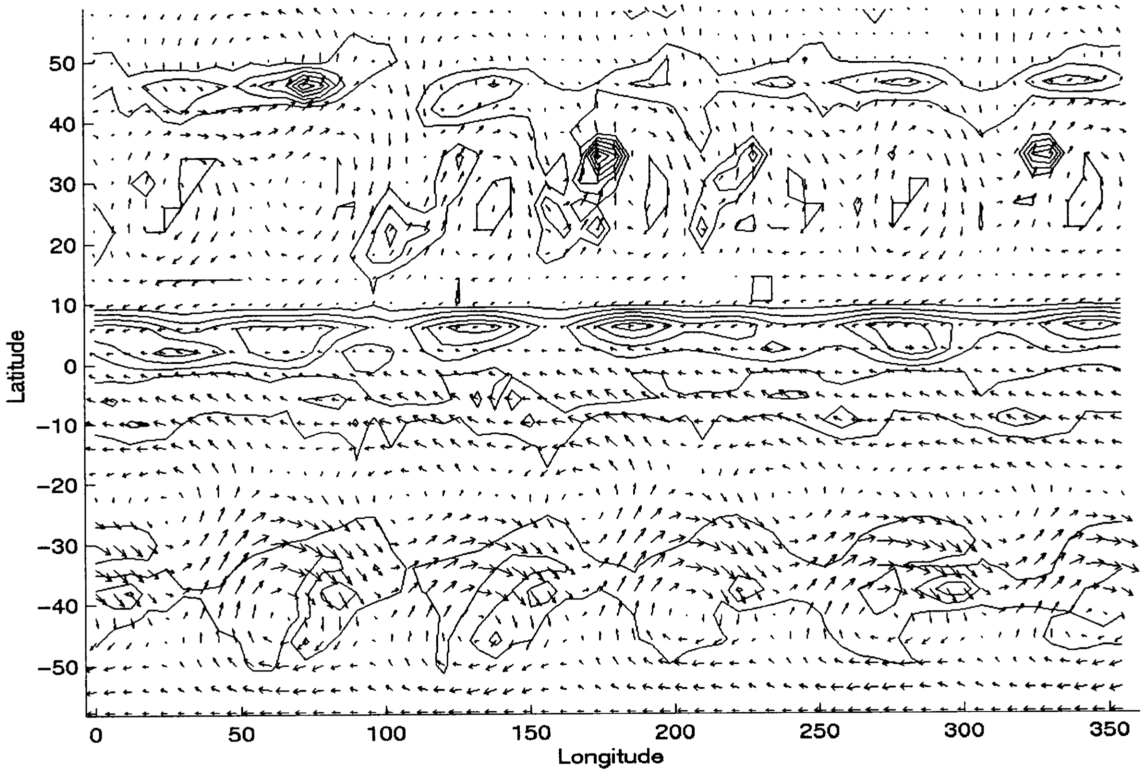

Figure 4-11: Winds at 1000 mb (arrows), mean days 297.5-300, with precipitation contours for the three dimensional run with $\Delta T = 30$K. Precipitation contour interval 3 mm/day, wind speed maximum of 17.3 m/s.

eddy flux convergence in the lower tropospheric subtropics of the northern hemisphere is somewhat stronger in this run, however. The wave activity in the equatorial upper troposphere is considerably weaker than in the $\Delta T = 20$K run. The easterly jet aloft in over the equator is stronger in this run, and the westerly forcing due to the divergence of the EP flux is weaker. The zonal mean potential vorticity field shows a region where the PV gradient is near zero and may change signs at low levels between 10N and 30N, as seen in Figure 4-13. This indicates that baroclinic instability may occur in the subtropics, whereas barotropic instability is unlikely at low levels since the absolute vorticity meridional gradient is positive throughout the low and mid troposphere in the northern hemisphere.

The zonal wavenumber covariance spectra at 750 mb for heat and momentum fluxes at 21N and 42N are shown in Figure 4-14. The eddy fluxes at 21N are concentrated in wavenumber 7 disturbances with eastward phase speed of 4 m/s. The waves at 42N which are responsible for the heat and momentum fluxes are also primarily of wavenumber 7 with phase speed of 3 m/s. The heat flux also has a weaker maximum in covariance at wavenumber 6 with eastward phase speed of 6 m/s. Since the wavenumber 7 signature which accounts for the majority of the heat and momentum fluxes is predominant both over the subtropical continent and in the midlatitudes, these waves may stem from the same source. The latitudinal difference between 21N and 42N accounts for the phase speed difference between the wavenumber 7 disturbances, which have approximately the same period for traversing the globe.

4.3 $\Delta T = 35K$

The zonal mean of the $\Delta T = 35$K run is very similar to the previous case. The ITCZ in this run has moved slightly equatorward, with maximum zonal mean precipitation around 2N, as seen in Figure 4-15, although the zonally averaged maximum near-surface θ_e is located near 10N. The northern Hadley cell also seems to be split at lower levels in the Eulerian mean circulation, which is due to eddy activity over the land. The residual mean circulation lacks this low-level split, and the residual mean 'summer' Hadley cell has its southern boundary at 20N, as seen in Figure 4-16. The northward eddy moisture flux is stronger in this run over the land surface, and is positive over the latitudinal extent of the continent, as seen in Figure 4-17. The mean meridional circulation tends to transport moisture southward across the coastline, but the northward moisture transport by eddies is greater through the subtropics. The northward net moisture flux results in the gradual filling of buckets in the midlatitudes over the continent, but not in the subtropics.

The latent heat flux associated with the convecting disturbance on the land is on the order of 300-350 W/m^2. The sensible heat flux over the dry land is of the order 150 W/m^2,

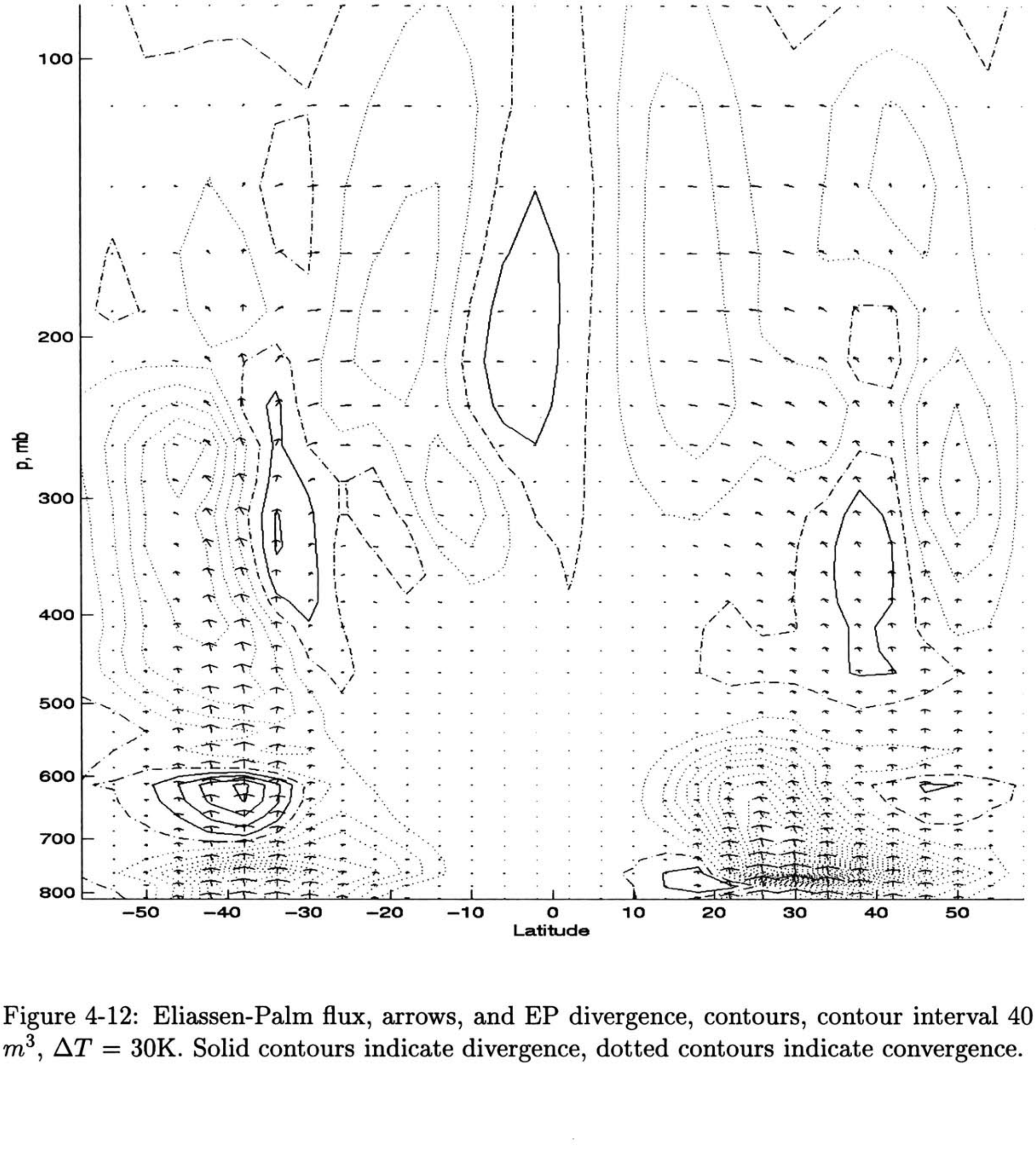

Figure 4-12: Eliassen-Palm flux, arrows, and EP divergence, contours, contour interval 40 m^3, ΔT = 30K. Solid contours indicate divergence, dotted contours indicate convergence.

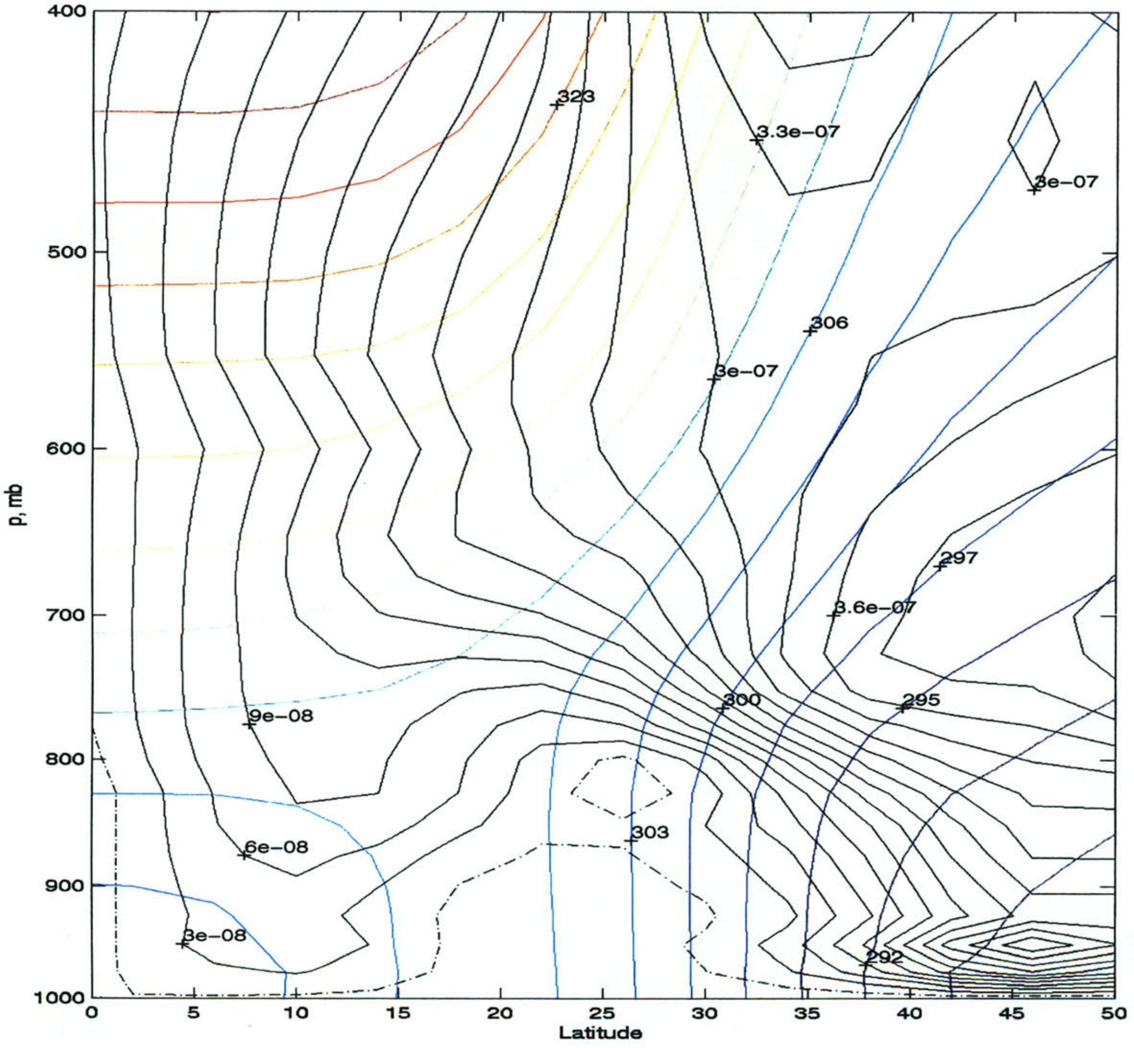

Figure 4-13: Zonal mean Ertel's PV, contour interval 3E-8 $Km^2kg^{-1}s^{-1}$, solid black lines indicate positive values, dotted indicate negative values. Zonal mean θ_v, contour interval 2K, color lines. 3D run with $\Delta T = 30$K.

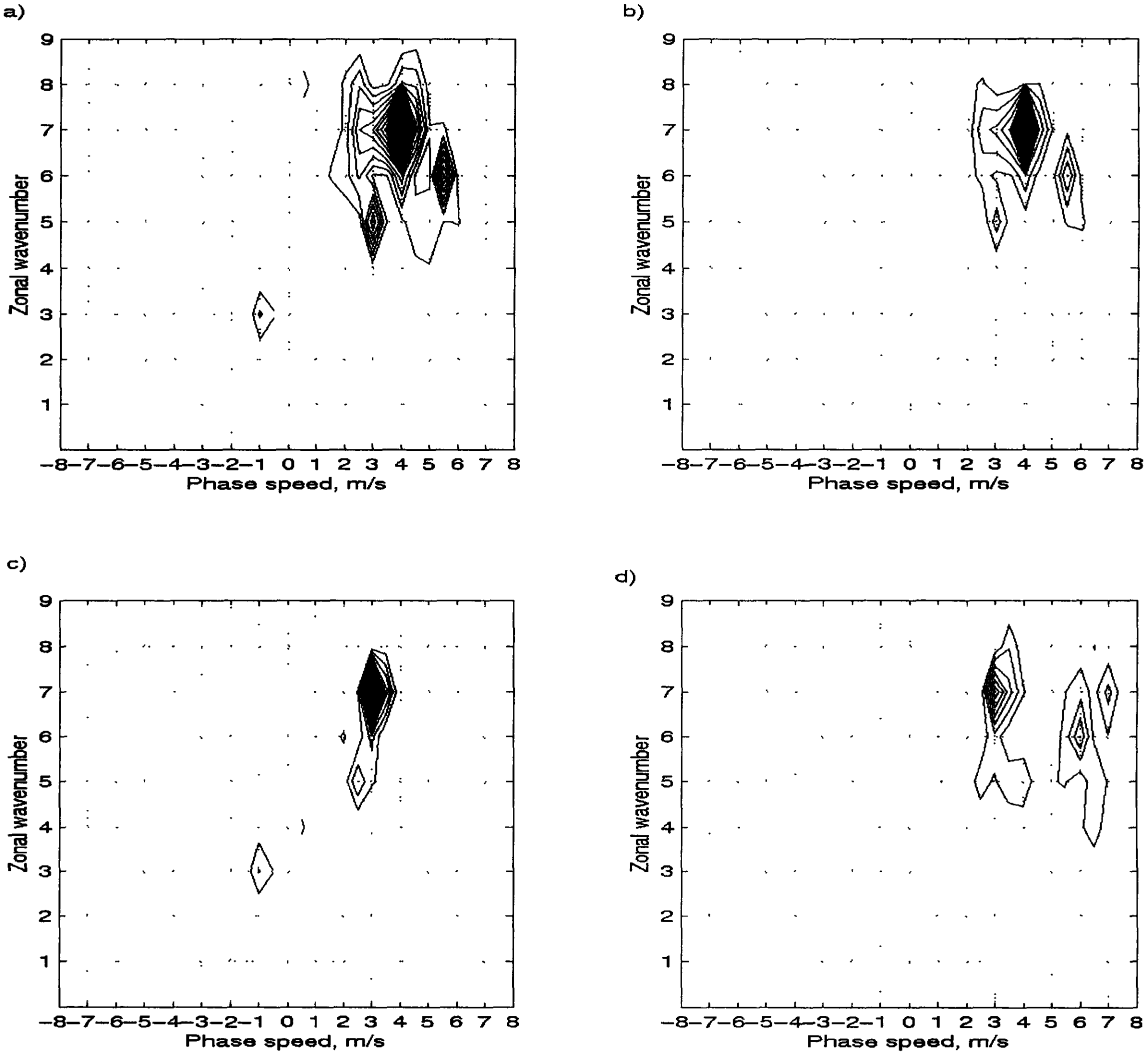

Figure 4-14: Zonal wavenumber phase speed covariance spectra, ΔT = 30K at 750 mb. a) spectra for $[u^*v^*]$ at 21N, contour interval 2.5E-8 m^3s^{-3}; b) $[v^*T^*]$ at 21N, contour interval 3.5E-8 Km^2s^{-3}; c) $[u^*v^*]$ at 42N, contour interval 2.5E-8 m^3s^{-3} d) $[v^*T^*]$ at 42N, contour interval 3.5E-8 Km^2s^{-3}

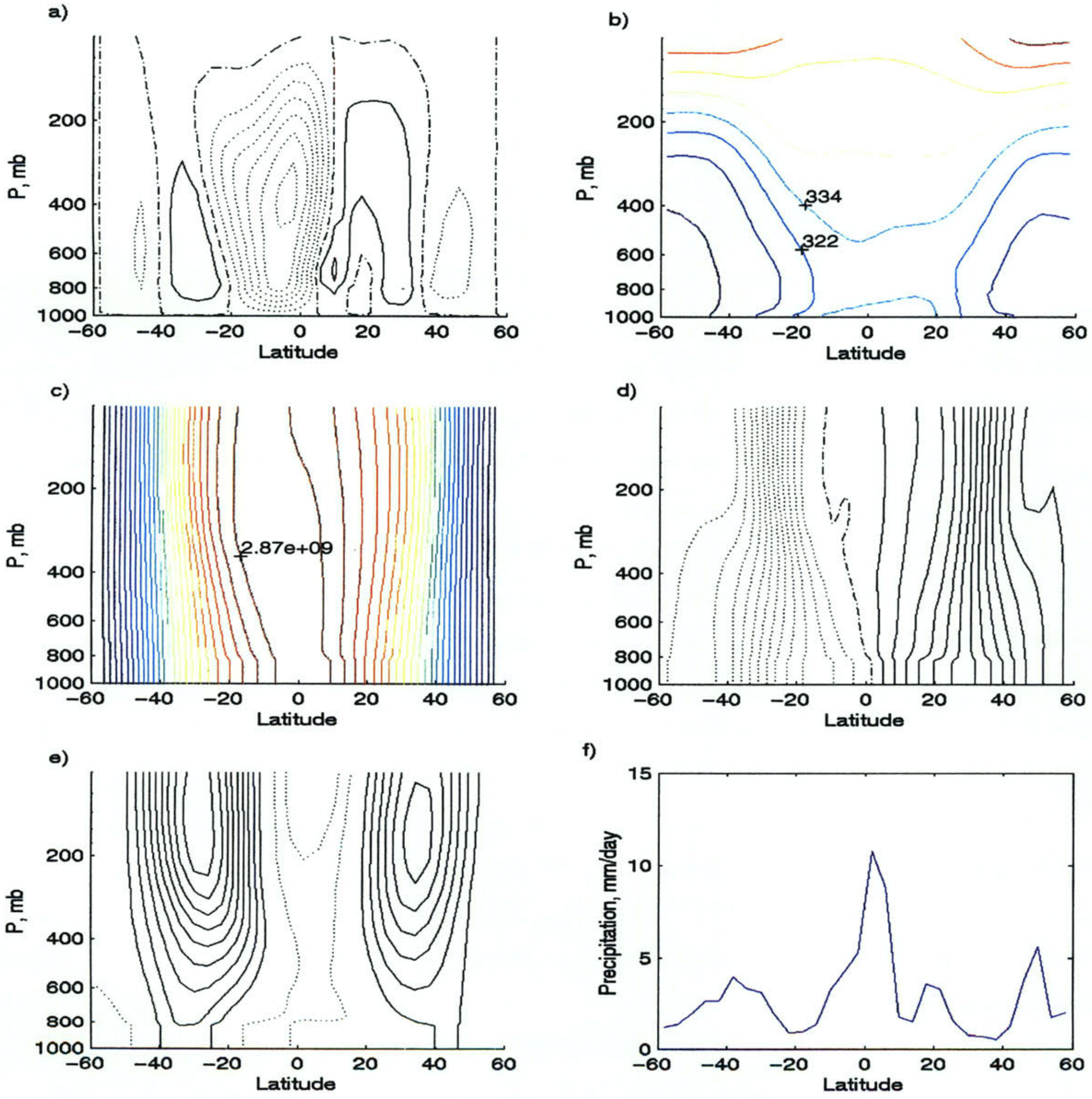

Figure 4-15: Model results for 3D run with $\Delta T = 35K$, all fields averaged over days 200-300. Solid lines indicate positive contours, dotted lines indicate negative contours, zero contour in dash-dots. a) Streamfunction, contour interval 2.5E10 kg/s; b) θ_e, contour interval 12 K; c) M, contour interval 8.6E7 m^2/s; d) absolute vorticity, ζ_a, contour interval 1.0E-5 1/s ; e) zonal wind u, contour interval 6 m/s; f) precipitation, mm/day.

not unreasonably higher than that observed over the Tibetan Plateau prior to monsoon onset (Xu and Chan, 2001). The land surface temperature over dry regions reaches up to 320K, while the land surface in deep convecting areas is reduced to less than 305K by the strong latent heat flux.

The EP flux field (Figure 4-18) shows a large region of waves with characteristic baroclinic structure at lower levels between 20N and 50N, and is very similar to the $\Delta T =$ 30K case. There is stronger wave generation in the midlatitudes near 400 mb in this run, however. There is a region where the Ertel's PV gradient switches signs along θ_v contours below 700 mb between 15N and 30N, shown in Figure 4-19. Positive northward PV gradient and negative surface θ gradient in the midlatitudes offer another region which may be baroclinically unstable. As the meridional gradient of absolute vorticity is positive throughout the northern hemisphere in the mid and lower troposphere, barotropic instability is again unlikely.

The zonal wavenumber phase speed covariance spectra for the eddy fluxes of heat and momentum at 750 mb are seen in Figure 4-20. At 21N, the waves which contribute the most to the eddy fluxes have eastward phase speeds between 3 and 4 m/s. There is a broad maximum of covariance from wavenumber 5 to wavenumber 7, and a weaker maximum at wavenumber one. The eddy flux covariance spectra at 42N is similarly concentrated in wavenumbers 5, 6, and 7, with eastward phase speed of approximately 3 m/s. The eddy heat flux at 42N also has a weaker peak at wavenumber one, with eastward phase speed of 3 m/s.

The behavior of the eddies over the coastal land is seen in the longitude-time diagram of precipitation at 22N in Figure 4-21. Although the first 100 days of this run are very similar to the behavior of the $\Delta T = 30$K run, the eventual 'steady' state eddy behavior is quite different. The precipitating eddies are not as transient as in previous runs. Instead, one or two neighboring eddies merge into a larger disturbance, and travel eastward while the other disturbances die out. This single, larger disturbance is probably responsible for the wavenumber one spectral peak seen in Figure 4-20. The smaller eddies which compose this large anomaly are represented by the higher wavenumber signatures, and all of the wave components are observed to move with the same phase speed. The eddies which persist and then grow induce a low-level southwesterly flow onto the land surface, which supplies moisture to drive the convection, as seen in Figure 4-22. Once this low-level flow initiates, the precipitating region grows and intensifies. Most of the precipitation events over the subtropical continent which occur during spin-up do not show this type of behavior, and become cut-off from moisture supply from the ocean, leading to their deaths. The precipitation tends to occur on the east side of the cyclonic low-level eddies, where northward flow from the ocean is greatest.

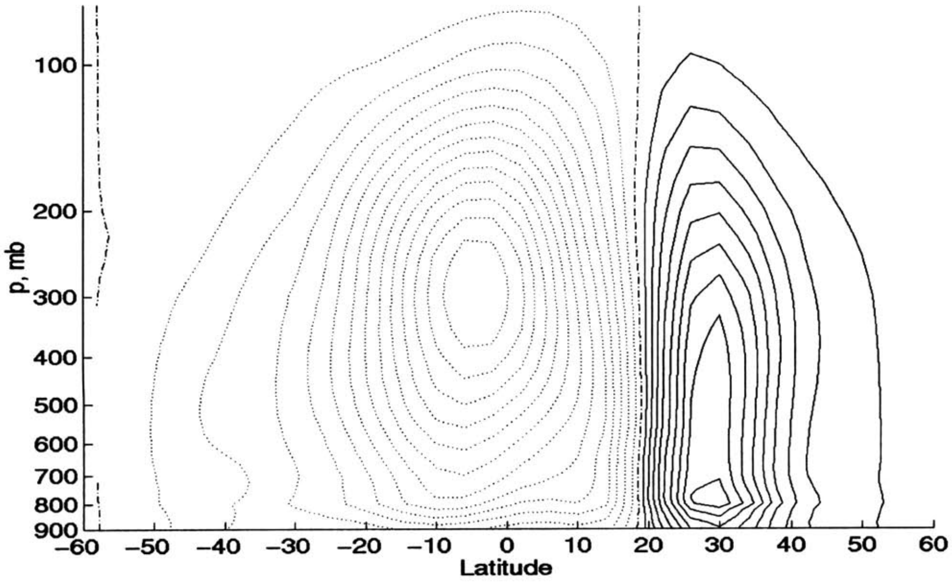

Figure 4-16: Residual mean zonal mean streamfunction, $\Delta T = 35$K, mean days 200-300. Contour interval kg/s.

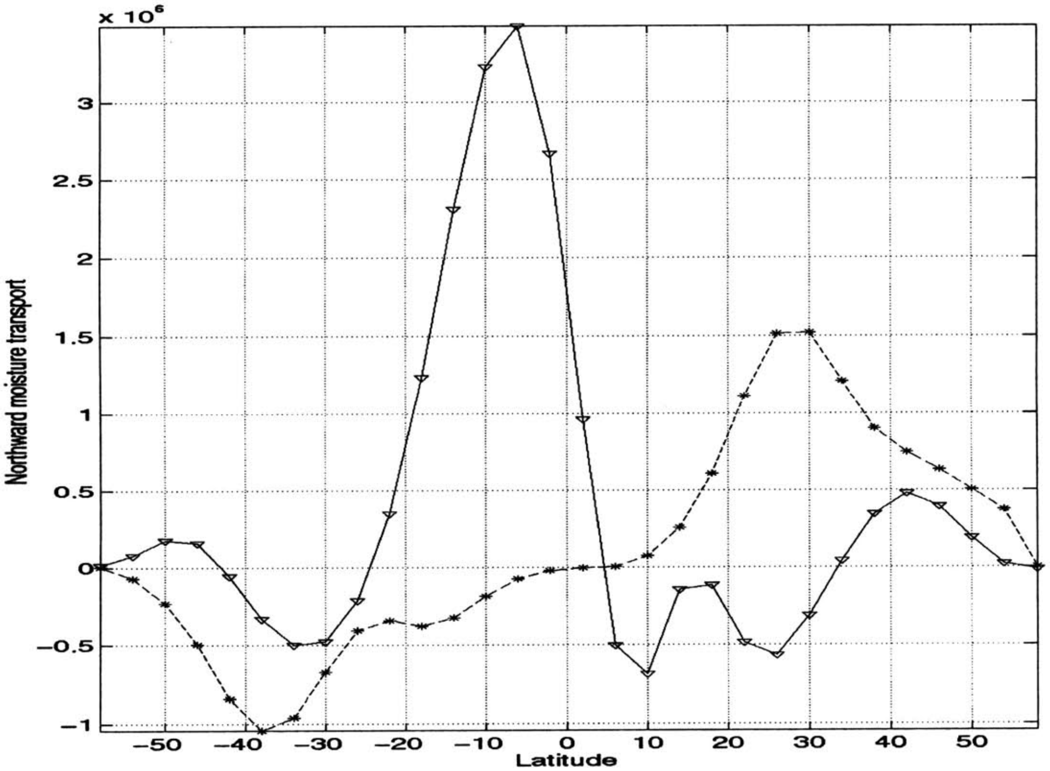

Figure 4-17: Zonal mean northward water vapor flux, kg/s, mean days 200-300, $\Delta T = 35K$. Solid line with triangles indicates [q][v], dashed line with circles indicates eddy flux $[q^*v^*]$.

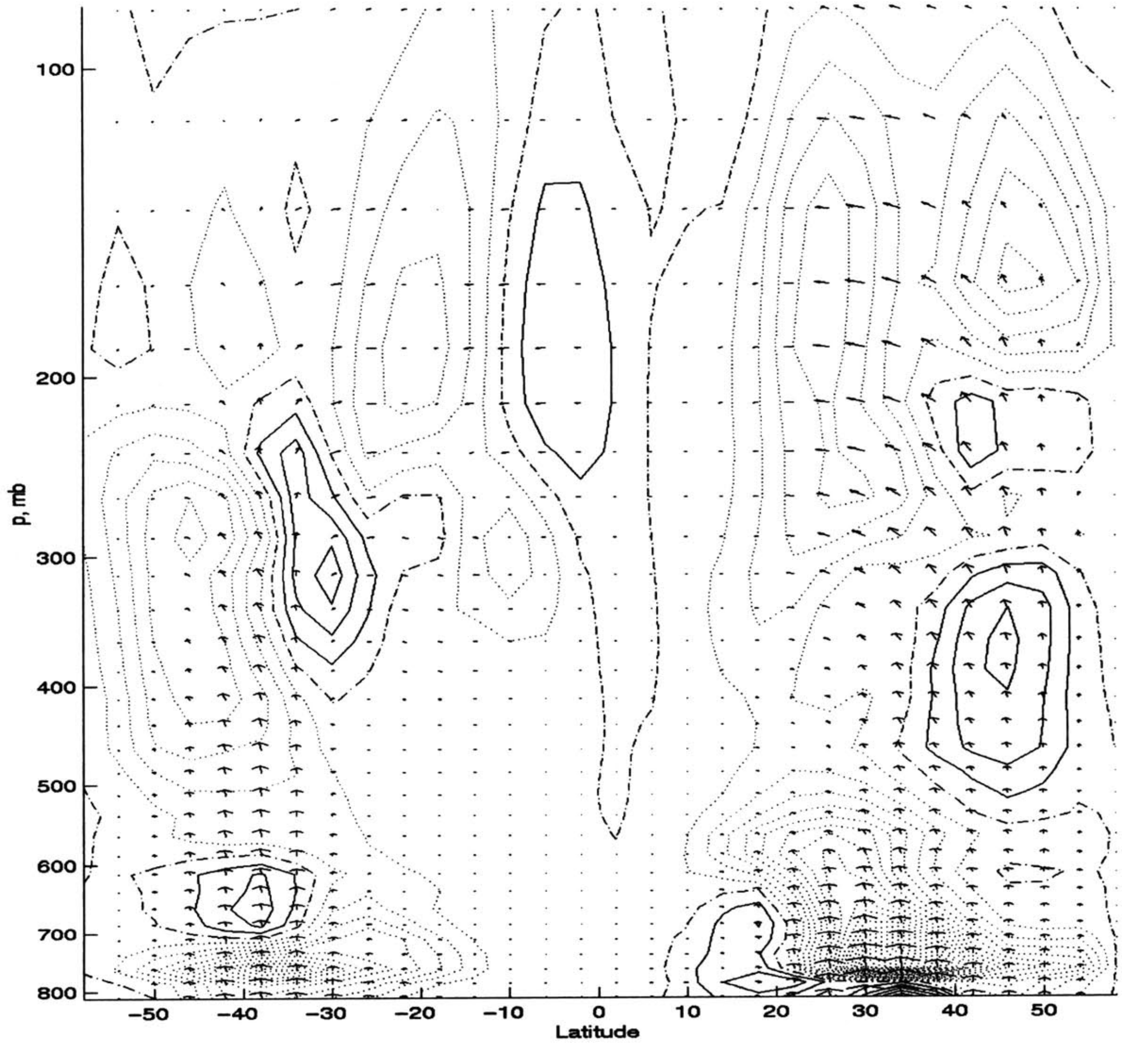

Figure 4-18: Eliassen-Palm flux, arrows, and EP divergence, contours, contour interval 40 m^3, $\Delta T = 35$K. Solid contours indicate divergence, dotted contours indicate convergence.

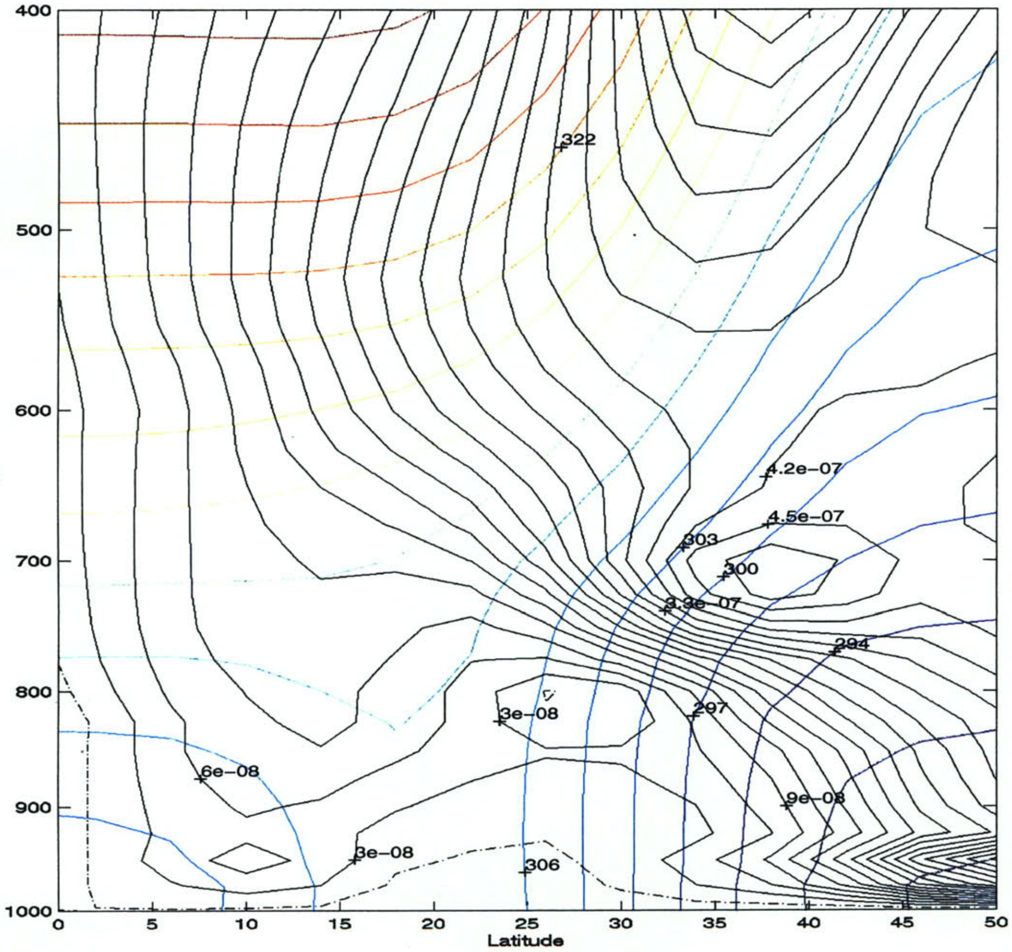

Figure 4-19: Zonal mean Ertel's PV, contour interval 3E-8 ,$Km^2kg^{-1}s^{-1}$ solid black lines indicate positive values, dotted indicate negative values. Zonal mean θ_v, contour interval 2K, color lines. 3D run with $\Delta T = 35$K.

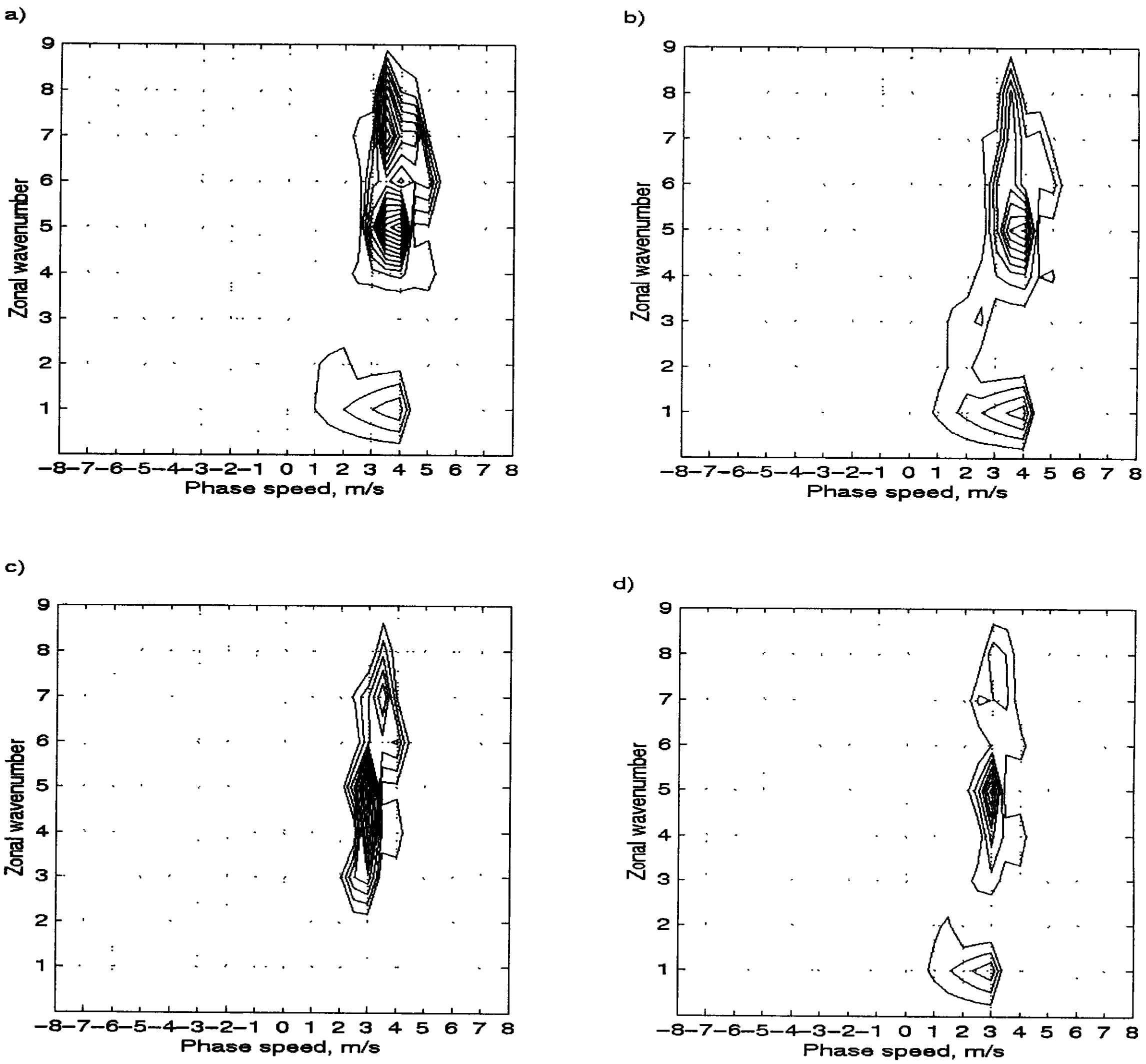

Figure 4-20: Zonal wavenumber phase speed covariance spectra, ΔT = 35K at 750 mb. a) spectra for $[u^*v^*]$ at 21N, contour interval 2.5E-8 m^3s^{-3}; b) $[v^*T^*]$ at 21N, contour interval 3.5E-8 Km^2s^{-2}; c) $[u^*v^*]$ at 42N, contour interval 2.5E-8 Km^2s^{-2}; d) $[v^*T^*]$ at 42N, contour interval 3.5E-8 m^3s^{-3}

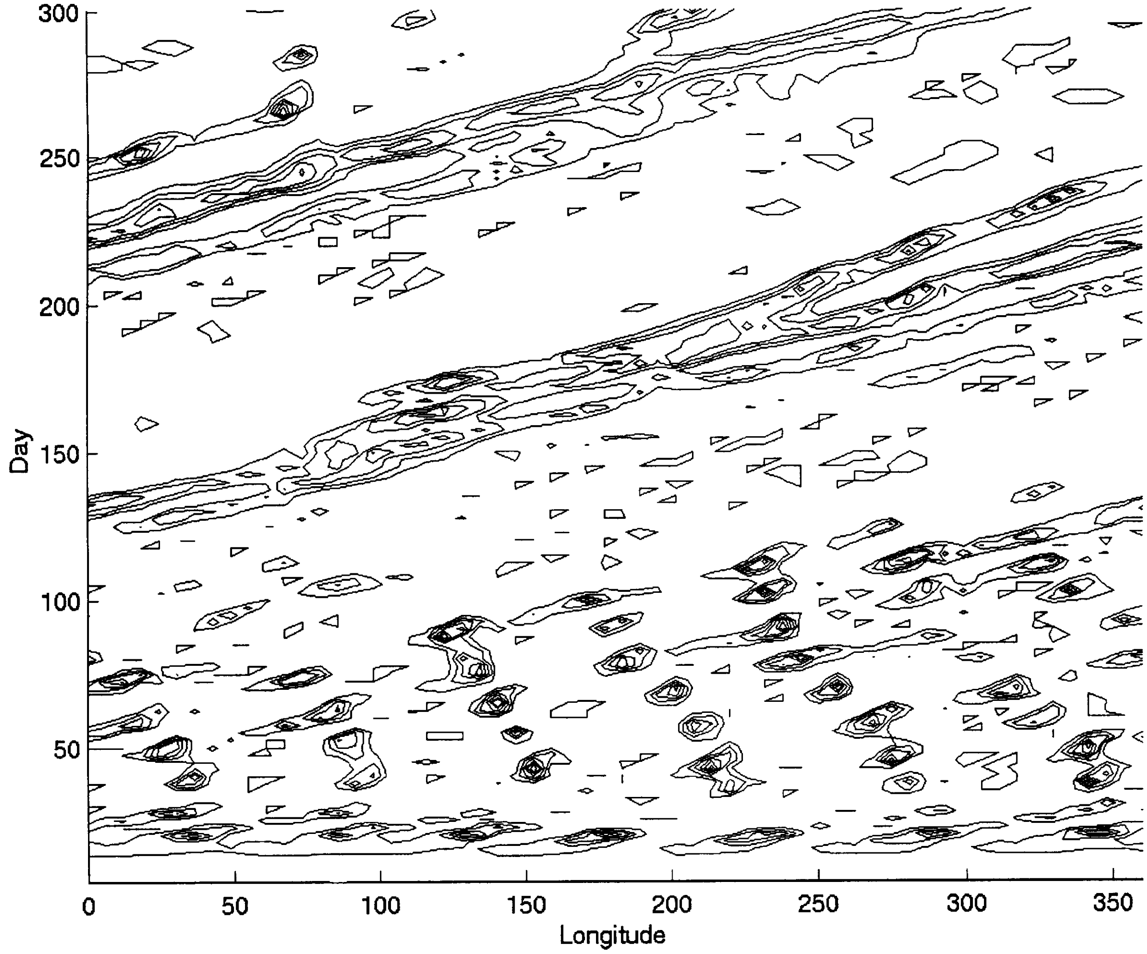

Figure 4-21: Longitude-time diagram of precipitation at 22N for three dimensional run with $\Delta T = 35$K. Precipitation contour interval 3 mm/day.

At times, new disturbances seem to form to the west of the existing large anomaly, and may die out or merge with the initial disturbance. The strength of the convection associated with the large disturbance varies, and examination of snapshots of the flow show that when the disturbance strengthens significantly, large eddies often form to the north of the disturbance, and blobs of convection are shed into the midlatitudes. If the eastern portion of the strong low-level cyclonic circulation strengthens, the anomaly may split into two smaller disturbances by the forcing dry air into the middle of the convective disturbance, weakening it in the center. The large anomaly dominates the flow along the coast, and there is a large region of suppressed convection over the rest of the coastal land, as seen in Figure 4-21.

The large anomaly does show some hallmarks of a monsoon: there is low-level cross-equatorial flow which feeds the monsoon from the southwest; there is strong convection and precipitation associated with the disturbance over the continent; there is low-level cyclonic flow near the disturbance, and upper-level anticyclonic flow; the ITCZ is located in the near-equatorial region except in the monsoonal regions, where the ITCZ is disrupted. However, the disturbance is limited to a longitudinal extent of approximately 40-50 degrees as seen in Figure 4-21, so that the zonal mean fields are not strongly affected by the disturbance. As the anomaly constantly moves eastward, it is difficult to evaluate the zonal average of the fields only over the region occupied by the disturbance.

4.4 $\Delta T = 45K$

The zonal mean steady state for the $\Delta T = 45$K case is monsoonal in nature. The zonal mean circulation features a strong ascent region between 15N and 25N, with a cross-equatorial circulation cell which extends to 25S, as seen in Figure 4-23. The cross-equatorial cell is nearly AMC near the equator, although the flow does cross M contours along the subtropical edges of the cell. The low-level return flow shows only a slight inclination to jump over the equator. The 'summer' Hadley cell is clearly not AMC, and is instead driven by eddies. There are two strong subtropical jets, the southern hemisphere jet being the stronger of the two. There is a strong easterly jet aloft across the equator, with the maximum easterly wind near 40 m/s near the tropopause. At low levels, there is a local easterly maximum near 10S, and a weaker region of easterlies from 25N to 35N. A region of low-level westerlies lies between 5N and 25N.

During spin-up, precipitating eddies form over the subtropical continent. Several of these eddies develop strong low-level southwesterly flow onto the land, and grow in extent and strength. Southwesterly low-level flow develops along much of the coastline, and the precipitating regions become longitudinally wider during the first 100 days of the run as seen

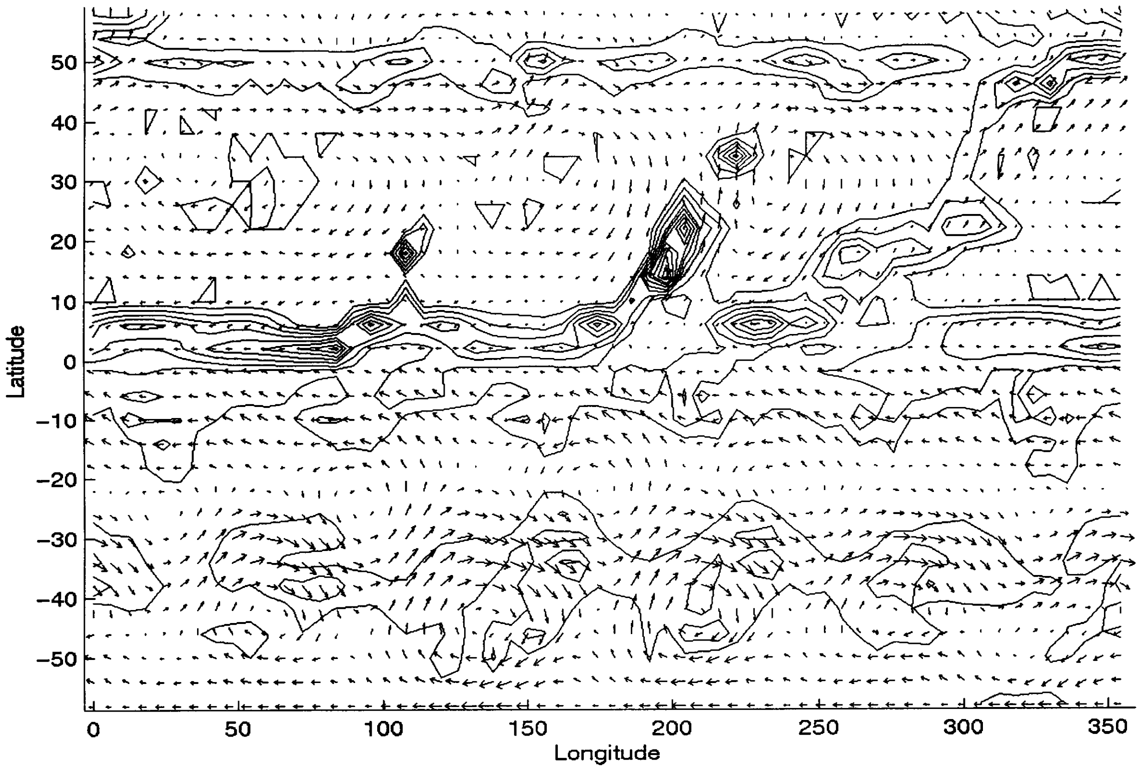

Figure 4-22: Winds at 1000 mb (arrows), mean days 297.5-300, with precipitation contours for the three dimensional run with ΔT = 35K. Precipitation contour interval 3 mm/day, maximum wind speed 19.1 m/s.

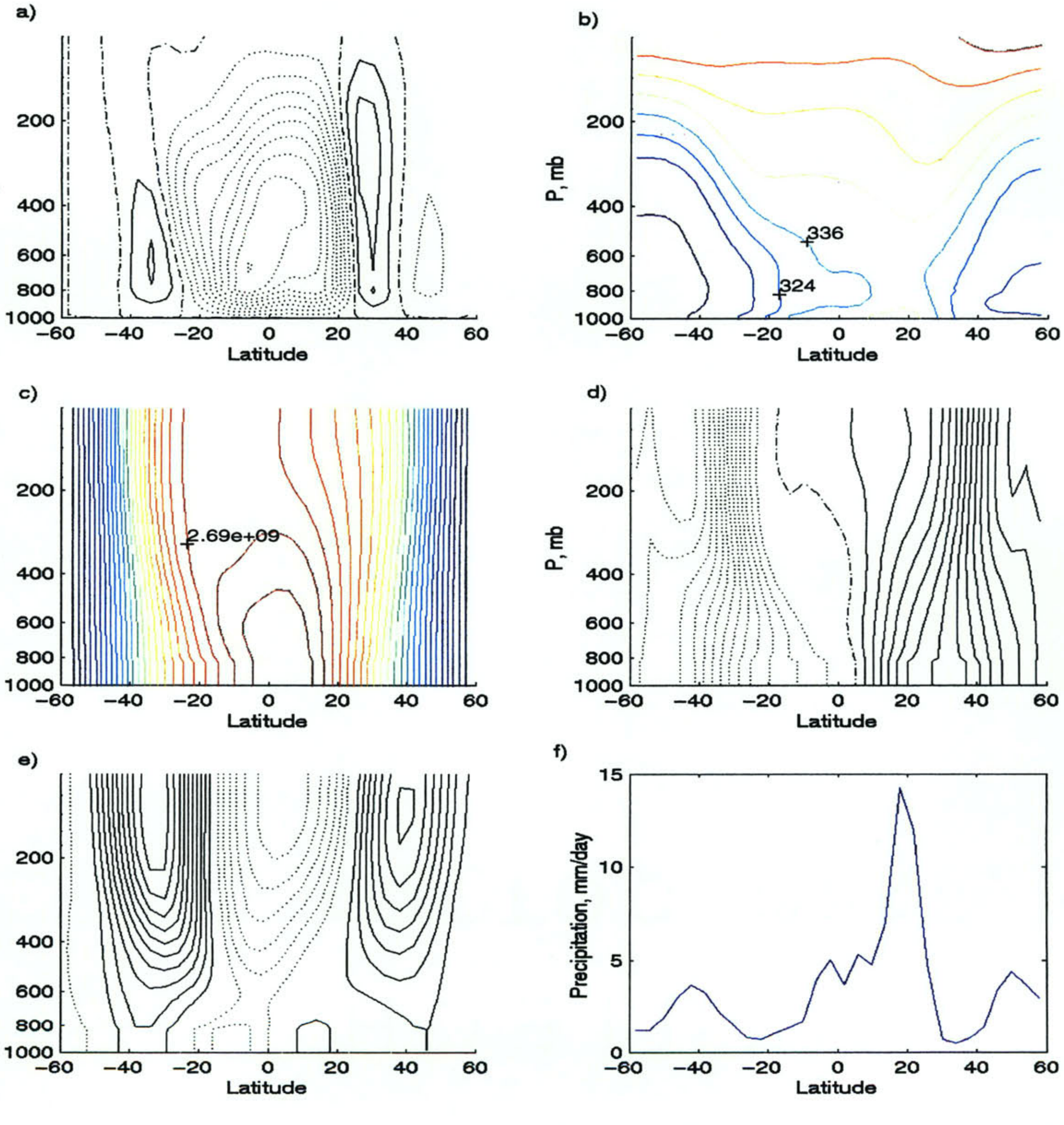

Figure 4-23: Model results for 3D run with $\Delta T = 45K$, all fields averaged over days 200-300. Solid lines indicate positive contours, dotted lines indicate negative contours, zero contour in dash-dots. a) Streamfunction, contour interval 2.5E10 kg/s; b) θ_e, contour interval 12 K; c) M, contour interval 8.6E7 m^2/s; d) absolute vorticity, ζ_a, contour interval 1.0E-5 1/s ; e) zonal wind u, contour interval 6 m/s; f) precipitation, mm/day.

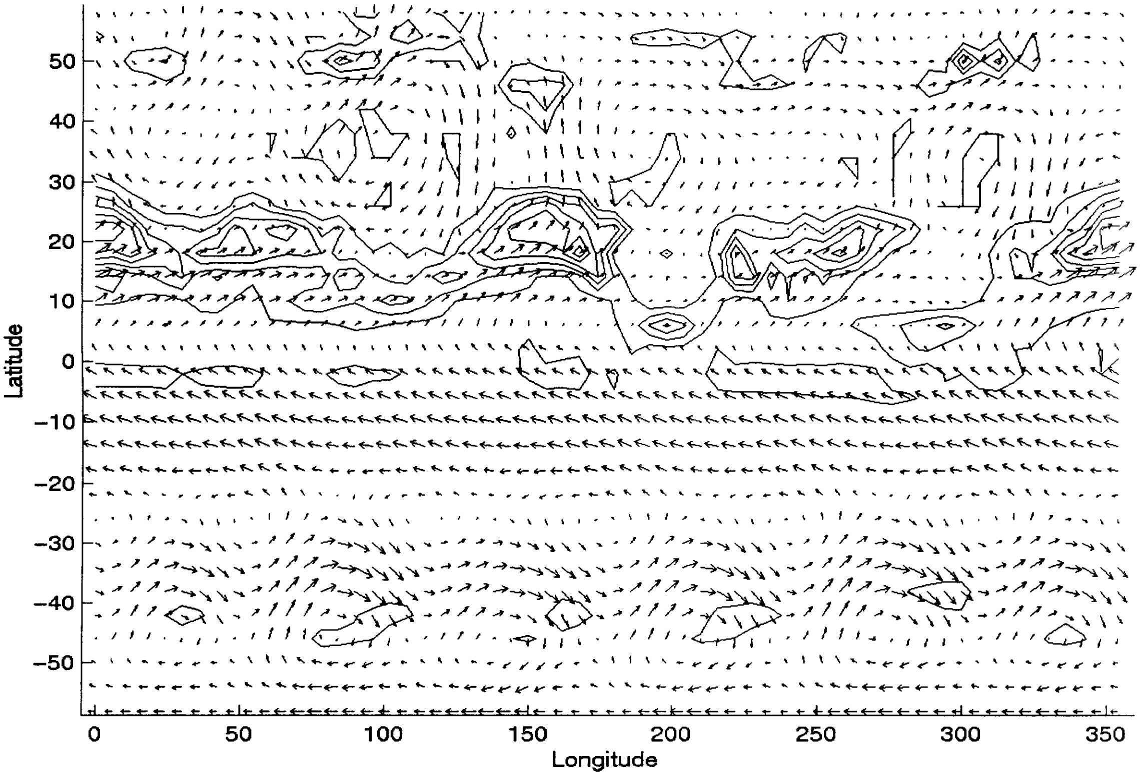

Figure 4-24: Winds at 1000 mb (arrows), mean days 297.5-300, with precipitation contours for the three dimensional run with ΔT = 45K. Precipitation contour interval 5 mm/day, maximum wind speed 18.5 m/s.

in Figure 4-25. These deep convective anomalies develop associated southwesterly low-level flow across the coastline, which travels with the monsoonal disturbances and supplies them with moisture.

The zonal mean precipitation has a broad maximum between 15N and 25N, with moderate precipitation across the equatorial region. There are several large precipitating disturbances over the land surface, which vary in longitudinal extent, and which sometimes merge together or break into smaller disturbances, as seen in Figure 4-25. In some areas, the buckets become completely saturated under heavy rainfall (4 cm/day), and new disturbances may form in the wake of a departed anomaly in the region of wetted buckets. The monsoon disturbances are associated with low-level cyclonic flow, and with anticyclonic flow at upper levels. The precipitation tends to be slightly out of phase with the vorticity, with the precipitation occurring on the eastern side of the low-level cyclones, as in the ΔT = 35K run. The upper-level anticyclonic flow is shifted to the the west of the deep convection.

In between the deep convecting regions on the land are strong low-level anticyclones, which tend to suppress convection on the western side of the precipitating anomalies by

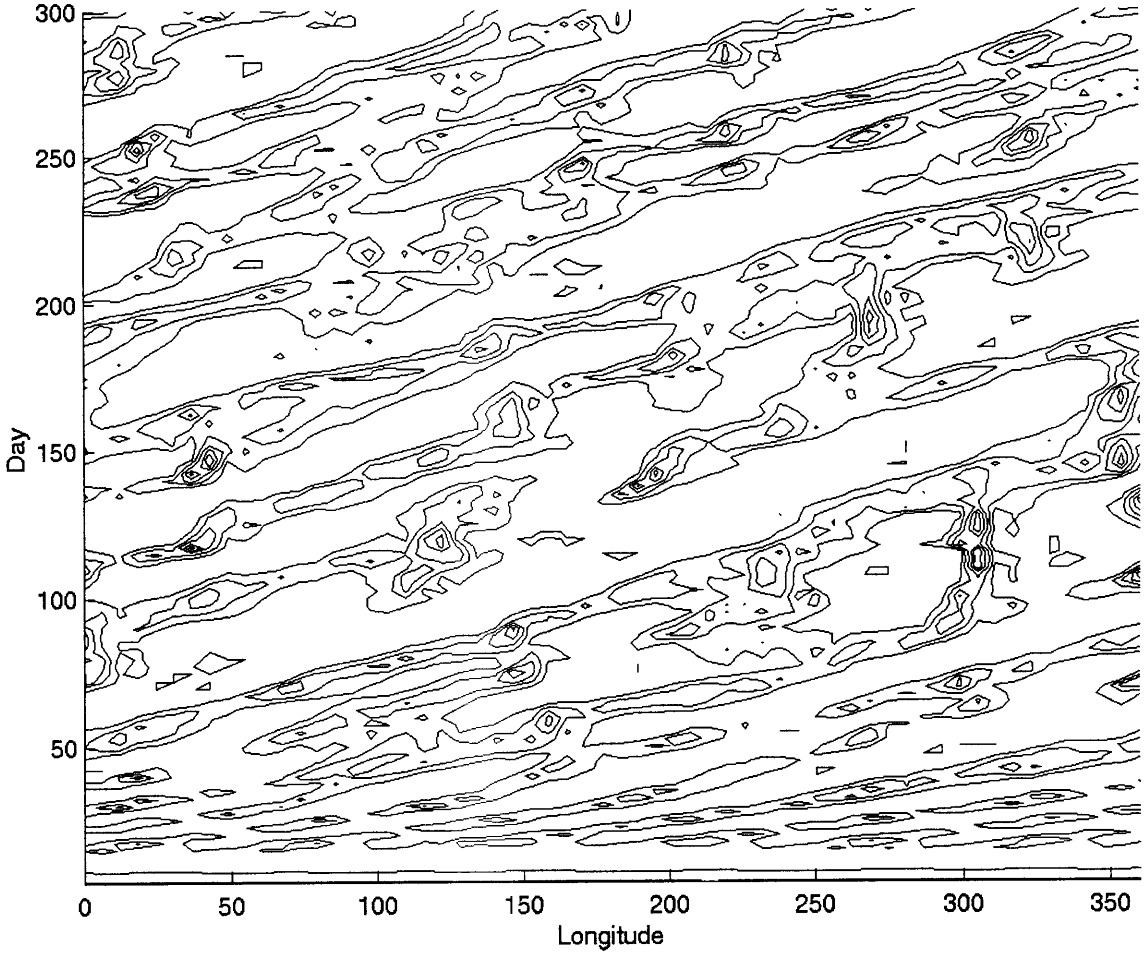

Figure 4-25: Longitude-time diagram of precipitation at 22N for three dimensional run with ΔT = 45K. Precipitation contour interval 10 mm/day.

drawing dry air from the interior of the continent southward. In these areas, the intense precipitation is located over the ocean. If the low-level winds are weak over the ocean and coastline, the oceanic deep convection in these areas tends to be located around 6N. However, if there are sufficiently strong winds along the coast, the precipitation maximum at that longitude is located near 10-12N, probably due to the enhanced surface fluxes in these regions. These deep convection regions can set up meridional circulation which features subsidence over the coastal continent, further suppressing convection there. Several large regions with weak precipitation are sustained over the subtropical continent for long periods of time, as seen in Figure 4-25.

Moisture is supplied to the monsoon circulation by both the mean flow and the eddies, with the mean flow providing most of the transport, as seen in Figure 4-26. The eddy water

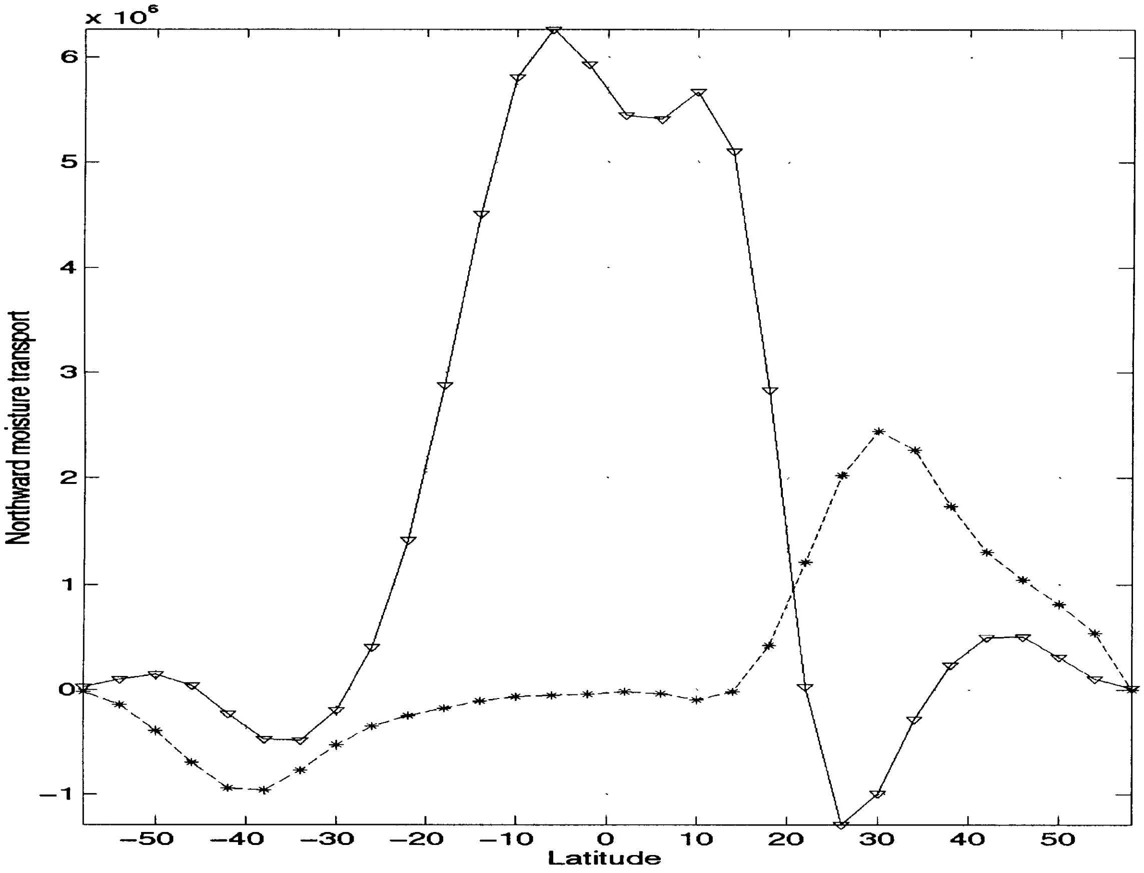

Figure 4-26: Zonal mean northward water vapor flux, kg/s, mean days 200-300, $\Delta T = 45K$. Solid line with triangles indicates [q][v], dashed line with asterisks indicates eddy flux $[q^*v^*]$..

vapor flux is only slightly higher than in the non-monsoonal runs, and carries moisture from the monsoon region to the midlatitudes. The magnitude of the moisture transport onto the continent by the mean flow is similar to that found in the monsoonal axisymmetric runs. The latent heat flux in the monsoon regions of the ΔT = 45K run is again somewhat high, around 450 W/m^2 on average in the deep convecting regions. The sensible heat fluxes, however, seem to be relatively close to observations. The zonal mean surface temperatures for the monsoonal run with ΔT = 45K are between 305K and 310K in the zonal mean, and surface air temperatures are near 305K. Observed surface temperatures tend to drop by several degrees after monsoon onset (Hsu et al., 1999), once precipitation develops over the land.

The Eliassen-Palm flux diagram seen in Figure 4-27 shows a broad region of low-level waves between 20N and 50N, similar to previous runs. The configuration of Ertel's potential vorticity in the northern hemisphere indicates possible baroclinic instability where the PV gradient changes sign near 800 mb between 10N and 25N, and also in midlatitudes where

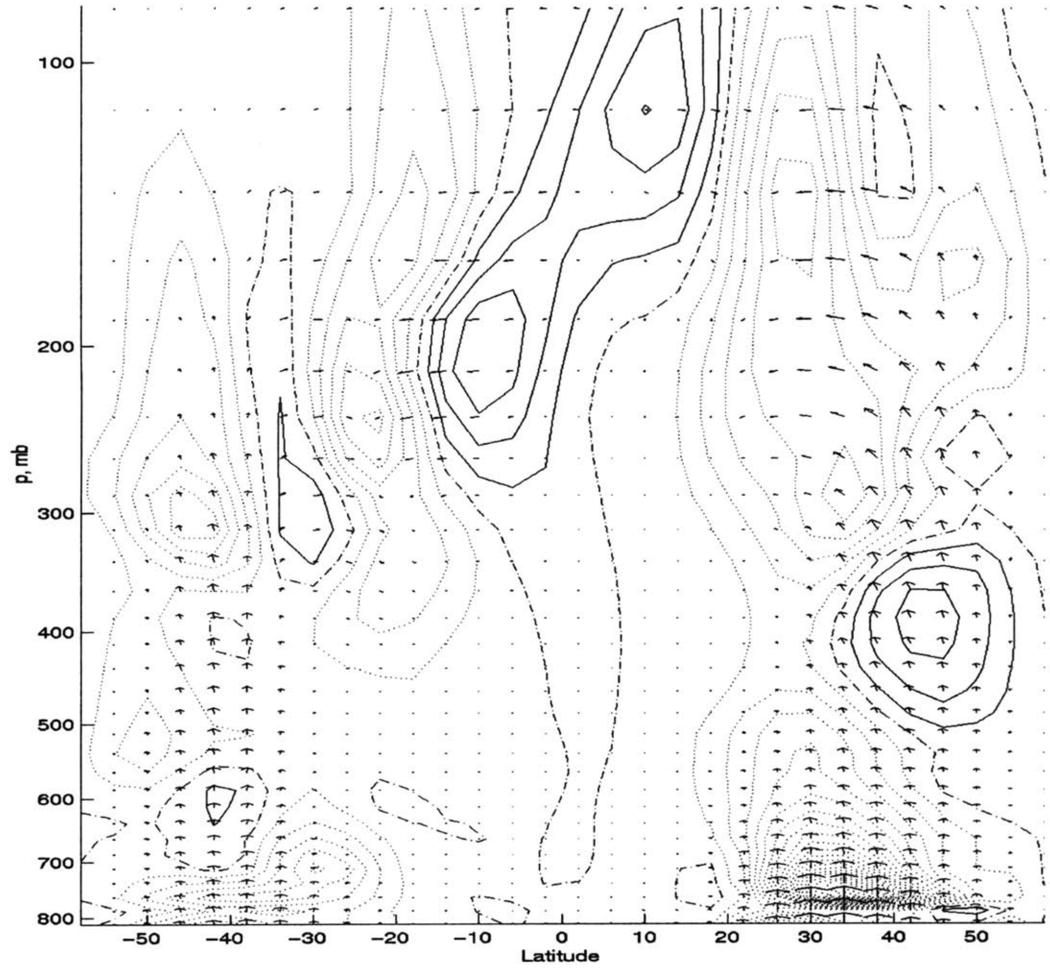

Figure 4-27: Eliassen-Palm flux, arrows, and EP divergence, contours, contour interval 40 m^3, $\Delta T = 45$K. Solid contours indicate divergence, dotted contours indicate convergence.

positive PV gradient and negative surface θ gradient occur. Barotropic instability is again unlikely as the absolute vorticity at lower levels has positive gradient through the mid troposphere across the entire northern hemisphere.

The zonal wavenumber covariance spectra at 750 mb, seen in Figure 4-29, shows much different wave structure than in the non-monsoonal runs. The momentum eddy flux at 21N has three different wavenumbers of peak covariance: wavenumber 2 with eastward phase speed between 3 and 4 m/s, wavenumber 3 with eastward phase speed of 1 m/s, and wavenumber 6 with eastward phase speed of approximately 3 m/s. The eddy heat flux at 21N is more concentrated in wavenumbers 2, 4, and 6, which all have eastward phase speed of 3 to 4 m/s. At 42N, the momentum eddy flux has a very strong spectral peak at wavenumber 4, with phase speed of 3 m/s to the east, which is only weakly echoed in the 21N spectra. The eddy heat flux at 42N has a broad range of waves, with spectral peaks

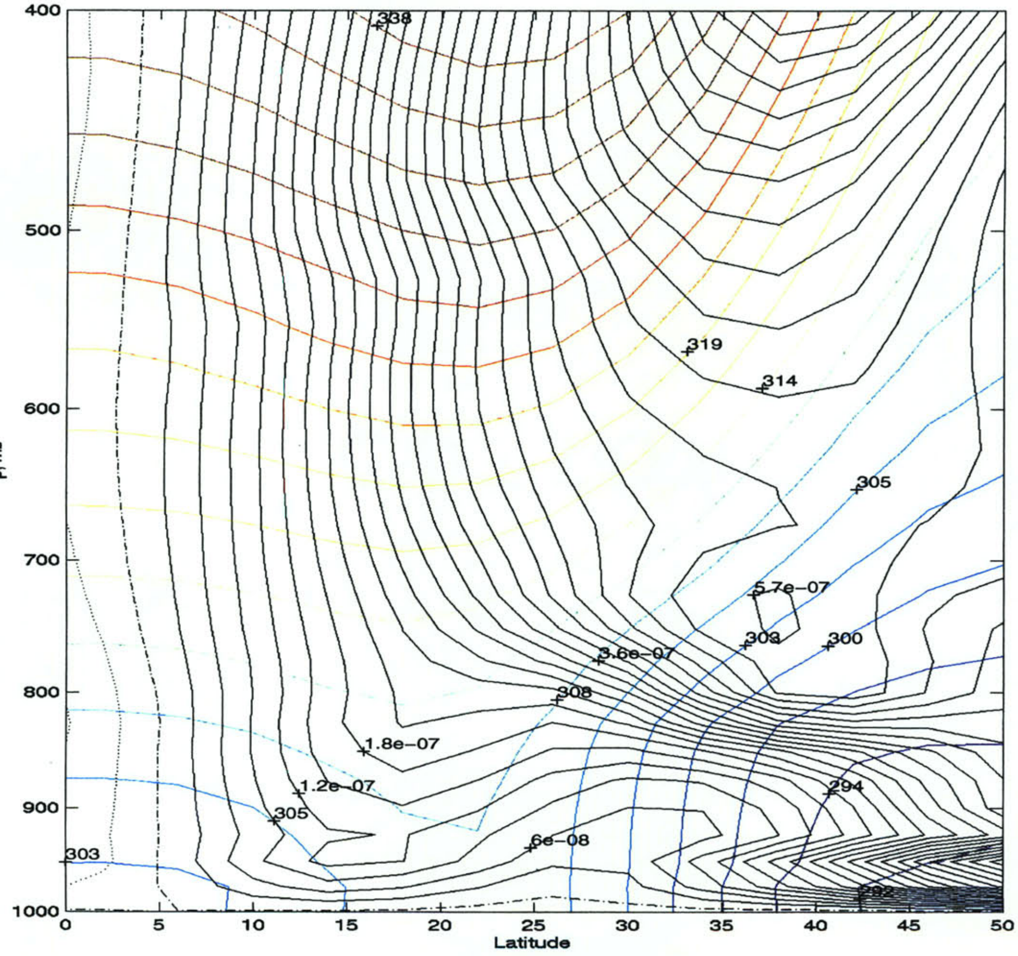

Figure 4-28: Zonal mean Ertel's PV, contour interval 3E-8 $Km^2kg^{-1}s^{-1}$, solid black lines indicate positive values, dotted indicate negative values. Zonal mean θ_v, contour interval 2K, color lines. 3D run with $\Delta T = 45$K.

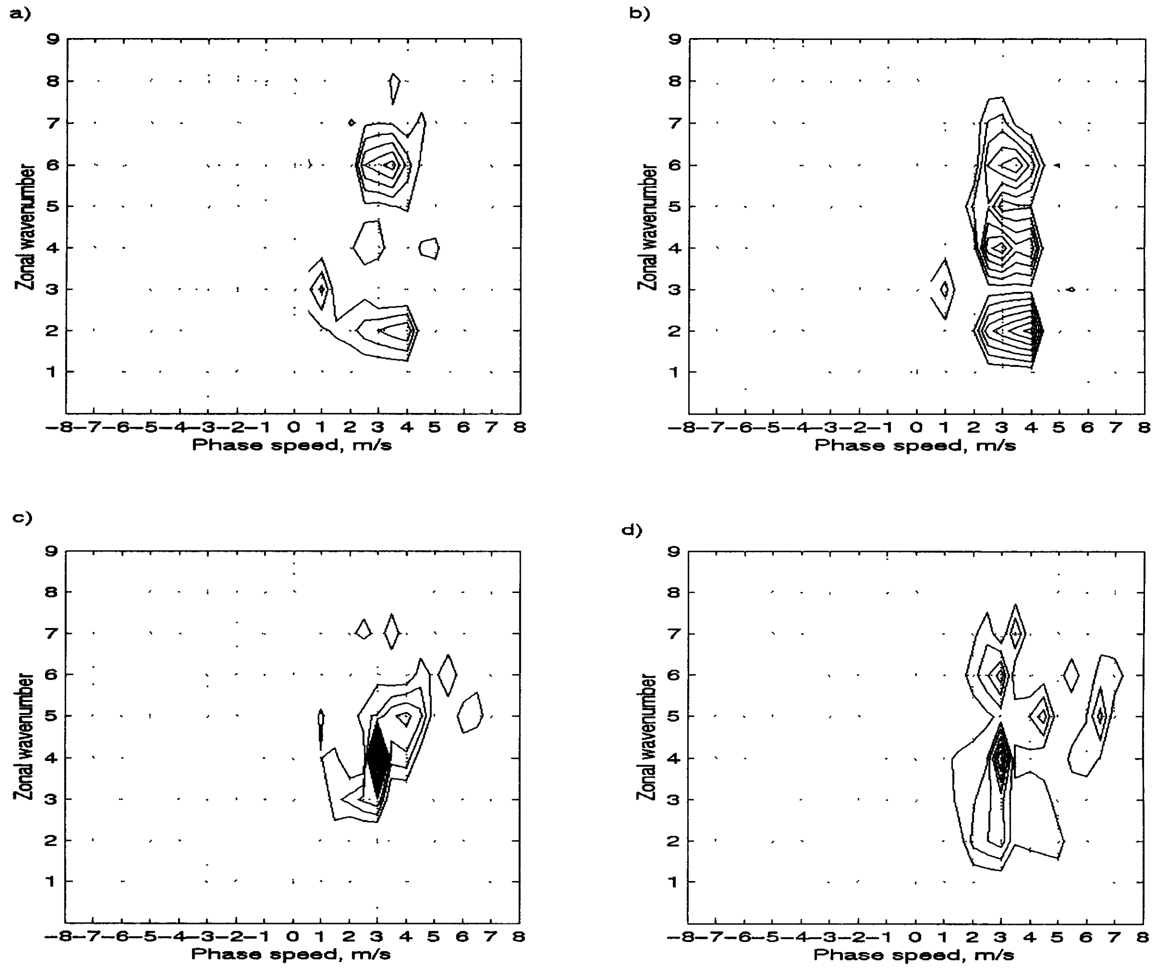

Figure 4-29: Zonal wavenumber phase speed covariance spectra, $\Delta T = 45$K at 750 mb. a) spectra for $[u^*v^*]$ at 21N, contour interval 2.5E-8 m^3s^{-3}; b) $[v^*T^*]$ at 21N, contour interval 2.5E-8 Km^2s^{-2}; c) $[u^*v^*]$ at 42N, contour interval 2.5E-8 m^3s^{-3}; d) $[v^*T^*]$ at 42N, contour interval 3.5E-8 Km^2s^{-2}

at wavenumbers 4 and 6 with eastward phase speed of 3 m/s, as well as others. The eddy momentum flux signatures are particularly different from each other at the two different latitudes, and the 21N spectra seem to be dominated by the monsoon. The wavenumber 2 peak seen at 21N is probably due to the large-scale monsoonal anomalies, in which are embedded smaller, higher wavenumber disturbances, which tend to travel eastward at the same speed.

Chapter 5

Discussion and Conclusions

5.1 Axisymmetric Runs

The axisymmetric model runs reveal several things:

1. To induce a monsoon circulation, we need to communicate the surface heating to the upper levels of the atmosphere. Precipitation over the land is necessary in order to moisten the heated land surface and create a low-level θ_e maximum over the continent.

2. The monsoon dynamics are strongly dependent on moisture availability, which is in turn affected by the large scale circulation and the land hydrology. The constraints of axisymmetric flow strongly affect the monsoon by discouraging low-level cross-equatorial flow, and limiting moisture transport onto the land. Differences in behavior at different meridional resolution are tied to moisture transport.

3. In order to induce a strong low-level cross-equatorial flow, a meridional temperature gradient in the boundary layer is necessary at the equator. In our runs, a northward SST gradient across the equatorial region is needed to generate sufficient low-level flow to maintain a realistic monsoon.

4. There seem to be three behavior regimes: i) the land surface forcing is too weak to result in a θ_e maximum over the continent even with adequate moisture supply, and the ascent region of the circulation cells is located over the ocean; ii) the land surface forcing is strong enough to result in a continental θ_e maximum in the presence of precipitation, but deep convection cannot be maintained over the land surface due to insufficient moisture transport and land surface processes. The ascent region of the steady circulation is poleward of the SST maximum, but located over the ocean surface; iii) There is a sustainable monsoon with deep convection over the land and a temperature maximum aloft, and strong AMC cross-equatorial circulation.

Our attempts to create a monsoon-type circulation in the 2D axisymmetric model were only partially successful. Moisture transport acted as a limiting factor for the monsoon in both the Case 1 and Case 2 scenarios. Although the land surface temperatures achieved in the model are reasonable for both monsoon and dry land regions, the surface latent heat flux is a little higher than observed for the monsoon regions. Given the crude surface parameterizations and simplified setup of our model, however, this level of surface forcing is not necessarily unreasonable. In the real world, factors which are not included in our simplified model, such as orography, may result in more effective forcing than the surface heating used in the model.

While the Case 1 axisymmetric runs seem to follow threshold behavior similar to that encountered in Plumb and Hou (1992), Emanuel (1995), and Zheng (1998), the dynamics are severely constrained by moisture transport problems. Whereas the forcing in Plumb and Hou (1992) and Zheng (1998) results in an upper-tropospheric temperature maximum for all applied positive forcings, this is not true of the land surface forcing in our setup. In our model runs, the land surface temperature forcing must be strong enough to maintain both warm land surface temperatures and sufficiently strong latent heat fluxes at the surface in order to result in a continental θ_e maximum. Deep convection acts to communicate the temperature maximum throughout the depth of the troposphere. The monsoon is dependent on the ground hydrology for its supply of moisture, so that the buckets provide most of the water for the monsoon. The circulation which results when deep convection is located over the land surface must result in a balance in the land surface hydrology in order to sustain a steady monsoon. When the surface forcing is insufficient, deep convection does not occur over the heated continent, and the upper-level temperature profile does not have a local maximum over the continent. The fixed moist bucket runs show threshold behavior very similar to that observed in the model runs of Zheng (1998), while the 'free' bucket hydrology runs are modified by the land surface parameterizations. The overall effect of the land surface hydrology and interactive temperature scheme is to sharpen the threshold behavior, and to limit the maximum strength of the cross-equatorial circulation. The crude nature of the land surface parameterizations and the dynamical limitations of axisymmetric flow in the Case 1 runs make it difficult to determine whether this limiting behavior is applicable to the real world.

In the Case 2 runs, Hadley cells are present when a monsoon circulation does not occur, so that AMC circulations are always at play. Instead of the two possible dynamical regimes being thermal equilibrium or an AMC circulation, the heated land region will either fall in the subsidence region of the summer Hadley cell, or the monsoonal circulation will attain. It would be desirable to be able to compare the results of Case 2 with those of Case 1 to determine whether the dynamical threshold behavior is altered by the change in possible regimes. However, differences in the crucial moisture transport between Case 1 and Case 2 due to jumping of the circulation in Case 1 make any direct comparison between these runs problematic at best. There is some indication of threshold behavior in Case 2 in that there is a significant jump in the strength of the cross-equatorial circulation streamfunction when a monsoon is induced. When the land surface temperature is too weak to result in a monsoon, the cross-equatorial circulation cell is the 'winter' Hadley cell, with ascent near the SST maximum. The strength of this 'winter' Hadley cell is primarily dependent on ocean surface fluxes, and is not significantly affected by increased land surface forcing. When the land surface temperature forcing is sufficient to result in a steady monsoon circulation, the cross-equatorial cell broadens slightly, and strengthens significantly. The strengthening of the circulation is expected, as a cell with a broader region of subsidence governed by radiative cooling requires stronger ascent.

In the axisymmetric case, strong easterlies aloft at the equator are due to the AMC nature of the cross-equatorial circulation when the ascent is located off of the equator. Thus, if a region of low-level heating or convergence encourages the formation of the ITCZ off of the equator in the axisymmetric case, the resultant easterlies over the equator will lead to a region of low pressure at the equator throughout the troposphere, and low-level convergence in the boundary layer. In cases where the meridional temperature gradient is very weak at the equator, the flow is reluctant to cross the equator at low levels, and instead enters the free troposphere and 'jumps' over the equator along M-contours. Even when there is a moderate meridional temperature gradient in the boundary layer due to the SST gradient, there is a tendency for the low-level flow to enter the free troposphere near the equator. This results in a secondary region of convection, which is seen in the model output as a broad region of precipitation throughout the near-equatorial region. The ITCZ cannot simply revert entirely to the equator in preference to the off-equatorial location because this would lead to the loss of the equatorial easterlies and thus loss of the source of the low-level convergence, and the off-equatorial heating would again be the preferential location for the ITCZ. Thus, the dual tendencies for convection manifest themselves as a strong ITCZ at the off-equatorial heat source with a broad region of weaker convection throughout the equatorial region, depending on the nature of the boundary layer flow. If the equatorial temperature gradient is weak, the low-level northward flow looses moisture content through precipitation near the equator, and the tendency of the flow to remain in the free troposphere prevents the replenishment of moisture content by surface evaporation. A meridional temperature gradient at the equator is necessary for the flow to cross the equator in the boundary layer and to transport sufficient moisture northward to supply the monsoon.

5.2 Three Dimensional Runs

A key factor in creating a zonal mean monsoon state in the three dimensional runs is the moisture supply to the precipitating eddy disturbances. In runs with weaker surface forcing, the deep convective regions over the coastal continent seem to be controlled by the eddies, and the precipitating anomalies do not induce their own flow. This means that each precipitation event over the continent must rely on the eddy to deliver adequate moisture to drive the convection: if the eddy fails to do so, the precipitating region dies off. In the runs with stronger forcing, some of the precipitating regions which first form due to the eddies seem to somehow induce (or be fortuitously located near) local low-level southwesterly flow along the coast. This allows moisture to be transported to the convecting region from the ocean, and the deep convection can intensify and broaden in extent. In the $\Delta T = 45$K run, the precipitating anomalies over the continent induce strong southwesterly flow and grow to large longitudinal extent. The strong precipitation locally fills the buckets, and encourages precipitation through the ground hydrology when the disturbance moves off to the east.

In all runs except for the $\Delta T = 45$K run, there is a broad region of minimum zonal mean pressure centered on the equator at low levels, although local pressure gradients are weak. This low is considerably wider than that seen in the axisymmetric runs, and helps to maintain a broad region of low-level convergence and precipitation in the equatorial region. The pressure gradient is in balance with the low level winds; there are easterlies in the lower troposphere throughout the entire tropics in all of the non-monsoonal runs.

The existence of eddies in the three-dimensional cases affects the large-scale meridional circulation. In addition to the creation of Ferrel cells in middle latitudes in the three-dimensional runs, the tropical Hadley cells and ITCZ are affected. Unlike the axisymmetric runs, strong easterlies can be maintained aloft at the equator without the presence of an off-equatorial ITCZ through eddy momentum transport. Thus, if eddies tend to create equatorial easterlies and thus induce convection at the equator, the Hadley cells may have ascent at the equator while maintaining easterlies aloft, and an off-equatorial heating region may not be sufficient to lure the ITCZ into relocating away from the equator. An ITCZ near the equator leads to subsidence of the northern Hadley cell between 10N and 20N, suppressing deep convection over this area and discouraging the formation of a monsoon.

Unlike in the perpetual runs of Xie and Saiki (1999), the monsoon region does not tend to spread inland with time, but instead remains confined to a region near the coast. As the same bucket hydrology is used in the MITGCM as in Xie and Saiki (1999), some process other than the hydrology must prevent the spread of precipitation inland with time. One possibility is tied to the zonal symmetry of the continent: the large-scale monsoon disturbances tend to move constantly to the east, so that there is not a tendency to gradually fill the buckets to the north and west of the monsoon, as in Xie and Saiki (1999).

One factor that may affect the zonal mean monsoon flow in the three dimensional runs is the so-called 'interactive Rodwell-Hoskins mechanism' (Rodwell and Hoskins, 1996). In this mechanism, localized subtropical heating due to the monsoon induces downwelling to the northwest of the heated region as a result of Rossby wave generation. Rodwell and Hoskins (1996) speculate that this subsidence region acts to quench convection to the west of the monsoon region, and may be responsible in part for the maintenance of observed desert regions to the west of monsoonal areas. The Rodwell-Hoskins mechanism may act to diminish the zonal mean monsoon by introducing longitudinally asymmetric regions in which deep convection is suppressed. Although the mechanism was used by Rodwell and Hoskins (1996) with a steady, stationary monsoon system, the monsoonal disturbances in our setup move relatively slowly, so that the theory may still apply.

We note that the deep convecting regions of the ΔT = 35K and 45K runs are interspersed with large regions of suppressed convection. We examine the vertical velocity at 500 mb for both of these cases to look for signs of the Rodwell-Hoskins mechanism. For the ΔT = 35K run, there is a single region of deep convection and ascent, and an associated longitudinally broad region of mean descent to the west of the deep convection. In the upper troposphere, a large anticyclone spreads from the precipitating area westward, and grows in longitudinal extent with time. However, the constant movement of the disturbance makes comparison of the flow to the ideal, steady flow studied by Rodwell and Hoskins (1996) difficult. In the ΔT = 45K case, there is pervasive deep convection throughout the subtropics, and it is more difficult to pair regions of strong convection with nearby areas of descent. Some areas of particularly strong and broad precipitation are accompanied by wide regions of subsidence to the west, while some strongly precipitating regions are not. The surface forcing may be strong enough to overwhelm the suppression of convection by subsidence in this case. As previously discussed, the lack of convection in these regions could be due to subsidence of meridional circulations stemming from the relocation of the ITCZ over the tropical ocean, so that it is difficult to determine how strongly the Rodwell-Hoskins mechanism might apply in these areas.

The three dimensional runs with weak surface forcing are dominated by waves of relatively high wavenumber, especially wavenumbers 6 and 7. As surface forcing is increased, low wavenumber eddy signatures become more prevalent in the subtropics, representing the large monsoon disturbances. These monsoon regions are composed of smaller eddies with higher wavenumber, but the eddies of different wavenumbers tend to have the same phase speed. In fact, a phase speed between 3 and 4 m/s is preferred for many of the disturbances over the subtropical continent at all levels of surface forcing. The waves in the midlatitudes show more variation in phase speed than those in the subtropics. The preferred phase speed of the disturbances may be due to interactions between the dynamics and the deep convection. The precipitation tends to occur on the eastern expanse of the low-level cyclonic flow, where moist inflow from the ocean is strongest. Thus, the deep convection and strong surface latent heat fluxes tend to lead the circulation, and the disturbance moves slowly to the east. This theory might be tested in the future by altering the bucket hydrology to see if the phase speed of the disturbances changes.

5.2.1 Comparison of Axisymmetric and 3D Results

Xie and Saiki (1999) found that baroclinic disturbances played a strong role in monsoon onset in their simplified GCM study. The presence of eddies may affect both the nature of the large-scale dynamics and the transport of moisture from the ocean to the continent. Axisymmetric runs from Case 2 can be compared with the three dimensional runs in order to determine the overall effects of the eddies on the monsoon circulation, since the same parameters and setup were used in both sets of runs.

The moisture transport plays an extremely important role in creating and maintaining a zonal mean monsoon. The mechanisms of moisture transport onto the continent differ between the axisymmetric and three dimensional model runs. In the axisymmetric runs, all moisture transport from the ocean onto the land must be due to the mean meridional circulation, while in the three-dimensional cases, eddies may carry moisture northward onto the land. This is especially important in light of the difficulties in transporting moisture in the axisymmetric runs. We note, however, that the eddy moisture flux in the three dimensional runs is relatively small in both the monsoonal and non-monsoonal cases. In the monsoonal $\Delta T = 45$K run, the moisture transport across the coastline by the zonal mean meridional circulation is much stronger than the eddy moisture flux, and is of the same order as the moisture transport in the axisymmetric monsoonal runs. In the non-monsoonal three dimensional runs, the southward moisture flux due to the mean circulation opposes the eddy moisture flux, so that the net northward moisture flux is quite small. The overall influence of the eddy moisture flux on the monsoon seems to be minimal. Eddies may also act to carry dry continental air south to the subtropics, and interfere with convection at some longitudes.

Since we were able to achieve a steady monsoon state in the axisymmetric runs, eddies are not required in order to maintain a viable monsoon. Indeed, the land surface forcing required to incite a monsoon in the three-dimensional case is greater than in the axisymmetric runs. The three dimensional runs require very large latent heat fluxes at the surface in order to maintain a zonal mean monsoon, while the axisymmetric monsoon cases have a more reasonable land latent heat flux. The zonal mean surface pressure low over the heated land surface is much weaker in the three dimensional runs than in the axisymmetric runs with the same land surface forcing. The zonal mean surface air temperature is also considerably cooler in the three dimensional runs. The eddies will tend to destroy strong temperature gradients in the three dimensional runs that can otherwise develop in the axisymmetric runs.

In the three dimensional runs, monsoon-type behavior may occur over a limited longitudinal range, while non-monsoonal circulation with an oceanic ITCZ may occur at other latitudes. If a region of suppressed convection occurs over the land at some longitude so that a non-monsoonal circulation is established, there may be dynamical feedbacks from the circulation, the ground hydrology, and possibly from eddy effects (such as the Rodwell-Hoskins mechanism) which act to maintain the region of suppressed convection. The zonal mean monsoon in the three dimensional runs may then be weaker than in a similar axisymmetric run, as both monsoonal and non-monsoonal regimes are included in the zonal mean. This is exemplified by the three dimensional run with $\Delta T = 35$K, where a single monsoon-type disturbance develops, but is confined to a longitudinally narrow region, while suppressed convection occurs elsewhere.

5.3 Future Work

Many facets of monsoon dynamics can be studied through the use of a simplified general circulation model. Several direct extensions of this work are suggested here to further expand upon our findings.

The axisymmetric runs are computationally inexpensive, and are useful for testing different land surface parameterizations. It would be desirable to run the Case 2 experiments again with a more sophisticated ground hydrology and land surface parameterization, especially since the choice of these seems to have a strong impact on the existence of a monsoon. The axisymmetric case is also ideal for examining the effects of a full radiation scheme, instead of the Newtonian relaxation used here, which would also allow for a better land surface temperature parameterization based on radiative balance. The possibility of multiple equilibria is intriguing, and this could be investigated with a series of runs in which the model dynamics are spun up from rest before introducing the land surface temperature forcing. The role of orography in inducing the monsoon by directly heating elevated regions of the atmosphere could be examined once topography is developed for the MITGCM.

The effects of zonal asymmetry of the real monsoons could be explored with a series of three-dimensional runs. One set of runs might have a zonally symmetric continent with a longitudinally localized heated region. A second set of runs might have a zonally asymmetric continent, allowing zonal transport of moisture over the land. Moisture transport onto the land surface seems to be one of the sticking points in creating a viable steady monsoon over the land in the current work, and it would be desirable to know to what extent the moisture transport controls the monsoon. An exploration of the moisture sources of the real monsoon through observational data might be very helpful in determining how relevant the model results are to the real world dynamics of the monsoon.

Bibliography

Cook, K. and A. Gnanadesikan: 1991, Effects of saturated and dry land surfaces on the tropical circulation and precipitation in a general circulation model. *J. Climate*, 873–889.

Emanuel, K. A.: 1991, A scheme for representing cumulus convection in large-scale models. *J. Atmos. Sci.*, **48**, 2313–2335.

— 1995, On thermally direct circulations in moist atmospheres. *J. Atmos. Sci.*, **52**, 1529–1534.

Emanuel, K. A. and M. Živković Rothman: 1999, Development and evaluation of a convection scheme for use in climate models. *J. Atmos. Sci.*, **56**, 1766–1782.

Held, I. M. and A. Y. Hou: 1980, Nonlinear axially symmetric circulations in a nearly inviscid atmosphere. *J. Atmos. Sci.*, **37**, 515–533.

Hide, R.: 1969, Dynamics of the atmospheres of the major planets with an appendix on the viscous boundary layer at the rigid bounding surface fo an electrically-conducting rotating fluid in the presence of a magnetic field. *J. Atmos. Sci.*, **26**, 841–853.

Hsu, H.-H., C.-T. Terng, and C.-T. Chen: 1999, Evolution of large-scale circulation and heating during the first transition of the Asian summer monsoon. *J. Climate*, **12**, 793–809.

Lindzen, R. S. and A. Y. Hou: 1988, Hadley circulations for zonally averaged heating off the equator. *J. Atmos. Sci.*, **45**, 2416–2427.

Luo, H. and M. Yanai: 1984, The large-scale circulation and heat sources over the Tibetan Plateau and surrounding areas during the early summer of 1979. Part ii: heat and moisture budgets. *Mon. Wea. Rev.*, **112**, 966–989.

Manabe, S.: 1969, Climate and the ocean circulation: the atmospheric circulation and the hydrology of the earth's surface. *Mon. Wea. Rev.*, **97**, 739–773.

Marshall, J., A. Adcroft, C. Hill, L. Perelman, and C. Heisey: 1997a, A finite-volume, incompressible Navier Stokes model for studies of the ocean on parallel computers. *J. Geophys. Res.*, **102**, 5753–5766.

Marshall, J., C. Hill, L. Perelman, and A. Adcroft: 1997b, Hydrostatic, quasi-hydrostatic, and nonhydrostatic ocean modeling. *J. Geophys. Res.*, **102**, 5733–5752.

Pauluis, O.: 2001, Axially symmetric circulations in a moist atmosphere. *Thirteenth Conference on Fluid Dynamics of the AMS*, American Meteorological Society.

Plumb, R. and A. Hou: 1992, The response of a zonally symmetric atmosphere to subtropical forcing: threshold behavior. *J. Atmos. Sci.*, **49**, 1790–1799.

Rodwell, M. and B. Hoskins: 1996, Monsoons and the dynamics of deserts. *Quart. J. Roy. Meteor. Soc.*, **122**, 1385–1404.

Schneider, E.: 1977, Axially symmetric steady-state models of the basic state for instability and climate studies. Part II. Nonlinear calculations. *J. Atmos. Sci.*, **34**, 280–296.

Schneider, E. and R. Lindzen: 1977, Axially symmetric steady-state models of the basic state for instability and climate studies. Part I. Linearized calculations. *J. Atmos. Sci.*, **34**, 263–279.

Webster, P.: 1983, Mechanisms of monsoon low-frequency variability: surface hydrological effects. *J. Atmos. Sci.*, **40**, 2110 - 2124.

Xie, S.-P. and N. Saiki: 1999, Abrupt onset and slow seasonal evolution of summer monsoon in an idealized gcm simulation. *J. Met. Soc. Japan*, **77**, 949–968.

Xu, J. and J. C. L. Chan: 2001, First transition of the Asian summer monsoon in 1998 and the effect of the Tibet-tropical Indian Ocean thermal contrast. *J. Met. Soc. Japan*, **79**, 241 - 253.

Zheng, X.: 1998, The response of a moist zonally symmetric atmosphere to subtropical surface temperature perturbation. *Quart. J. Roy. Meteor. Soc.*, **124**, 1209 - 1226.